TABLE OF CONTENTS

Autor's signature

Autor's signature

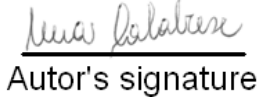

Autor's signature

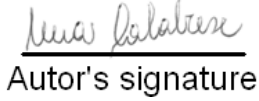

LIST OF TABLES

Autor's signature

LIST OF FIGURES

Autor's signature

Autor's signature

Autor's signature

Autor's signature

Autor's signature

INTRODUCTION

Currently, silicon solar cells cover more than 85% of the market of photovoltaic. However, silicon cells technology is still not cheap enough to allow a wide diffusion of photovoltaic energy conversion in the absence of government incentives. For this reason huge efforts of research and development have been spent in the last years to find alternative and improved solutions in this field [1].

Polymer solar cells (PSCs) represent a new technology that in the mid-long term could lead to affordable energy since they offer low cost, low thermal budget, solution processing, flexible substrates and a very high speed of processing.

In the active layer of a PSC, the conjugated polymer plays the key role of absorbing light, creating excitons for the subsequent charge separation, and transporting holes to the anode. To further improve the device performance, one approach is to adopt materials that harvest more light from the solar spectrum. The solar emission spectrum ranges from 350 to 1500nm, with a maximum flux at 700nm about. Nevertheless, the best PSC material developed to date, poly(3-hexylthiophene) (P3HT), absorbs only a part of the visible light spectrum (in the range from 350 to 650nm) and thus the possibility to harvest up of 22.4% of the available photons giving a maximum theoretical current density of 14.3mA/cm^2 [2].

To enhance the absorption of semiconducting polymers, several effective approaches have been reported, including the preparation of low band-gap (LBG) polymers and side chain-conjugated polymers. Using donor-acceptor strategies [2], several new polymers have been developed to better harvest the solar spectrum in the region 1.4-1.9eV. Unfortunately, LBG polymers exhibit often relatively low hole mobility and poor solubility. Thus, the main challenge of conjugated polymer engineering is to prepare materials that simultaneously exhibit high mobility and a better utilization of the solar spectrum.

OUTLINE

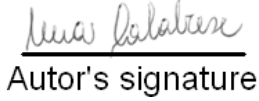

Autor's signature

This thesis is organized as follows. In the chapter 1 is reported an brief overview on organic semiconductors with particular reference to conjugated polymers. In the chapter 2, device physics, the working principle of organic solar cells is discussed in detail. Also, the current limitations concerning the power conversion efficiency will be explained. Most of these limitations can be circumvented by applying novel concepts, as outlined in chapter 3: material engineering as well as novel concept for solar cells are covered. In the chapter 4, the characterization methods of polymers and organic solar cells will be briefly described. Finally, in the chapter 5, the results and discussion will lead to the conclusions and to an outlook on the future opportunities, defined in the chapter 6. Experimental part is described in the chapter 7.

REFENENCES

[1] Po, R.; Maggini, M.; Camaioni, N., *J. Phys. Chem. C*, (2010) **114**, 695.

[2] Krebs, F. C.; Bundgaard, E., *Sol. Ener. Mat. and Sol. Cells.*, (2007) **91**, 954.

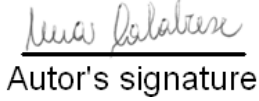

Autor's signature

1 ORGANIC SEMICONDUCTORS

1.1 INTRODUCTION

With the invention of the transistor around the middle of the last century, inorganic semiconductors such as Si or Ge began to take over the role as the dominant material in electronics from the previously dominant metals. At the same time, the replacement of vacuum tube based electronics by solid state devices initiated a development which by the end of the 20th century has lead to the omnipresence of semiconductor microelectronics in our everyday life. Now, at the beginning of the 21st century, we are facing a new electronics revolution that has become possible due to the development and understanding of a new class of materials, commonly known as *organic semiconductors*. The atoms, which form the backbone of organic semiconductors, are predominantly carbon atoms, sometimes in combination with oxygen and/or nitrogen. The nature of the chemical bonding in these materials directly influences the electrical properties. The enormous progress in this field has been driven by the variety of novel applications, such as large area, flexible light sources and displays, low-cost printed integrated circuits or plastic solar cells based on these materials. Traditional optoelectronic devices are composed of inorganic semiconductors such as amorphous, polycrystalline or single crystalline silicon that are usually processed under high temperature and high vacuum conditions. Compared to inorganic semiconductors, organic semiconducting materials are characterized by immense structural flexibility such that their optical and electronic properties can be easily tuned. They can also have excellent solubility in various organic solvents, which can potentially enable low-cost solution processing techniques. The field of electronics based on conjugated materials started in 1977 when Heeger, MacDiarmid, and Shirakawa discovered that the conductivity of the conjugated polymer polyacetylene (PA, Figure 1.4) can be increased by seven orders of magnitude upon oxidation with iodine, for which they were awarded the Nobel Prize in Chemistry in 2000 [1-3]. This discovery led,

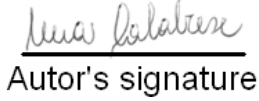

subsequently, to the develop and study of many innovative materials for the use in opto-electronic applications. There are two major classes of organic semiconductors: *low molecular weight* materials and *polymers*. Both have in common a conjugated π-electron system but an important difference between the two classes of materials lies in the way how they are processed to form thin films. Whereas small molecules are usually deposited from the gas phase by sublimation or evaporation, conjugated polymers can only be processed from solution, e. g. by spin-coating or printing techniques. Additional, a number of low molecular weight materials can be grown as single crystal allowing intrinsic electronic properties to be studied on such model systems. The controlled growth of highly ordered thin films either by vacuum deposition or solution processing is still subject of ongoing research, but will be crucial form many applications. Today, organic semiconductors are investigated for a variety of applications including organic light-emitting diodes (OLEDs) [4, 5], organic solar cells [6, 7], organic field-effect transistors (OFETs) [8], biosensors [9], etc. Here a short overview on organic semiconducting materials is given with particular reference to conjugated polymers, object of this work, to clearly understand the priorities and complexity involved in the design and development of organic materials for electro-optical applications.

1.2 CONJUGATED POLYMERS

Among organic semiconductors, *conjugated polymers* are considered promising materials owing to their potential of providing environmentally safe, flexible, lightweight, inexpensive electronics. They combine the electronic properties known from the traditional semiconductors and conductors with the ease of processing and mechanical flexibility of plastics. The particular bonding arrangement of the carbon atoms in the polymer backbone is the reason for the characteristic electronic properties of tunable conductivity, electrochromism, electroluminescence and electro-activity.

1.2.1 CHEMICAL STRUCTURE

The carbon atoms in a polymer are primarily bound together by covalent bonds formed by the interaction of two electrons, one from each of the atoms linked by the bond. This process can be easily explained with the simpler example of bond formation between two hydrogen atoms. As the atoms are brought together their 1s-electron orbitals overlap forming two new σ-orbitals around the atoms, which are symmetric and have zero angular momentum with respect to the interatomic axis. One orbital, the *bonding orbital*, is formed by the linear superposition of the two s-orbitals. This gives a high electron density between the hydrogen nuclei which reduces their electrostatic repulsion. Thus the nuclei are drawn together and an electron in the bonding orbital has a lower energy than one in the isolated atom orbital. The other, the *antibonding orbital* (generally labeled with an asterisk *), is formed by the superposition of s-orbitals with opposite sign, giving a lower electron density between the nuclei. The electrostatic repulsion between the nuclei is not screened and the energy of an electron in this orbital is increased as showed in Figure 1.1. The Pauli exclusion principle allows the two electrons from the hydrogen atoms to pair in the bonding orbital, if they are of opposite spin, to give a stable molecule with total energy less than that of the two isolated hydrogen atoms.

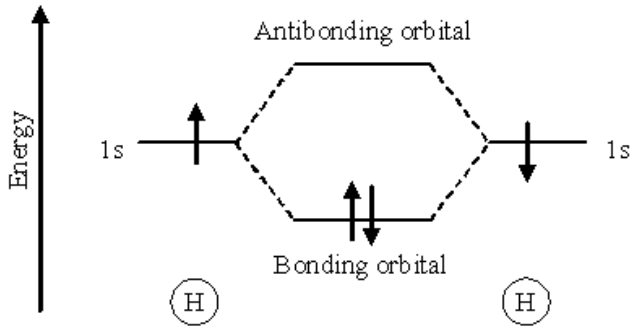

Figure 1.1 Overlap of hydrogen atom orbitals to from bonding and antibonding orbitals.

A neutral carbon atom has six electrons, which occupy the *1s*, *2s* and *2p* orbitals giving an electronic configuration of $1s^2 2s^2 2p^2$. The electrons in the core orbitals do not contribute to the chemical bonding. Since the *2s* shell is filled, this would suggest that carbon would form two bonds with its neighbors, with the unpaired $2p^2$ electrons, but we know that it

Autor's signature

forms four. The four valence electrons in the $2s^2 2p^2$ shells combine to a hybridized structure when forming covalent bonds. The *s* and *p* orbitals combine to form hybrid orbitals (sp^1, sp^2, and sp^3, depending upon the number of orbitals that is combined), which give rise to triple, double, or single bonds. In conjugated polymers, one *2s* orbital pairs with the two 2*p* orbitals to form $3sp^2$ hybrid orbitals, leaving one *p* orbital unhybridized. Two of the sp^2 orbitals on each carbon atom form covalent bonds with neighboring carbons, the third generally forms a covalent bond with a hydrogen or side group. This is called a σ-*bond,* which is any bond with cylindrical symmetry around the internuclear axis. The unhybridized p_z orbital overlaps with the unhybridized p_z orbital on the neighboring carbon. This is called a π-*bond*, as is any bond which arises from electrons approaching side by side, off the internuclear axis. Figure 1.2 summarizes the preceding explanation.

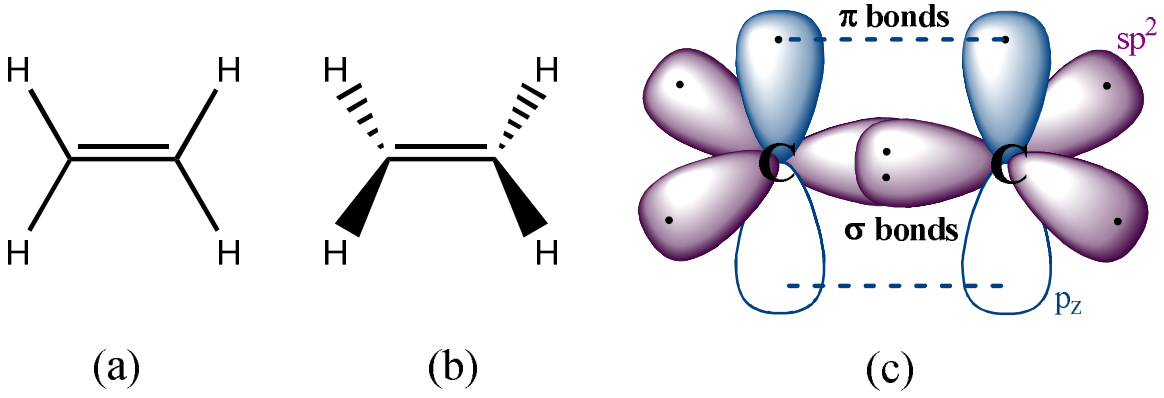

Figure 1.2 Conducting conjugated polymers: ethylene (C_2H_4). (a) Top (b) Front (c) Bonding. The sp^2 hybrid orbitals are shown in purple, and the unhybridized p_z orbitals in blue. Electrons are represented by the dots.

The electrons in the π-*bonds* are weakly bound thus they are relatively easily delocalized. These delocalized π electrons are the conduction electrons in these materials. In summary, the sp^2 hybridization in conducting polymers is important because this leaves one *p* electron per atom to form its own band. The resulting π-bond formed parallel to the underlying σ-bond, resulting in a multiple (double) bond. Compounds where orbitals are used in this way to form double bonds between carbon atoms, rather than to form single bonds with other atoms, e.g. hydrogen, are said to be unsaturated. The length of the single and double bonds are not identical and the Peierls instability [10] splits this simple band into two sub-bands. The antibonding orbitals (π*), located higher in energy, form a

Autor's signature

conduction band, with the lowest state named LUMO (Lowest Unoccupied Molecular Orbital). The valence band is formed by the molecular orbitals with lower energy, the bonding orbitals (π), with the HOMO (Highest Occupied Molecule Orbital) as an upper energy limit (Figure 1.3).

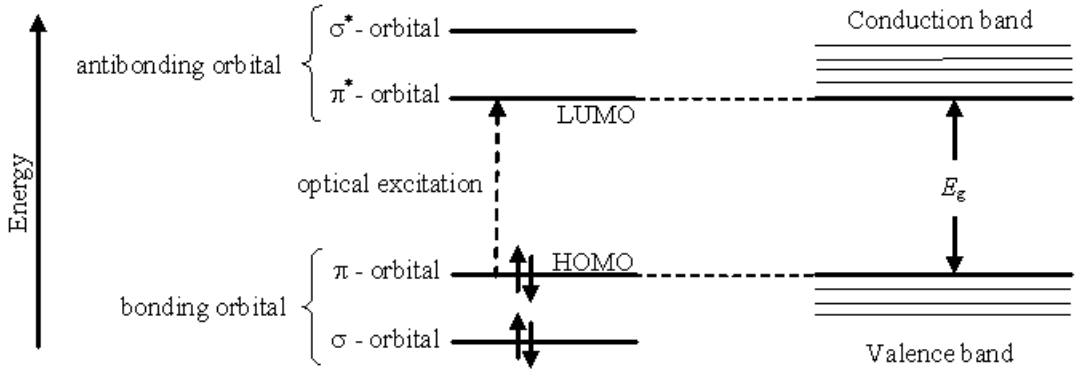

Figure 1.3 Energy level in organic semiconductors.

When successive carbon atoms in a chain engage in π-bonding, the structure is said to be *conjugated*, and may be represented as a sequence of alternating single and double bonds. Some common conjugated polymers are shown in Figure 1.4.

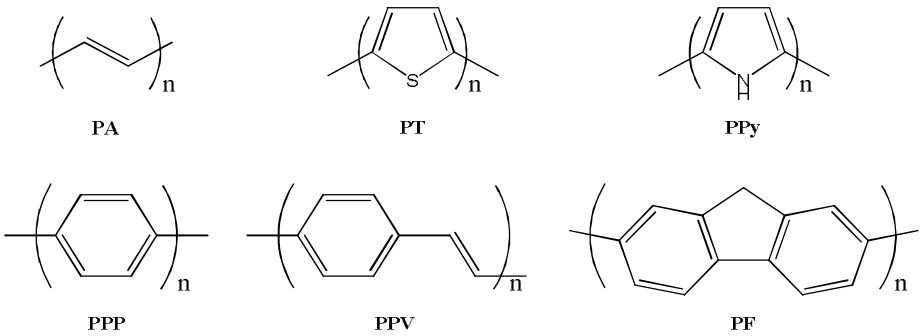

Figure 1.4 Molecular structures of several common conjugated polymers: poly(acetylene) (PA), poly(thiophene) (PT), poly(pyrrole) (PPy), poly(pphenylene) (PPP), poly(p-phenylenevinylene) (PPV) and poly(fluorene) (PF).

For a non-degenerate ground state conjugated polymer the sense of bond alternation between single and double bonds affects the energy of the organic semiconductor. The two different senses of bond alternation in non-degenerate ground state polymers are often

Autor's signature

referred to as the aromatic (low-energy) and quinoid (high-energy) structures. This implicates an important property of π-conjugated polymers: *the electronic structure and, hence, the energy are strongly coupled with the geometric structure.*

The nature of bonding in organic semiconductors is fundamentally different from their inorganic counterparts. Organic molecular crystals are Van der Waals bonded solids implying a considerably weaker intermolecular bonding as compared to covalently bonded semiconductors like Si or GaAs. The consequences are seen in mechanical and thermodynamic properties such as reduced hardness or lower melting point, but even more importantly in a much weaker delocalization of electronic wavefunctions amongst neighboring molecules, which has direct implications for optical properties and charge carrier transport. The situation in polymers is somewhat different since the morphology of polymer chains can lead to improved mechanical properties. Nevertheless, the electronic interaction between adjacent chains is usually also quite weak in this class of materials.

1.2.2 OPTICAL PROPERTIES

Organic semiconductors have two important peculiarities as compared to their inorganic counterparts. One is the existence of well-defined spin states (*singlet* and *triplet*) as in isolated molecules which has important consequences for the photophysics of these materials displayed in Figure 1.5. Usually the ground state of an organic molecule is a singlet state (S_0) and absorption of a photon leads to the first excited singlet state (S_1). Typical lifetimes of the S_1 state are in the range 1-10 ns [11], thus leading to a rapid transition back to the S_0 ground state via fluorescence or non radiative transitions. In the excited singlet state there is a small probability for intersystem crossing (ISC) to the triplet state (T_1), from which the excitation energy can be released either by phosphorescence or non-radiatively. However, since intersystem crossing is a weak process, triplet lifetimes are usually in the millisecond range for pure aromatic hydrocarbons, and radiative decay via phosphorescence is usually not observed at room temperature. Triplet lifetimes can be considerably shorter in molecules incorporating heavy atoms, such as Pt or Ir. Therefore metal organic complexes incorporating these elements are becoming more important in devices as light emitting diodes (LEDs). Conjugated polymers generally have broad

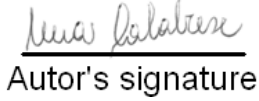

absorption and emission spectra, which be explained by the polydispersity of the material and the variation in conjugation length, as well as different degrees of polymer inter-chain interactions. Shifts in the absorption and emission spectra are strongly associated with conformational changes in the polymer backbone and/or the degree of inter-chain interactions. Alternations of the torsion angle between the polymer rings, through rotation around the π-bonds, in a conjugated polymer will affect the effective conjugation length [12]. An alternation from a non-planar to planar conformation, the torsion angle approaches 180° (trans conformation) or less common 0° (cis conformation), will give a longer conjugation length, seen as a red shift in absorption and emission [13, 14]. A more planar structure increases the propensity of π-stacking of the polymer chains, which also will lead to red shifts in the optical spectra, due to the possible inter-chain energy migration. Red shifts associated with aggregation is often seen as a new vibronic structure, a distinct absorption shoulder in the longer wavelengths of the visible spectra □□□□. The emission intensity of a conjugated polymer is highly dependent on the degree of aggregation, a consequence of the higher probability of a non-radiative decay in the aggregated phase. A second important difference between organic and inorganic semiconductors, is originate from the fact that optical excitations (excitons) are usually localized on one molecule and therefore have a considerable binding energy. In photovoltaic cells this binding energy has to be overcome before a pair of independent positive and negative charge carriers is generated. The excited states of neutral and charged conjugated polymers and their decay processes strongly affect the performance of polymer (opto)electronic devices such as LEDs and solar cells.

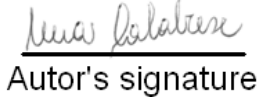

Autor's signature

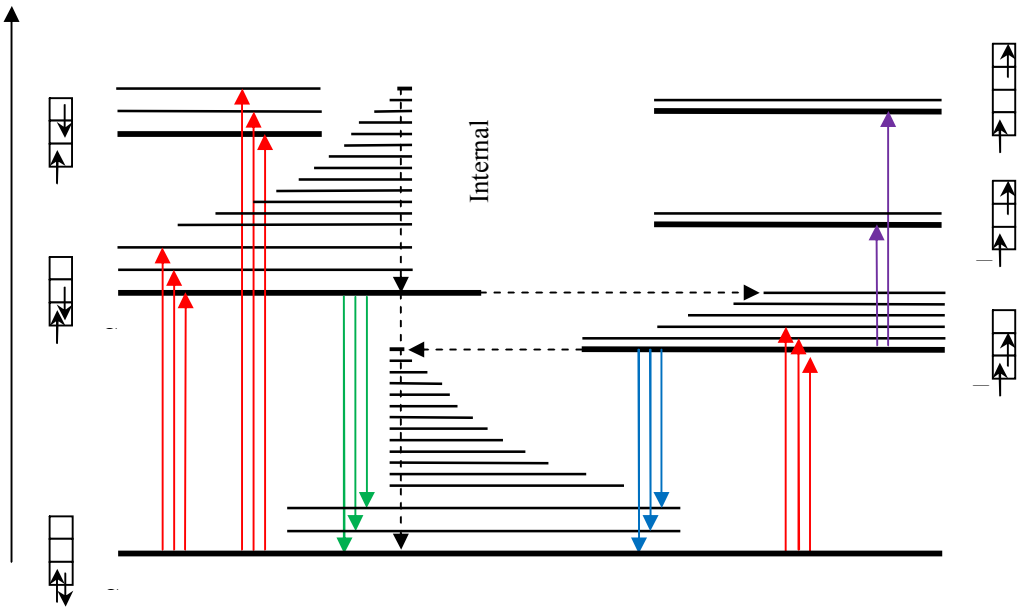

Figure 1.5 Schematic drawing of common photophysical processes for a conjugated molecule or polymer.

1.2.3 ELECTRICAL PROPERTIES

Conjugated polymers in the pristine state have, in contrast to crystalline materials, extremely low conductivity and exhibit strong temperature and electric field dependence. In order to overcome the limitations posed by the low intrinsic carrier density, different means can be applied in organic semiconductors such as: (electro-)chemical doping, photogeneration of carriers, carrier injection from contacts, and field-effect doping.

The first method concerns the introduction of charges either by electron-removal (oxidation or p-doping) or electron-injection (reduction or n-doping). The major part of conjugated polymers known today is built up of electron-releasing units, making them p-type semiconductors which can be doped with oxidants like I_2, $FeCl_3$, etc. The structural changes that occur in a conjugated polymer upon oxidation are illustrated in Figure 1.6 for polythiophene.

When this polymer is *p*-type doped (oxidized), the electron-phonon coupling leads to the formation of self trapped charged species, because the positive charge and unpaired electron cannot move independently as they are bound by a quinoid chain segment. As a result, the positive charge and the unpaired electron can only move with mutual interaction

Autor's signature

along the chain thus causing a local, geometric deformation, which is referred to as a positive *polaron* (see Figure 1.6). Upon further oxidation either, a second electron is removed from a different segment of the polymer creating a new polaron, or the unpaired electron of the previously formed polaron is removed and, hence, a bipolaron is formed. Conduction by (bi)polarons is generally accepted as the mechanism of intrachain charge transport in conjugated polymers. Hence, the intrachain conductivity relies on extension of the conjugation along the chain. In the bulk, charges should also be transported from chain to chain, which can occur via several mechanisms, such as hopping of charges between localized sites or band-like transport.

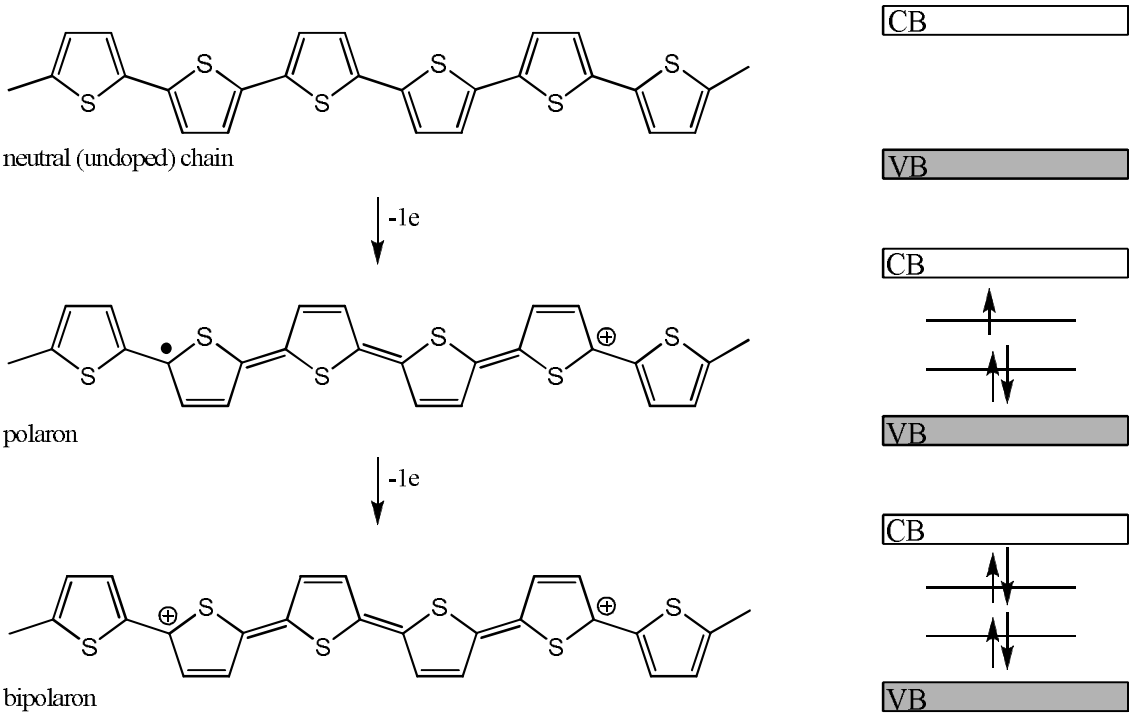

Figure 1.6 Change of geometric structure of polythiophene upon doping.

Interchain charge transport depends on the overlap of wave functions on different chains and can be increased by improving the macroscopic ordering of the polymer chains (for example via a liquid crystalline phase). When the polymer is doped, the electronic band structure of the polymer is changed and characteristic in-the-gap states are formed, which are associated with the lattice distortion due to the strong electron-phonon interaction (polaron formation). This geometric distortion causes an upward shift of the highest occupied level and a downward shift for the lowest unoccupied level. These new energy

Autor's signature

levels are associated with the quasi-particles (polarons, bipolarons) that are formed, in proportion to the doping level and the degeneracy of the ground state, (i.e. two equivalent resonance forms) (see Figure 1.6). Owing to the extensive conjugation of □-electrons, conjugated polymers can also be easily oxidized (*p*-doping) or reduced (*n*-doping) electrochemically with the conjugated polymer acting as either an electron source or an electron sink. In particular, the doping reaction can be accomplished by applying a direct current power source between a *polymer*-coated positive electrode and a negative electrode immerse in a particular solution. Compared with chemical doping, electrochemical doping has several distinct advantages. Firstly, a precise control of the doping level can be achieved simply by monitoring the amount of current passed. Secondly, doping-undoping is highly reversible with no chemical products requiring removal. Finally, both *p*- or *n*-type doping can be achieved even with dopant species that cannot be introduced by conventional chemical means. In both cases, however, counter dopant ions are introduced for stabilizing the charge along the polymer backbone. The incorporation of counter ions can be both a hindrance and an advantage. While the counter ions may cause an undesirable structural distortion and a deteriorated effect on conductivity, they facilitate conjugated conducting polymers for actuation applications. In order to eliminate the incorporation of counter ions, photo-doping and charge-injection doping methods have been exploited to achieve the redox doping effects. In organic solar cells, indeed, the conjugated polymers become charged in a photoinduced electron transfer reaction rather than by chemical doping. The irradiation of a conjugated polymer with a light beam of energy equal or greater than its band gap could promote electrons from the valence band into the conduction band [16]. Although the photogenerated charge carriers may disappear once the irradiation ceases, the application of an appropriate potential during irradiation could separate electrons from holes, leading to photoconductivity. In spite of their high absorption coefficient, typically in the range of 10^5-10^7 cm^{-1} [17] in most organic materials, the application of organic semiconductors in organic photovoltaic cells (OPVCs) faces the problem of the large exciton binding energy which prohibits efficient exciton dissociation. This can be overcome by making use of a photoinduced charge transfer between an electron donor and the fullerene C_{60} as an acceptor [18]. Due to the short exciton diffusion length of typically 10 nm [19], efficient OPVCs use the so-called bulk-heterojunction concept of mixing donor and acceptor in one single layer. In spite of the huge progress

Autor's signature

recently achieved, there are still challenges to achieve sufficient lifetime of OPVCs under ambient conditions or the availability of low-band gap materials to make better use of the solar spectrum [20]. Another method to increase the low intrinsic carrier density of conjugated polymer is the carrier injection from contacts that essentially governs device operation in organic light-emitting devices (OLEDs). This requires low energetic barriers at the metal-organic interfaces for both contacts to inject equally large quantities of electrons and holes, which is necessary for a balanced charge carrier flow. Thus the interface energetic structure plays a very crucial role for achieving efficient OLEDs [21]. Using a field-effect transistor (FET) geometry, charge carriers can be also injected into the band gap of conjugated polymers by applying an appropriate potential on the metal/insulator/polymer multilayer structure [22]. Just like photodoping, the charge-injection doping does not generate counter ions, allowing a systematic study of the electrical properties as a function of the charge carrier density with a minimized distortion of the material structure.

1.2.4 CHARGE CARRIERS TRANSPORT

Charge-transport process in conventional inorganic semiconductors is usually described using a band model, in which the highest energy occupied band is called the valence band (VB) and the lowest energy unoccupied band is called the conduction band (CB). Charge carriers can be produced by removing electrons from the valence band, by adding electrons into the conduction band, or by promoting electrons from the valence band to the conduction band to generate excitons that may then dissociate into free charge carriers under an applied electric field or by contacting with an electrode. Free charge carriers can then move in the highly delocalized states within the bands. The charge-transport process in the band model is mainly limited by phonons (lattice vibrations), which scatter the charge carriers. As the temperature T increases, the frequency of the lattice vibrations and the scattering of charge carriers by phonons are increased and thus the charge carrier mobility is decreased. Generally the band model is no longer applicable for materials with low charge carrier mobilities (usually $\mu \leq 1$ cm^2/Vs), including amorphous silicon and organic semiconductors. For disordered organic materials, intermolecular interactions are

Autor's signature

weak and are classified as Van der Waals forces. Such weak intermolecular interactions lead to the formation of discrete energy levels instead of energy bands. Thus, charge-transport process is considered as a *hopping* process of charge carriers between localized states. In such a hopping regime in low mobility materials, the charge carriers can reside on a molecule for a sufficiently long time such that localization of the charge carriers is accompanied by geometry relaxation of the molecules. In contrast to the phonon-limited charge-transport process in the band model, the charge carrier hopping process is a phonon assisted process and thus the charge carrier mobilities are usually increased with increasing temperatures. In addition, the hopping process of charge carriers in organic semiconductors is often complicated by the presence of traps. Traps are usually localized at lattice defects (vacant positions which should be otherwise occupied by molecules as in single crystalline materials), impurities and domain boundaries in the materials.

1.3 REFERENCES

[1] Heeger, A. J.: Semiconducting and Metallic Polymers: The Fourth Generation of Polymeric Materials (Nobel Lecture). Angew. Chem. Int. Ed. 40, 2591-2611 (2001)

[2] MacDiarmid, A. G.: Synthetic Metals: A Novel Role for Organic Polymers (Nobel Lecture). Angew. Chem. Int. Ed. 40, 2581-2590 (2001)

[3] Shirakawa, H.: The Discovery of Polyacetylene Film: The Dawning of an Era of Conducting Polymers (Nobel Lecture). Angew. Chem. Int. Ed. 40, 2574-2580 (2001)

[4] Burroughes, J. H., Bradley, D. D. C., Brown, A. R., Marks, R. N., Mackay, K., Friend, R. H., Burns, P. L., Holmes, A. B.: Light-emitting diodes based on conjugated polymers. Nature. 347, 539-541 (1990)

[5] Tang, C. W., VanSlyke, S. A.: Organic electroluminescent diodes. Appl. Phys. Lett. 51, 913-915 (1987)

[6] Tang, C. W.: Two-layer organic photovoltaic cell. Appl. Phys. Lett. 48, 183-185 (1986)

[7] Yu, G., Gao, J., Hummelen, J. C., Wudl, F., Heeger, A. J.: Polymer Photovoltaic Cells: Enhanced Efficiencies via a Network of Internal Donor-Acceptor Heterojunctions. Science. 270, 1789-1791 (1995)

[8] Drury, C. J., Mutsaers, C. M. J., Hart, C. M., Matters, M., Leeuw, D. M. d.: Low-cost all-polymer integrated circuits. Appl. Phys. Lett. 73, 108-110 (1998)

[9] Vidal, J.-C., Garcia-Ruiz, E., Castillo, J.-R.: Recent Advances in Electropolymerized Conducting Polymers in Amperometric Biosensors. Microchimica Acta. 143, 93-111 (2003)

[10] Peierls, R. E.: Quantum Theory of Solids. Oxford University Press, USA (1955)

[11] Samuel, I. D. W., Crystall, B., Rumbles, G., Burn, P. L., Holmes, A. B., Friend, R. H.: Time-resolved luminescence measurements in poly(p-phenylenevinylene). Synthetic Metals. 54, 281-288 (1993)

[12] Bredas, J. L., Street, G. B., Themans, B., Andre, J. M.: Organic polymers based on aromatic rings (polyparaphenylene, polypyrrole, polythiophene): Evolution of the electronic properties as a function of the torsion angle between adjacent rings. The Journal of Chemical Physics. 83, 1323-1329 (1985)

[13] Faïd, K., Leclerc, M.: Responsive Supramolecular Polythiophene Assemblies. Journal of the American Chemical Society. 120, 5274-5278 (1998)

[14] Kim, J., Swager, T. M.: Control of conformational and interpolymer effects in conjugated polymers. Nature. 411, 1030-1034 (2001)

[15] Langeveld-Voss, B. M. W., Janssen, R. A. J., Meijer, E. W.: On the origin of optical activity in polythiophenes. Journal of Molecular Structure. 521, 285-301 (2000)

[16] Heeger, A. J., Kivelson, S., Schrieffer, J. R., Su, W. P.: Solitons in conducting polymers. Rev. Mod. Phys. 60, 781 (1988)

[17] Skotheim, T. A., Reynolds, J. R.: Conjugated Polymers: Processing and Applications CRC Press Taylor & Francis Group, USA (2006)

[18] Sariciftci, N. S., Smilowitz, L., Heeger, A. J., Wudl, F.: Photoinduced Electron Transfer from a Conducting Polymer to Buckminsterfullerene. Science. 258, 1474-1476 (1992)

[19] Nunzi, J. M.: Organic photovoltaic materials and devices. C. R. Physique. 3, 523-542 (2002)

Autor's signature

[20] Sun, S.-S., Sariciftci, N. S.: Organic photovoltaics: mechanism, materials, and devices. CRC Press, Boca Raton, Florida (2005)

[21] Salaneck, R. W., Seki, K., Kahn, A., Pireaux, J.-J.: Conjugated polymer and molecular interfaces: science and technology for photonic and optoelectronic applications. Marcel Dekker, Inc., (2002)

[22] Garnier, F., Hajlaoui, R., Yassar, A., Srivastava, P.: All-Polymer Field-Effect Transistor Realized by Printing Techniques. Science. 265, 1684-1686 (1994)

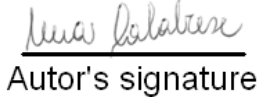

Autor's signature

2 ORGANIC SOLAR CELLS

2.1 INTRODUCTION

Solar cell manufacturing based on the technology of crystalline silicon devices is growing by approximately 40 % per year and this growth is increasing. This has been realized mainly by special market implementation programs and government grants encouraging the consumers to install photovoltaic devices at suitable, sunny places. However at the current status, photovoltaics hardly contribute to the energy market, because it is far too expensive. The great manufacturing costs for silicon solar cells originate from the energy intensive production of highly pure silicon are one of the major drawbacks for a large scale distribution. To ensure a sustainable technology path for photovoltaics, efforts to reduce the cost of the current silicon technology are needed while at the same time new solar cell technologies have to be placed in the consumer market. In the field of inorganic photovoltaics, thin-film technologies based on cheaper production processes are currently under investigation. Other approaches to cheaper solar cells are based on dye-sensitized nanocrystalline titanium dioxide which has been discovered by Grätzel *et al*. in 1990. Another interesting alternative to inorganic cells is given by the semiconducting polymers, which combine the opto-electronic properties of conventional semiconductors with the excellent mechanical and processing properties of polymeric i.e. plastic materials. These can be processed from solution at room-temperature onto e.g. flexible substrates using simple and therefore cheaper deposition methods like spin or blade coating. Compared with the established solar cell technologies, solar cells made of organic semiconductors offer many promising possibilities. The greatest potential of organic solar cells lies in the prognosis of low production costs and mechanical flexibility. Both characteristics open up a fully new range of possible solar cell applications. At present, basic research work is necessary in order to create the prerequisites required for a commercialization of organic

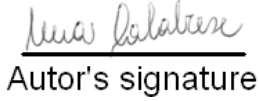

solar cells. The most important factors for the implementation and the dissemination of solar cells are manufacturing costs, efficiency and long term stability. Here a brief introduction and overview is given of the field of organic solar cells with particular reference to polymer solar cells.

2.2 BRIEF HISTORY

The first organic solar cells were based on an active layer made of a single material sandwiched between two electrodes of different work functions. By the absorption of light, strongly Coulomb-bound electron-hole pairs are created, so-called *singlet excitons*, with a binding energy of about 0.4 - 0.5 eV [1]. The excitons need to be separated to finally generate a photocurrent. In order to overcome the exciton binding energy, one has either to rely on the thermal energy, or dissociate the exciton at the contacts. Unfortunately, both processes have a rather low efficiency: under the operating conditions of solar cells, the temperature is not high enough, and the sample thickness is higher than the exciton diffusion length. The consequence is that not all excitons are dissociated, and may hence recombine radiatively by photoluminescence. Consequently, the single layer organic solar cells had power conversion efficiencies far below 1%. A major breakthrough was realized by C. W. Tang in the mid eighties [2], who introduced a double-layer structure of two organic semiconductors with different electron affinity. The introduction of a second organic semiconductor layer was a quantum leap in terms of power conversion efficiency though still on a low level. The light is usually absorbed in the so-called donor material, a hole conducting small molecule such as copper phthalocyanine. In bilayer devices, the photogenerated singlet excitons could diffuse within the donor towards the planar interface to the second material, the acceptor, which is usually chosen to be strongly electronegative. The acceptor material provides the energy needed for the singlet exciton to be separated, as the electron can go to a state of much lower energy within the acceptor. This charge transfer dissociates the exciton, the electron moving to the acceptor material, whereas the hole remains on the donor. A prominent example for an electron acceptor material is the buckminsterfullerene (C_{60}) [3]. The difference between the electron energy on the donor

Autor's signature

and the corresponding acceptor level has to be larger than the exciton binding energy, in order to initiate a charge transfer from donor to acceptor material. If the exciton reaches this donor-acceptor hetero-interface by diffusion, it is energetically favorable for the electron to be transferred to the acceptor molecule. This charge transfer, or electron transfer, is reported to be very fast. Indeed, it was found to be faster than 100 fs in polymer-fullerene systems, and very efficient, as the alternative loss mechanisms are much slower [4]. Thus, the exciton is dissociated and the resulting charge carriers are spatially separated. Even though the electron and the hole now reside on two separate materials, they are still Coulomb bound due to the weak screening of the electric field in organic semiconductors. Therefore, a further step is needed for the final charge pair dissociation, for instance initiated by an electric field or the energetic disorder of the organic semiconductors. Thus, the mutual Coulomb attraction is overcome. This dependence becomes evident in the strongly field and temperature dependent photocurrent of organic solar cells, which also influences fill factor and short circuit current: only if this charge carrier separation is successful, can electron and hole hop towards their respective contacts, in order to generate a photocurrent. The organic bilayer solar cells invented by C. W. Tang were made of two conjugated small molecules, and achieved a power conversion efficiency of about 1 % [2]. The limiting factor in this concept is that for a full absorption of the incident light, a layer thickness of the absorbing material has to be of the order of the absorption length. This is much more than the diffusion length of the excitons [5] so the potential of the bilayer solar cell is difficult to exploit. In the early nineties, a novel concept was introduced, accounting for the low exciton diffusion length in disordered organic semiconductors, as well as the required thickness for a sufficient light absorption: the so-called *bulk heterojunction solar cell* [6]. This approach features a distributed junction between donor and acceptor material: both components interpenetrate one another, so that the interface between them is not planar any more, but spatially distributed. This concept is implemented by spin coating a polymer-fullerene blend, or by co-evaporation of conjugated small molecules. Bulk heterojunctions have the advantage of being able to dissociate excitons very efficiently over the whole extent of the solar cell, and thus generating electron-hole pairs throughout in the film. The disadvantages are that it is somewhat more difficult to separate these still strongly Coulomb bound charge carrier pairs due to the increased disorder, and that percolation to the contacts is not always given

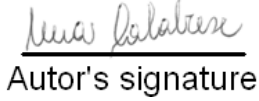

in the disordered material mixtures. Also, it is more likely that trapped charge carriers recombine with mobile ones. However, the positive effects on the device performance exceed the drawbacks. For an efficient bulk heterojunction solar cell, a good control of the morphology is very important. Rather simple methods of optimization have been successfully performed in the last decade. The choice of solvents [7] as well as the annealing of the solution processed polymer-fullerene solar cells [8] both lead to a more favorable inward structure in view of the dissociation of bound electron-hole pairs and the subsequent charge transport. Thus, the power conversion efficiency was increased many fold, in case of the annealing from a bare half percent to above 3 %. Indeed, optimization by novel routes is an ongoing process, and within the last five years, further steps in improving the power conversion efficiency have been made. Co-evaporated copper phthalocyanine/fullerene solar cells have reached 5.0 % efficiency using a concept called planar-mixed heterojunction [9], and solution processed polythiophene-fullerene cells achieved between 6 and 8% efficiency by the use of novel materials as well as additives optimizing the phase separation [10].

2.3 OPERATING PRINCIPLES

Photovoltaic cell configurations based on organic materials differ from those based on inorganic semiconductors due to the fact that the physical properties of inorganic and organic semiconductors are significantly different. Inorganic semiconductors generally have a high dielectric constant and a low exciton binding energy. Hence, the thermal energy at room temperature is sufficient to dissociate the excitons created by absorption of photons into a positive and negative charge carriers. The formed electrons and holes are easily transported as a result of the high mobility of the charge carriers and the internal field of the p-n junction. Organic materials have a lower dielectric constant and the exciton binding energy is larger than for inorganic semiconductors, hence dissociation into free charge carriers does not occur at room temperature. To overcome this problem, organic solar cells commonly utilize two different materials that differ in electron donating and accepting properties. These are called Donor (D) and Acceptor (A) materials respectively.

Charges are created by photoinduced electron transfer between the two components. This photoinduced electron transfer between donor and acceptor boosts the photogeneration of free charge carriers compared to the individual, pure materials, in which the formation of bound electron-hole pairs, or excitons is generally favored. Various architectures for organic solar cells have been investigated in recent years. The Figure 2.1 illustrates the physic processes involved in transformation of solar energy into electricity in organic photovoltaic device. This scheme, despite its limitations, is generally accepted to explain the mechanism operating in an organic solar cell [11]. In general, for a successful organic photovoltaic cell, five important processes have to be optimized to obtain a high conversion efficiency of solar energy into electrical energy.

1. *Photons absorption and generation of excitons*: light causes the promotion of electrons from the highest occupied molecular orbital (HOMO), analogous to valence band in the inorganic semiconductors, to the lowest unoccupied molecular orbital (LUMO), analogous to the conduction band in the inorganic semiconductors, of the donor material. The processes can also occur in an analogous manner in the case of an excited acceptor, and the details of these mechanistic steps have been described extensively in the literature but is not object of this work. This results in an excited but neutral state with a limited, finite lifetime; this state is termed *exciton* and consists of an electron and a hole paired by an energy E_{ex} that is smaller than the energy gap between the limits of the permitted bands (difference between LUMO and HOMO orbital of donor material). If E_g is the energy gap, then ($E_g - E_{ex}$) is the exciton binding energy (around 0.4 - 0.5 eV in conjugated polymer [1]) indicated with E_B. The amount of absorbed photons depends on the value of the optical absorption coefficient and on the thickness of the donor material.
2. *Excitons diffusion*: these quasi-particles diffuse within the material as long as recombination processes (of the hole-electron pair that forms/constitutes the excitons) do not take place.
3. *Hole-electron separation (excitons dissociation)*: if the offsets of the energy levels of the Donor and the Acceptor materials are higher than the exciton binding energy, excitons dissociate at the D/A interface. More precisely, the condition that must be fulfilled is $E_{ex} > IP - \chi$, where E_{ex} is the exciton energy, IP is the ionization energy

Autor's signature

of the acceptor, and χ is the electronic affinity of the acceptor [12]. Excitons photogenerated in the donor side will dissociate by transferring the electron to the LUMO level of the acceptor and retaining the positive charge, while those created in the other phase/component will transfer the hole to the HOMO of the donor while retaining the negative charge. This step leads to the formation of free charge carriers.

4. *Carrier transport towards the electrodes*: this transport involves the classic mechanism for hopping processes in organic materials.
5. *Charge collection at the respective electrodes*: for this to occur most efficiently, the following conditions (opposite to the injection conditions for OLEDs) must be met: E_F cathode < E_{LUMO} acceptor and E_F anode > E_{HOMO} donor.

Each of the above listed steps can be affected by several phenomena that decrease the efficiency of the global process, so that only a limited portion of the photons reaching the cell are able to generate useful charge carriers. Thus, the optimization of each step is extremely important to extract as much energy as possible from the device. This optimization encompasses the development of improved approaches in the design of materials and device structures.

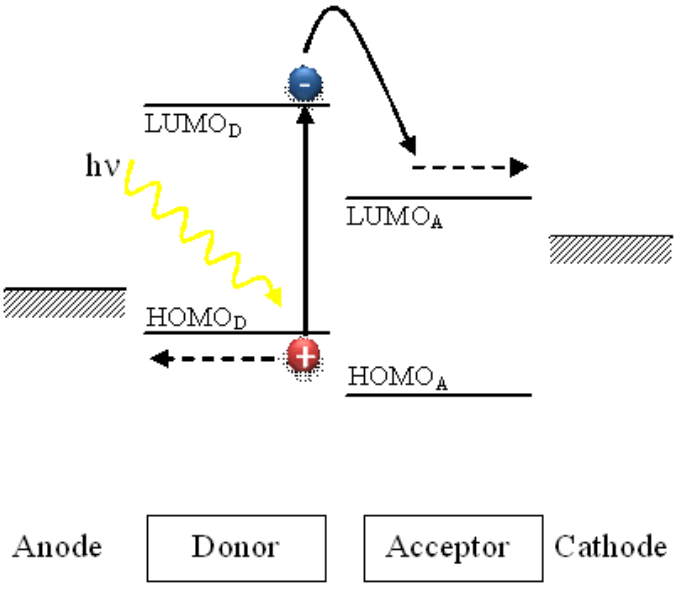

Figure 2.1 General mechanism for photoenergy conversion in organic solar cells.

Autor's signature

2.4 DEVICE PHYSICS

In this section, the function of an organic solar cell will be described in more detail as compared to the preview introduction, including loss mechanisms and other limitations. The section is ordered according to the different steps from photon absorption to photocurrent generation, as described above for a bulk heterojunction solar cell.

2.4.1 PHOTON ABSORPTION AND EXCITON GENERATION

A basic requirement in an organic photovoltaic cell is that the materials optical excitation energy gap (optical gap) should be equal or close to the incident photon energy. In most amorphous organic materials where electronic band structures are difficult to form, this gap is the energy gap between the Highest Occupied Molecular Orbital (HOMO) and the Lowest Unoccupied Molecular Orbital (LUMO), both are also called frontier orbitals. In organic conjugated system, HOMO is typically an occupied π bonding orbital, and LUMO is typically an unoccupied π^* anti-bonding orbital. Since an organic HOMO/LUMO excitation basically generates a tightly bound exciton instead of a free electron and hole, optical energy gap is therefore used instead of the conventional electronic energy gap that typically refers to the energy gap between the free holes at valence band (VB) and the free electrons at conduction band (CB) in inorganic semiconducting materials. In organics, the relationship between optical gap (Eg_{opt}) and electronic gap (Eg_e) may be approximated as:

$$Eg_e = Eg_{opt} + E_B \quad (1)$$

where E_B is called exciton binding energy that represents a minimum energy needed to separate an intra-molecular exciton into an inter-molecular radical ion pair [13]. Eg_{opt} values can be estimated directly from optical absorption band edge, and absolute Eg_e values may be estimated by electrochemical Redox analysis. Absolute HOMO/LUMO levels are typically estimated from a referenced half electrochemical analysis in

Autor's signature

combination with the optical absorption spectroscopy. Solar light radiation span a wide range with largest photo-flux between 600–1000nm (1.3–2.0 eV, on surface of the earth or 1.5 Air Mass) or 400–700 nm (1.8–3.0 eV, in space or Air Mass 0). So, for terrestrial applications, it is desirable that the energy gap of the donor material span a range from 1.3 to 2.0 eV. This may be achieved by incorporating a series of different energy gaped donor/acceptor or organic dyes that absorb light in that radiation range. However, while the solar photon loss can be minimized in this way, due to energy transfer processes where all high energy excitons will eventually become lowest energy excitons, the open circuit voltage (*V*oc) of the cell will also be reduced accordingly. Indeed, experimental studies have revealed certain correlations of *V*oc versus the gap of lowest acceptor LUMO and highest donor HOMO levels [14]. Actually, several widely used conjugated semiconducting polymers used in organic solar cell studies have optical gaps higher than 2.0 eV, well above the maximum solar photon flux range. This photon loss problem is in fact very common in almost all currently reported organic photovoltaic materials and devices. However, one advantage of organic materials is the versatility and flexibility of its energy levels being fine tuned via molecular design and synthesis, therefore, ample room exists for improvement.

2.4.2 EXCITON DIFFUSION

Once an organic exciton is photogenerated, it typically diffuses (e.g., via intra-chain or inter-chain energy transfer processes) to a remote site, and at the same time it quickly decays radiatively or non-radiatively to its ground state, having usually pico to nano seconds lifetime. Alternatively, in solid state, some excitons may be trapped in certain defect or impurity sites. Both exciton decay and trap contribute to the exciton loss. For most conjugated organic materials the average distance an organic exciton can travel within its lifetime is typically in the range of 5-10 nm [5, 15]. Since the desired first step of photovoltaic process is that each photogenerated exciton will be able to reach the donor/acceptor interface where charge separation can occur, one way to minimize the exciton loss would be to make a defect-free, a donor/acceptor phase separated and ordered

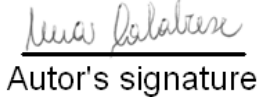

material. This could be obtained by a bulk hetero-junction structure. This type of solar cells are desirable, as they not only minimize the exciton loss by increasing the donor/acceptor interface, they can also offer enough thickness for effective photon harvesting.

2.4.3 EXCITON SEPARATION AND CHARGE CARRIER GENERATION

As discussed, the exciton binding energy is much larger than the thermal energy in organic semiconductors. Thus, in view of photovoltaic current generation, a driving force is needed to dissociate them. As already outlined in the previous section, its lack is the reason why single layer organic solar cells doesn't work efficiently. A second organic semiconductor, the electronegative acceptor, has to be introduced either in a bilayer or bulk heterojunction device configuration in order to yield an efficient exciton dissociation. The class of materials with the currently best acceptor properties are the (buckminster)fullerenes, C_{60} and its derivatives. Polymer acceptors and non-fullerene small molecule acceptors have shown a less efficient excitons separation of charges up to now, which seems to be due to the LUMO not being electronegative enough for efficient electron accepting properties and too low electron mobilities [16].

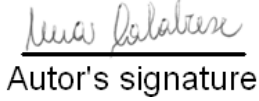

2.4.4 CARRIER DIFFUSION TO THE ELECTRODES

Once the carriers (free electrons or holes) are generated, holes need to diffuse toward the positive large work function electrode, and electrons need to diffuse toward the negative small work function electrode. The driving forces for the carrier diffusion may include the field created by the work function difference between the two electrodes, as well as a chemical potential driving force [17]. Mid-gap state species, such as impurities and defects, or intentionally doping redox species, can also facilitate the charged carrier generation and diffusion by providing splitting interfaces and hopping orbitals. However, right after electron-hole pair is separated at the interface, it can also recombine due to both the potential drop between the acceptor LUMO and donor HOMO, and the Coulomb force between the electron and the hole. Fortunately, the charge recombination rates in most cases are much slower than the charge separation rates (e.g., charge *recombination* rates are typically micro to milliseconds compared to femto/pico seconds charge *separation* rate) [18], so there is an opportunity (in the time domain) for the carriers to reach the electrodes before they recombine. In most currently reported organic solar cells, however, the diffusion of electrons and holes to their respective electrodes are not really smooth due to materials poor morphology. On this point of view the bulk heterojunction solar cell can be considered disadvantageous. If donor and acceptor phases are perfectly bicontinuous between the two electrodes, and all LUMO and HOMO orbitals are nicely aligned and overlapped to each other in both donor and acceptor phases, like in a molecularly self-assembled thin films or crystals, then the carriers should be able to diffuse smoothly in bands toward their respective electrodes. Currently, carrier thermal hopping and tunneling are believed to be the dominant diffusion and conductivity mechanism for most reported organic photovoltaic systems, therefore, the carrier loss is believed to be another key factor for the low efficiency of organic photovoltaic materials and devices.

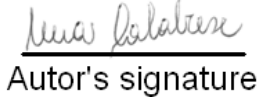

2.4.5 CHARGE-CARRIERS COLLECTION AT THE ELECTRODES

It has been proposed [6] that when the acceptor LUMO level matches the Fermi level of the small work function electrode, and the donor HOMO matches the Fermi level of the large work function electrode, an ideal ohmic contact would be established for efficient carrier collection at the electrodes. So far, there are no organic photovoltaic cells have achieved this desired ohmic contacts due to the availability and limitations of materials and electrodes involved. There were a number of studies, however, focusing on the open circuit voltage (*V*oc) dependence on materials LUMO/HOMO level changes, electrode Fermi levels, and chemical potential gradients [14, 19]. The carrier collection mechanisms at electrodes are relatively less studied and are not yet well understood. It is believed that the carrier collection loss at the electrodes is also a critical contributing factor for the low efficiency of the up to date reported organic solar cells. Buffer materials as interlayers between the active layer and the electrodes have been widely used in the literature to improve the contact characteristics [20].

2.5 DEVICE ARCHITECTURE

The photoactive layer - the heart of the cell - can be a single chemical species (*single layer*) or a pair of electron donor (D) and electron acceptor (A); the latter situation is more efficient. In the case of the two components system, the architecture of the cell can be a double layer of materials (*bilayer heterojunction*), a double layer with a diffuse interface, a mixture in which the two phases form a dispersion at nanometric level to form a high contact area (*dispersed heterojunction*, *bulk heterojunction*) or a double layer in which donor and acceptor materials are oriented, such that charges are transported directly through conducting pathways which are perpendicular to the electrodes (*ordered heterojunction*). In this paragraph a short overview on the architecture of organic solar cells is given, with particular attention on the bulk heterojunction solar cells, object of this work.

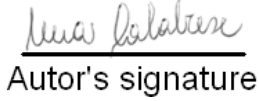

2.5.1 SINGLE LAYER DEVICES

Single layer structures consist of one semiconductor material sandwiched between two electrodes, one of them gives an ohmic contact (Transparent Oxide Conductive, TCO, in the case of *p*-type organic) and the other one gives a rectifying contact Figure 2.2. These cells are often referred to as *Schottky* type devices or *Schottky diodes* since charge separation occurs at the rectifying (Schottky) junction with the rectifying contact. The structure is simple but absorption covering the entire visible range is rare using a single type of molecule. Furthermore, the photoactive region (near the rectifying contact) is often very thin and since both positive and negative photoexcited charges travel through the same material recombination losses are generally high. Such cells have small efficiency and are used only to study specific device properties such as current densities regimes by I-V characteristics. In 1986, a major breakthrough was realized by Tang, who introduced a bilayer structure of a *p*- and *n*-type organic semiconductor [2]. The photoactive material was placed between two dissimilar electrodes, indium tin oxide (ITO) for collection of the positive charges and silver to collect the negative charges. A power conversion efficiency of about 1% was achieved under simulated AM2 illumination (691 W/m^2). An important aspect found in this concept is that the charge generation efficiency is relatively independent of the bias voltage.

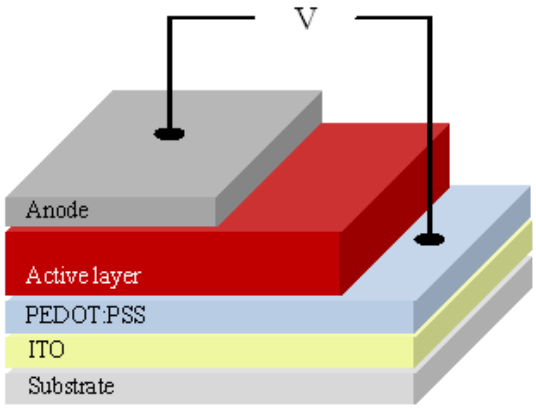

Figure 2.2 Schematic diagram of a single layer device.

Autor's signature

2.5.2 BILAYER HETEROJUNCTION DEVICES

In a bilayer heterojunction device, p-type and n-type semiconductors (Donor and Acceptor) are sequentially stacked together with a planar interface. The bilayer is sandwiched between two electrodes matching the donor HOMO and the acceptor LUMO, for efficient extraction of the corresponding charge carriers. The bilayer device structure is schematically depicted in Figure 2.3. In this structure the photoexcitations in the photoactive material have to reach the p-n interface where charge transfer can occur, before the excitation energy of the molecule is lost via intrinsic radiative and non-radiative decay processes to the ground state. Because the exciton diffusion length of the organic material is in general limited to 5-10 nm in polymeric materials [5] only absorption of light within a very thin layer around the interface contributes to the photovoltaic effect. This limits the performance of bilayer devices, because such thin layer cannot absorbs all the light. A strategy to improve the efficiency of the double-layer cell is related to structural organization of the organic material to extend the exciton diffusion length and, therefore, create a thicker photoactive interfacial area.

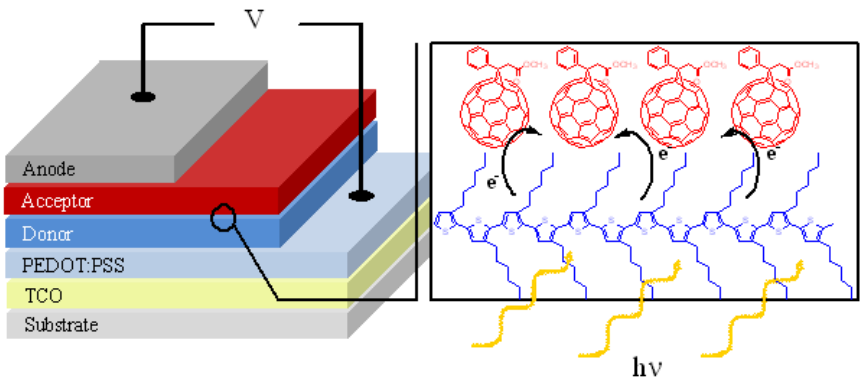

Figure 2.3 Schematic diagram of a bilayer heterojunction and subsequent photoinduced electron transfer at the interface of the two layers (P3HT/PCBM as an example).

Autor's signature

2.5.3 BULK HETEROJUNCTION DEVICES

When combining electron donating (*p*-type) and electron accepting (*n*-type) materials in the active layer of a solar cell, it must be considered that excitons created in either material can diffuse to the interface, to enable charge separation. Due to their short lifetime and low mobility, the diffusion length of excitons in organic semiconductors is limited to about 5-10 nm only [5, 15]. This imposes an important condition to efficient charge generation. Anywhere in the active layer, the distance to the interface should be on the order of the exciton diffusion length. Despite their high absorption coefficients, exceeding 10^5 cm^{-1} [21], a 20 nm bilayer of donor and acceptor materials would not be optical dense, allowing most photons to pass freely. The solution to this problem was solved by simply mixing the *p*- and *n*-type materials and relying on the intrinsic tendency of polymeric materials to give phase separation on a nanometer dimension, junctions throughout the bulk of the material are created that ensure quantitative dissociation of photogenerated excitons, irrespective of the thickness. Polymer-fullerene solar cells were among the first to utilize this bulk heterojunction (BHJ) principle [6]. Nevertheless, this attractive solution poses a new challenge. Photogenerated charges must be able to migrate to the collecting electrodes through this intimately mixed blend. Because holes are transported by the *p*-type semiconductor and electrons by the *n*-type material, these materials should be preferably mixed into a bicontinuous, interpenetrating network in which inclusions barrier layers are avoided. In Figure 2.4, a schematic for a bulk heterojunction device is shown.

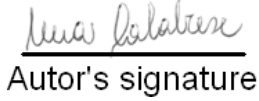

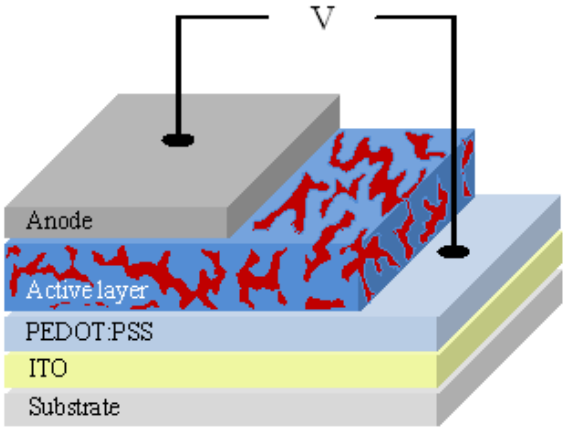

Figure 2.4 Schematic of a bulk heterojunction device. The donor (D) is blended with the acceptor (A) throughout the whole film.

BHJ is similar to the bilayer device with respect to the D-A concept, but it exhibits a largely increased interfacial area where charge separation occurs. While in the bilayer heterojunction the donor and acceptor phases are completely separated from each other and can selectively contact the anode and cathode, respectively, in the bulk heterojunction both phases are intimately intermixed. This mixture has a priori no symmetry breaking in the volume. There is no preferred direction for the internal fields of separated charges; that is, the electrons and holes created within the volume have no net resulting direction they should move [22]. Therefore, a symmetry breaking condition (like using different work-function electrodes) is essential in bulk heterojunctions. Otherwise, only concentration gradient (diffusion) can act as driving force. The different steps from photon absorption to photocurrent generation, are shown in Figure 2.5 from a kinetic and an energetic perspective. Microphase separated polymer bulk heterojunctions can be achieved with various combinations of donor and acceptor materials such as a semiconducting polymer as a donor and a fullerene, C_{60} derivative as acceptor or by mixing hole and an electron conducting polymers, because polymer blends tend to phase separate due to their low entropy of mixing. The obtained morphology of such blends is a crucial parameter and strongly depends on the processing conditions such as solvent and temperature.

Autor's signature

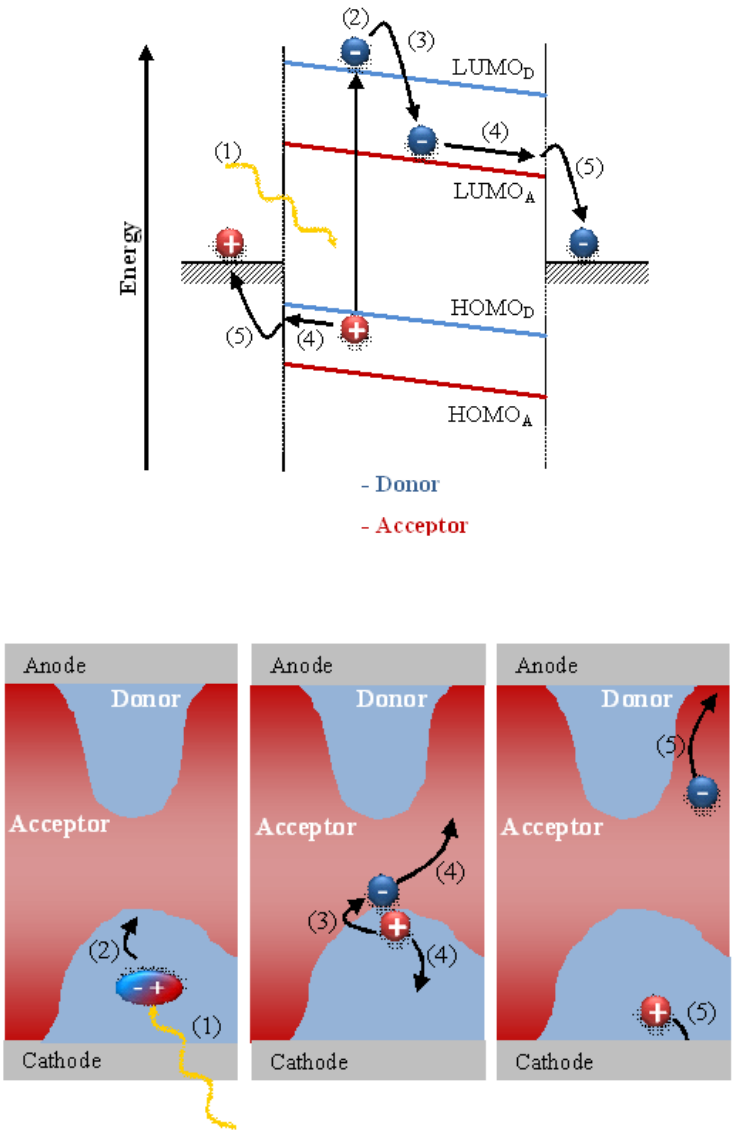

Figure 2.5 From light absorption to photocurrent in a BHJ solar cell. Up: simplified energy diagram (1) singlet exciton generation from an absorbed photon in the donor material, (2) exciton diffusion to the acceptor interface, (3) exciton dissociation by electron transfer to the electronegative acceptor molecules, (4) charge transport of electron resp. hole by hopping between localized states, (5) extraction of the charges: photocurrent. Down: from a kinetic point of view.

2.6 CHARACTERIZATION OF A SOLAR CELL DEVICE

The current-voltage characteristics of a solar cell in the dark and under illumination are shown in Figure 2.6. In the dark, there is almost no current flowing, until the contacts start to inject at forward bias for voltages larger than the open circuit voltage. In the fourth

Autor's signature

quadrant, the device generates power under light. At maximum power point (MPP), the product of current and voltage is the largest. The power conversion efficiency of a solar cell is determined by the following formula:

$$\eta_{eff} = \frac{P_{out}}{P_{in}} = \frac{V_{oc} J_{sc} FF}{P_{in}} \tag{2}$$

The following parameters are defined in this equation (2): open circuit voltage (V_{oc}) in V, as the bias voltage at which no net current flows, short circuit current density (J_{sc}) in mA/cm^2, as the current that flows at short circuit conditions, fill factor (FF), and P_{in} as the incident light power in mW/cm^2. This light intensity is standardized at 100 mW/cm^2 with a spectral intensity distribution matching that of the sun on the earth's surface at an incident angle of 48.2° which is called the AM 1.5G spectrum. The fill factor itself is defined as follows:

$$FF = \frac{V_{MPP} J_{MPP}}{V_{oc} J_{sc}} \tag{3}$$

The maximum power point (MPP) is the point on the current voltage curve at which the product of current and voltage, which is the power output, is at its maximum value (Figure 2.6). The corresponding voltage and current values are equal to V_{MPP} and J_{MPP}.

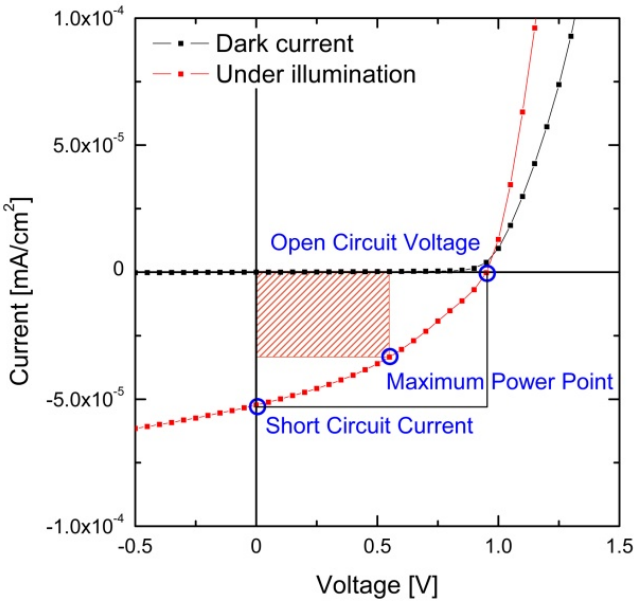

Figure 2.6 Schematic diagram of I-V characteristics of a photovoltaic cell in the dark (dark) and under illumination (red) in which are represented *V*oc, *J*sc, the maximum power point, and the fill factor which can be regarded as the ratio of the colored rectangle and larger uncolored rectangle.

2.7 CRITICAL PARAMETERS FOR SOLAR CELL EFFICIENCY

2.7.1 OPEN CIRCUIT VOLTAGE

In organic solar cells, the open circuit voltage is found to be function of the highest occupied molecular orbital HOMO level of the donor (p-type semiconductor quasi Fermi level) and lowest unoccupied molecular orbital LUMO level of the acceptor (n-type semiconductor quasi Fermi level) according with the following equation/law [23]:

$$V_{oc} = \frac{HOMO(D) - LUMO(A)}{q} - \frac{KT}{q}\ln\left[\frac{(1-P)\gamma N_c^2}{PG_M}\right] \quad (4)$$

where q is the elementary charge, P is the dissociation probability of a bound electron-hole pair into free charge carriers, G_M is the generation rate of the bound electron-hole pairs, γ is

Autor's signature

the Langevin recombination constant, N_c is the effective density of states, K is the Boltzmann constant, and T is the temperature. However, this relation is only valid when the electrodes form ohmic contacts with the HOMO of the donor and the LUMO of the acceptor. If this is not the case the Voc will be limited to the difference in the work function of the electrodes, which is generally lower. This is often observed when aluminum is used as cathode without a lithium fluoride (LiF) or other low work function interlayer, reducing the voltage significantly. On the other hand an ill-defined cathode interface can give rise to a distinct S shape of the I-V curve at open circuit conditions resulting in a relatively high voltage which is, however, always accompanied by low fill factors and should thus be avoided. A low amount of photogenerated charges as well as a recombination with charge traps will result in a lower Voc as can be seen from equation (4). Open circuit voltage is also affected by the nanomorphology of the active layer in the polymer fullerene bulk heterojunction solar cells.

2.7.2 SHORT CIRCUIT CURRENT

In the ideal, loss free contacts, the short circuit current, I_{sc}, is determined by the product of the photoinduced charge carrier density and the charge carrier mobility within the organic semiconductors [24]:

$$I_{sc} = ne\mu E \tag{5}$$

where n is the density of charge carriers, e is the elementary charge, μ is the mobility, and E is the electric field. Assuming the 100% efficiency for the photoinduced charge generation in a bulk heterojunction mixture, n is the number of absorbed photons per unit volume.

The current generated by a solar cell is hence governed by the amount of absorbed photons. Because of the low exciton diffusion coefficients in the donors [5] a bulk heterojunction is employed to harvest all the excitons. The domain size of donor and

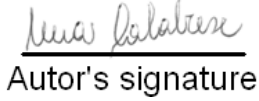

acceptor phases thus plays a very important role in the actual short-circuit current measured in a device. In fact, the control of this morphology is the most difficult and most investigated part of the solar cell fabrication. Typically a large range of solvents, polymer: fullerene ratios, annealing effects and additives are required to induce the correct morphology. When domain sizes are too large, excitons will be lost due to the decay process. Photophysical studies can be employed to see whether all excitons are able to reach an interface. However, too small domain sizes can induce an enhanced recombination of the charge carriers. Moreover, the donor and acceptor domains need to have a percolated pathway towards anode and cathode, respectively, to allow charge collection. Even when all of the generated excitons reach an interface, this does not automatically imply that all charges are actually converted into free charge carriers. Due to the low dielectric constant of the polymer and fullerene, the electron and hole are coulombically bound at the interface and need to be dissociated into free carriers by an electric field. Plotting the photocurrent as a function of the effective field can be useful to determine the dissociation efficiency of a device.

2.7.3 FILL FACTOR

The fill factor is the most sensitive parameter in a solar cell compared to the open circuit voltage (V_{oc}) and the short circuit current density (J_{sc}). It depends in a complicated way on the charge dissociation, the charge carrier transport, the recombination processes, the thickness of the active layer and on the morphology of the cathode/polymer interface. A good hole transport capability is of vital importance for proper device operation. Charge carrier photogeneration is preceded by the dissociation of exciton at the D/A interface. Once the exciton is dissociated, the charge collection efficiency does not approach 100% under short-circuit condition [25] since, the polaron pair (with hole on the D-chain and electron on the A-chain) created after dissociation is still bound by mutual coulombic interaction and this charge-transfer exciton has finite lifetime. The formation of free electron and hole pair is highly field and temperature-dependent process which is reflected in the reverse bias photocurrent (J_{ph}) behavior. In P3HT:PCBM devices where a good FF

Autor's signature

(45%) has been observed, the J_{ph} essentially saturates at high reverse bias indicating the fact that almost all the photogenerated free charge carriers are extracted from the device. However, in most of these systems J_{ph} in the reverse bias shows mild field dependence. A strong field dependence of J_{ph} reduces the FF significantly. Since near V_{oc} the effective field in the device is low, a strong field-dependent exciton dissociation rate changes the curvature of the *J-V* response and it tends to become concave. Besides the field-dependent exciton dissociation rate, unbalanced transport of charge carriers can also play a major role. In case of perfect ohmic contacts (non-injecting in the reverse bias mode), the behavior of the illuminated *J-V* response depends on the drift length of the electrons (e) and holes (h) and the ratio (*b*) of their drift lengths, reported in (6) and (7) equation respectively, where μ is the mobility, τ is the lifetime of the charge carriers and *E* is the field across the device:

$$L_D = \mu\tau E \tag{6}$$

$$b = \frac{\mu_e \tau_e}{\mu_h \tau_h} \tag{7}$$

For balanced transport (*b*~1), J_{ph} varies linearly with *V* at lower voltage regime and at higher voltage it saturates to a value reported in the equation (8), where *q* is the charge, *G* is the generation rate, *E* is the electric field, *T* is the temperature and d is the active-polymer layer thickness:

$$J_{ph} = qG(E,T)d \tag{8}$$

In case of unbalanced transport (*b*<1 or *b*>1) carrier accumulation takes place near both the contacts modifying the field and in absence of any recombination the thickness of the accumulation region(s) is governed by the smaller μτ. This process is also known as μτ-limited process. When hole and electron transport are strongly unbalanced (*b*<<1 or *b*>>1) the slower charge carrier will accumulate near one of the electrode to a greater extent leading to build up of an internal field. When the field in this region becomes equal to the

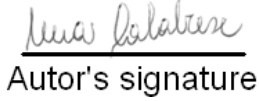

external applied voltage (V), the current becomes space charge limited (SCL). Under SCL condition J_{ph} follow the relation:

$$J_{ph} = qG\left[\left(\mu\tau\right)_{slow\ carrier}\right]^{0.5} V^{0.5} \tag{9}$$

In this condition a build up of space charge results in a square root dependence of the photocurrent on voltage, resulting in low fill factors [26]. Even a difference in hole and electron mobility of only one order of magnitude can influence the device performance, imposing limitations on the active layer thickness in order to avoid space charge problems [27]. The thickness d also determines the slope ($=\mu\tau/d^2$) of the J-V curve (in the range $V_{sat}<V_{oc}<V_{sat}$, V_{sat} is the saturation voltage at which J_{ph} switches from linear to saturation regime). A steeper slope moves V_{sat} closer to V_{oc} and hence increase the FF. The electrode active-layer interface also plays an important role; the deposition conditions of cathode lead to a variety of physical and chemical defect features which can be dangerous and can be decrease the FF [28].

2.8 REFERENCES

[1] Arkhipov, V. I., Bässler, H.: Exciton dissociation and charge photogeneration in pristine and doped conjugated polymers. Phys. Status Solidi A. 201, 1152-1187 (2004)

[2] Tang, C. W.: Two-layer organic photovoltaic cell. Appl. Phys. Lett. 48, 183-185 (1986)

[3] Smalley, R. E.: Discovering the fullerenes. Rev. Mod. Phys. . 69, 723-730 (1997)

[4] Sariciftci, N. S., Smilowitz, L., Heeger, A. J., Wudl, F.: Photoinduced Electron Transfer from a Conducting Polymer to Buckminsterfullerene. Science. 258, 1474-1476 (1992)

[5] Nunzi, J. M.: Organic photovoltaic materials and devices. C. R. Physique. 3, 523-542 (2002)

[6] Yu, G., Gao, J., Hummelen, J. C., Wudl, F., Heeger, A. J.: Polymer Photovoltaic Cells: Enhanced Efficiencies via a Network of Internal Donor-Acceptor Heterojunctions. Science. 270, 1789-1791 (1995)

[7] Shaheen, S. E., Brabec, C. J., Sariciftci, N. S., Padinger, F., Fromherz, T., Hummelen, J. C.: 2.5% efficient organic plastic solar cells. Appl. Phys. Lett. 78, 841-843 (2001)

[8] Padinger, F., Rittberger, R. S., Sariciftci, N. S.: Effects of postproduction treatment on plastic solar cells. Adv. Funct. Mater. 13, 85-88 (2003)

[9] Xue, J. G., Rand, B. P., Uchida, S., Forrest, S. R.: Mixed donor-acceptor molecular heterojunctions for photovoltaic applications. II. Device performance. J. App. Phys. 98, (2005)

[10] Park, S. H., Roy, A., Beaupre, S., Cho, S., Coates, N., Moon, J. S., Moses, D., Leclerc, M., Lee, K., Heeger, A. J.: Bulk heterojunction solar cells with internal quantum efficiency approaching 100%. Nat. Photon. 3, 297-U295 (2009)

[11] Brabec, C. J., Hummelen, J. C., Sariciftci, N. S.: Plastic Solar Cells. Adv. Funct. Mater. 11, 15-26 (2001)

[12] Peumans, P., Yakimov, A., Forrest, S. R.: Small molecular weight organic thin-film photodetectors and solar cells. J. Appl. Phys. 93, 3693-3723 (2003)

[13] Knupfer, M.: Exciton binding energies in organic semiconductors. Appl. Phys. A Materials Science & Processing. 77, 623-626 (2003)

[14] Kroon, R., Hummelen, J. C., Lenes, M., Blom, P. W. M., De Boer, B.: Small bandgap polymers for organic solar cells (polymer material development in the last 5 years). Polym. Rev. 48, 531-582 (2008)

[15] Markov, D. E., Amsterdam, E., Blom, P. W. M., Sieval, A. B., Hummelen, J. C.: Accurate Measurement of the Exciton Diffusion Length in a Conjugated Polymer Using a Heterostructure with a Side-Chain Cross-Linked Fullerene Layer. J. Phys. Chem. A. 109, 5266-5274 (2005)

[16] McNeill, C. R., Greenham, N. C.: Conjugated-Polymer Blends for Optoelectronics. Advanced Materials. 21, 3840-3850 (2009)

[17] Gregg, B. A.: Excitonic solar cells. J. Phys. Chem. B 107, 4688-4698 (2003)

Autor's signature

[18] Kraabel, B., Hummelen, J. C., Vacar, D., Moses, D., Sariciftci, N. S., Heeger, A. J., Wudl, F.: Subpicosecond photoinduced electron transfer from conjugated polymers to functionalized fullerenes. J. Chem. Phys. 104, 4267-4273 (1996)

[19] Brabec, C. J., Cravino, A., Meissner, D., Sariciftci, N. S., Fromherz, T., Rispens, M. T., Sanchez, L., Hummelen, J. C.: Origin of the Open Circuit Voltage of Plastic Solar Cells. Adv. Funct. Mater. 11, 374-380 (2001)

[20] Po, R., Carbonera, C., Bernardi, A., Camaioni, N.: The role of buffer layers in polymer solar cells. Energy Environ. Sci. (2010)

[21] Skotheim, T. A., Reynolds, J. R.: Conjugated Polymers: Processing and Applications CRC Press Taylor & Francis Group, USA (2006)

[22] Hoppe, H., Sariciftci, N. S.: Organic solar cells: An overview. J. Mater. Res. 19, 1924-1945 (2004)

[23] Koster, L. J. A., Mihailetchi, V. D., Ramaker, R., Blom, P. W. M.: Light intensity dependence of open-circuit voltage of polymer:fullerene solar cells. Appl. Phys. Lett. 86, 123509 (2005)

[24] Sariciftci, N. S., Günes, S., Neugebauer, H.: Conjugated Polymer-Based Organic Solar Cells. Chem. Rev. 107, 1324-1338 (2007)

[25] Peumans, P., Forrest, S. R.: Separation of geminate charge-pairs at donor-acceptor interfaces in disordered solids. Chemical Physics Letters. 398, 27-31 (2004)

[26] Mihailetchi, V. D., Wildeman, J., Blom, P. W. M.: Space-Charge Limited Photocurrent. Phys. Rev. Lett. 94, 126602 (2005)

[27] Lenes, M., Koster, L. J. A., Mihailetchi, V. D., Blom, P. W. M.: Thickness dependence of the efficiency of polymer:fullerene bulk heterojunction solar cells. Appl. Phys. Lett. 88, 243502-243503 (2006)

[28] Gupta, D., Mukhopadhyay, S., Narayan, K. S.: Fill factor in organic solar cells. Sol. Ener. Mat. and Sol. Cells. 94, 1309-1313 (2010)

Autor's signature

3 MOTIVATION AND AIM

3.1 INTRODUCTION

Efforts to optimize the performance of organic solar cells should find their basis in the fundamental steps by which light energy is converted into electrical energy in the devices, from light absorption to charge extraction - discussed in detail in Chapter 2.
It is clear that in each step several phenomena can take place that decrease the efficiency of the global process , so that only a limited portion of the photons reaching the cell are able to generate useful electrons. Thus the optimization of each step is fundamental to extract as much energy as possible from the device. This optimization encompasses the development of new approaches in the design of materials and of the device structure. In this chapter, the factors limiting state-of-the-art organic solar cells are briefly summarized on basis of the current knowledge about the elementary processes of photogeneration in these devices. Approaches for avoiding the limitation or improving the process will be discussed subsequently and the focus of this work is described.

3.2 LIMITS OF STATE OF THE ART ORGANIC SOLAR CELLS

3.2.1 LIGHT ABSORPTION

The first process in a solar cell is the absorption of light by the active layer. Since PCBM possesses a relatively low extinction coefficient, in particular at longer wavelengths, most of the solar radiation needs to be absorbed by the p-conjugated polymer. To absorb as much light as possible, a good overlap between the polymer absorption spectrum and the

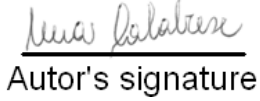

solar emission is essential. Figure 3.1 shows that an organic solar cell with an absorption edge at 650 nm, typical for the common poly(3-hexylthiophene-2,5-diyl) (P3HT) absorber material, can generate up to 20 % of the maximum available photocurrent, whereas silicon solar cells achieve up to 60 %. Hence it is important to extend absorption at higher wavelengths (beyond 650 nm) i.e. decreasing the energy gap. However, lowering of the polymeric energy gap can eventually result in a decrease in power conversion efficiency (PCE) due to a decrease in open circuit voltage. Based on these simple considerations the low band gap (LGB) polymers have the possibility to improve the efficiency of solar cells due to a better overlap with the solar spectrum.

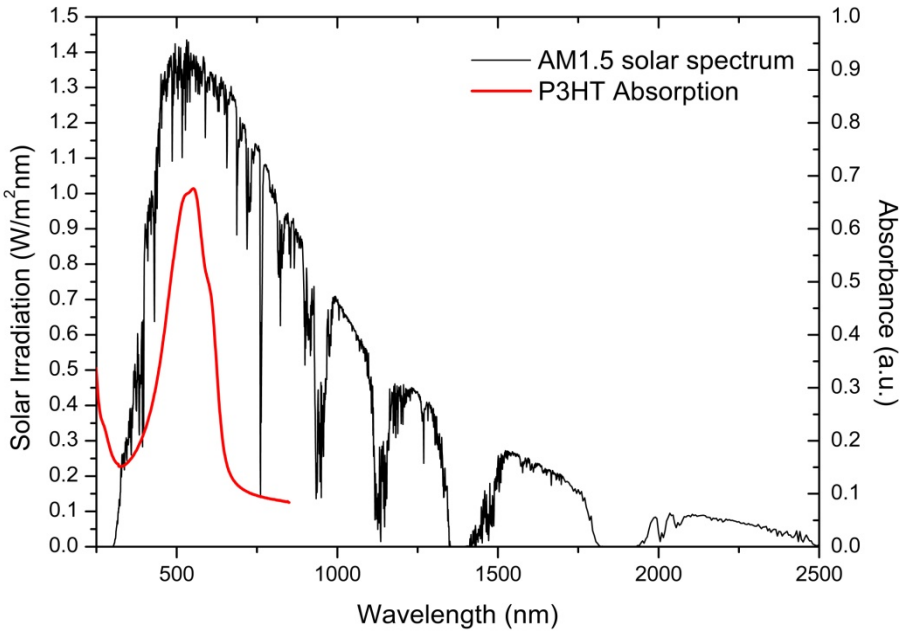

Figure 3.1 AM1.5 solar spectrum (Direct + Circumsolar, after ASTMG173). The absorption spectrum of the commonly used absorber material for bulk heterojunction solar cells, P3HT, is included for comparison.

Autor's signature

3.2.2 ENERGY LEVELS ALIGNMENT

After absorption of light by the semiconducting polymer, the exciton needs to be dissociated into free charges. This charge generation is suggested to be initiated by the difference in LUMO levels of the donor and acceptor [1-3]. Therefore, certain guidelines need to be taken into account when designing small band gap polymers for photovoltaic application. The first constraint is that the donor must be capable of transferring charge to the fullerene upon excitation. An energetic driving force is necessary for this process to be favorable and the driving force must exceed the exciton binding energy. This binding energy is the Coulombic attraction of the bound electron-hole pair in the donor, and typical values are estimated to be 0.4-0.5 eV [1] for conjugated polymers. The energetic driving force effects the dissociation of the exciton with the formation of a geminate pair. An additional energetic driving force is required to separate this geminate pair bound by Coulombic forces to generate free charges. This process is aided both thermally and by the intrinsic electric field in the device. The overall energetic driving force for a forward electron transfer from the donor to the acceptor is represented by the energy difference between the LUMOs of the donor and acceptor. It appears that a minimum energy difference of 0.3 eV is required to affect the exciton splitting and charge dissociation [4, 5]. Furthermore, an energy difference between the LUMOs larger than this minimum value does not seem to be advantageous, and indeed results in wasted energy that does not contribute to the device performance [3]. The ideal polymer would have a minimum energy difference between the LUMOs; in this way wasted energy upon exciton splitting would be avoided and the energy gap of the polymer would be minimized so as to maximize the absorption of light. The HOMO energy of the ideal donor polymer would then be determined by considering the energy gap of the polymer, and hence the light absorption, as well as the influence on the open circuit voltage. The lower the energy of the HOMO, the greater the maximum theoretically attainable *V*oc value, but the larger the energy gap, the poorer the spectral overlap with the photon flux from the sun. Therefore, it is important to find a compromise between these factors.

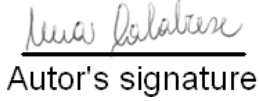

3.2.3 CHARGE TRANSPORT AND RECOMBINATION

The charge mobility limits the power conversion efficiency in bulk heterojunction solar cells to a certain degree. As the recombination rate at short circuit current is rather low, the extraction depth is sufficient for state-of-the-art devices, but is limited for devices further beyond 200 nm thickness. At voltages approaching the open circuit voltage, charge recombination is also critical, limiting the maximum open circuit voltage. Possible approaches for improvements are the synthesis of novel materials with higher charge carrier mobility for improved transport. Unfortunately, in the regime of Langevin recombination, the loss rate increases linearly with mobility [6, 7]. Hence, it is important to design a polymer with good charge transport properties, i.e. make a polymer that exhibits mesoscopic order and crystallinity in the solid state. Furthermore, the electron and hole mobility should be balanced in a BHJ solar cell. Unbalanced and slow charge transport has been shown to lead to space charge effects that lower *J*sc and FF consequently reducing device performance [8].

3.2.4 CHARGE EXTRACTION

The charge extraction in bulk heterojunction solar cells is more limited in comparison to bilayer solar cells. However, in general terms the low but sufficient surface recombination velocity ensures an efficient charge extraction in state-of-the-art solar cells. It is unclear whether or not the charge extraction in bulk heterojunctions can be improved further. If yes, then by using a more advanced device layouts, such as donor/donor–acceptor/acceptor configurations or blocking layers. In all cases, more research is needed on the fundamental processes governing energy conversion by organic solar cells, in order to find the most promising optimization routes.

3.3 NEW MATERIALS

In the previous section the importance of optimizing the electronic structure of both the donor and the acceptor as well as the morphology of the composite was discussed. The recent records in power conversion efficiency of organic solar cells, 3.5 % for modules and 7.9 % for small devices [9], were not achieved by using the well researched Poly(3-hexylthiophene) blended with fullerene derivatives but using novel materials. Indeed, several aspects of organic solar cells can potentially be optimized on the molecular level by synthetic design. New and adapted synthetic strategies can lead to the desired properties of organic semiconducting materials. Nowadays, in most cases only the donor material absorbs light efficiently; an absorbing acceptor has a large potential for increasing the photocurrent. Additionally, by a variation of the relative energy levels of donor and acceptor material, thus optimizing the energetic position of the charge transfer complexes, the energy loss due to the electron transfer can be minimized. An alternative approach is to use low band gap polymers. These have an enhanced absorption in the red part of the spectrum, in order to shift the absorption gap and provide a better harvesting of the solar spectrum. Recently, low band gap novel donor polymers with an absorption up to 1300 nm have been presented. Devices derived from blends with PCBM, however, showed that the open circuit voltage and the photocurrent are too low to yield a good solar cell [10]. Many of the novel copolymer low band gap systems show either an overall lower charge generation efficiency [11] or have absorption bands as narrow as P3HT and thus absorb little in the blue part of the visible spectrum [12]. Nevertheless, the efficiency records in the last months were also achieved with low band gap donor materials. Indeed, recently a trend towards using copolymers can be observed in order to address the issue of narrow absorption width. These conjugated polymers can have low band gaps resulting from the intrachain coupling between the electron donating and accepting units on each monomer [13]. Some of these concepts embed metals or elemental (inorganic) semiconductors into the chemical structure, thus showing that further enhancements of the absorption width as well as the charge generation and transport properties are to be expected. Alternatively (or additionally), nanoparticle sensitisers and the multijunction approach can be used to improve the photon harvesting. A class of promising materials utilizing the donor-acceptor

approach are the alternating copolymers of Donor-Acceptor-Donor (D-A-D) segments and dialkylated fluorene segments reported by Svensson *et al* [14]. The choice of the fluorene unit in these polymers was motivated by the fact that polyfluorenes (PFOs) have shown good stability [15] and can form liquid crystalline phases [16], which improve charge mobility. The donor molecules most of the time based on thiophene, pyrroles, carbazole, are electron rich and able to increase the electron density between the repeating units. A wide variety of acceptors have been used, the most common ones being based on the cyano group, the benzothiadiazole, and the thienopyrazine moiety. Examples are reported in Figure 3.2. Several polymers in this category have previously been synthesized and evaluated and they has been shown good performance in optoelectronic devices. In particular, poly{9,9-bisalkylfluorene-2,7-diyl-*alt*-[4,7-bis(thien-2-yl)-2,1,3-benzothia-diazole]-5',5"-diyl} with alkyl = hexyl, 2-ethylhexyl, octyl, decyl, dodecyl [17-20], containing fluorene-thiophene-benzothiadiazole-thiophene units in a strictly alternating sequence, have led to solar cells having power conversion efficiencies in the range 0.6-4.5% and for this reason has represented a reference for this work.

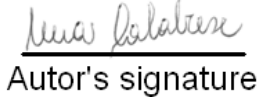

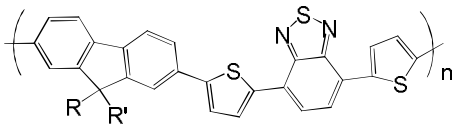

APFO-1, R=R'=C_6H_{13}
APFO-2, R=C_6H_{13}, R'=$CH_2CH(C_2H_5)C_4H_9$
APFO-3, R=R'= C_8H_{17}
APFO-4, R=R'=$C_{12}H_{25}$

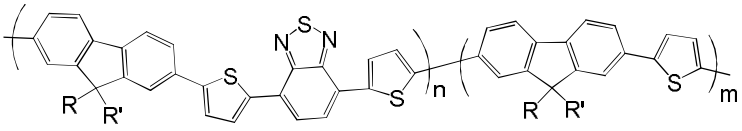

APFO-5 R=C_6H_{13}, R'=$CH_2CH(C_2H_5)C_4H_9$, n=50%, m=50%

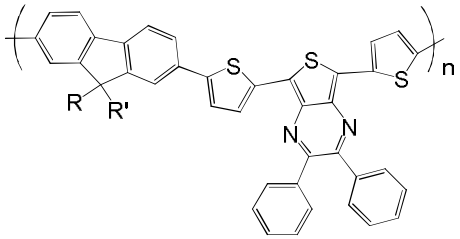

APFO-6

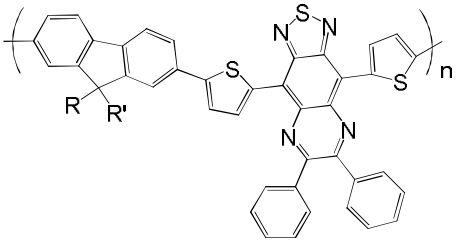

APFO-7

Figure 3.2 Chemical structures of some alternating PFO polymers.

3.4 AIM OF RESEARCH

The focus of this work is the design, the synthesis and the characterization of a novel family of pseudo-random copolymers based on fluorene (F), thiophene (T) and benzothiadiazole (B) monomer units. The synthesis of random instead of alternating copolymers has the aim to improve the harvesting of the sunlight. Indeed, while the disordered structure, typical of the random polymers, may hamper the crystallization and decrease the carrier mobility, the presence of different monomer units sequences generate a distribution of energy gaps and increase the light harvesting ability. This is one of the fundamental prerequisite to obtain high efficiency photovoltaic devices. Another advantage

Autor's signature

of random copolymers lies in their simplicity of synthesis that consists in a one-pot polymerization step from readily available precursors. In the synthesis of these novel copolymers care was taken to introduce solubilizing groups so that the resulting copolymers are soluble and, hence, the solutions processable. These substituents generally do not absorb light and do not contribute to the photocurrent and hence should be kept to a minimum. The chemical nature, position and size of the side chains do have a pronounced effect on the (photo)physical properties. The effect of the molecular weight on optical and electrical properties was investigated. Solution and solid-state characterization of the envisaged donor-acceptor molecules should establish structure-property relationships which can be exploited for the fabrication of organic solar cells. Optical measurements provide vital information about the electronic properties and can be used as a proof of an ongoing electron-transfer within these donor-acceptor materials. Furthermore, the energetic levels of the corresponding frontier orbitals can be determined by cyclic voltammetry which is essential with respect to the applied electrodes and acceptors in organic solar cells. These analysis methods allow the selection of the most promising candidates which can be employed for the fabrication of efficient organic solar cells. In order to understand the correlations between chemical property and structure, theoretical calculations were carried out. The calculations of HOMO/LUMO distribution of the copolymers were performed using Hartree Fock methods and density functional theory approach. The performed calculations showed how HOMO and LUMO levels are affected by the incorporation of electron donating and electron-withdrawing groups into polymer backbone. Additionally, the predictions data obtained were compared with the experimental data, taking into account the different measurement condition.

3.5 REFERENCES

[1] Arkhipov, V. I., Bässler, H.: Exciton dissociation and charge photogeneration in pristine and doped conjugated polymers. Phys. Status Solidi A. 201, 1152-1187 (2004)

[2] Scharber, M. C., Brabec, C. J., Heeger, A. J., Mühlbacher, D., Koppe, M., Denk, P., Waldauf, C.: Design Rules for Donors in Bulk-Heterojunction Solar Cells - Towards 10 % Energy-Conversion Efficiency. Adv. Mater. 18, 789-794 (2006)

[3] Koster, L. J. A., Mihailetchi, V. D., Blom, P. W. M.: Ultimate efficiency of polymer/fullerene bulk heterojunction solar cells. Appl. Phys. Lett. 88, (2006)

[4] Brabec, C. J., Sariciftci, N. S., Hummelen, J. C., Janssen, R. A. J., Winder, C., Dhanabalan, A., Hal, P. A. v.: A Low-Bandgap Semiconducting Polymer for Photovoltaic Devices and Infrared Emitting Diodes. Adv. Funct. Mater. 12, 709-712 (2002)

[5] Brabec, C. J., Sariciftci, N. S., Hummelen, J. C., Cravino, A., Meissner, D., Rispens, M. T., Sanchez, L., Fromherz, T.: The influence of materials work function on the open circuit voltage of plastic solar cells. Thin Solid Films. 403-404, 368-372 (2002)

[6] Juska, G., Sariciftci, N. S., Sliauzys, G., Arlauskas, K., Pivrikas, A., Osterbacka, R., Scharber, M., Mozer, A.: Recombination of photogenerated and injected charge carriers in pi-conjugated polymer/fullerene blends. Thin Solid Films. 511, 224-227 (2006)

[7] Sariciftci, N. S., Juska, G., Mozer, A. J., Dennler, G., Pivrikas, A., Österbacka, R., Fuchsbauer, A.: Charge carrier mobility and lifetime versus composition of conjugated polymer/fullerene bulk-heterojunction solar cells. Organic Electronics. 7, 229-234 (2006)

[8] Kroon, R., Hummelen, J. C., Lenes, M., Blom, P. W. M., De Boer, B.: Small bandgap polymers for organic solar cells (polymer material development in the last 5 years). Polym. Rev. 48, 531-582 (2008)

[9] Green, M. A., Emery, K., Hishikawa, Y., Warta, W.: Solar cell efficiency tables (version 36). Progress in Photovoltaics: Research and Applications. 18, 346-352 (2010)

[10] Gong, X., Tong, M., Xia, Y., Cai, W., Moon, J. S., Cao, Y., Yu, G., Shieh, C.-L., Nilsson, B., Heeger, A. J.: High-Detectivity Polymer Photodetectors with Spectral Response from 300 nm to 1450 nm. Science. 325, 1665-1667 (2009)

Autor's signature

[11] Peet, J., Kim, J. Y., Coates, N. E., Ma, W. L., Moses, D., Heeger, A. J., Bazan, G. C.: Efficiency enhancement in low-bandgap polymer solar cells by processing with alkane dithiols. Nat Mater. 6, 497-500 (2007)

[12] Völker, S. F., Uemura, S., Limpinsel, M., Mingebach, M., Deibel, C., Dyakonov, V., Lambert, C.: Polymeric Squaraine Dyes as Electron Donors in Bulk Heterojunction Solar Cells. Macromol. Chem. Phys. 211, 1098-1108 (2010)

[13] Kim, J. Y., Qin, Y., Stevens, D. M., Kalihari, V., Hillmyer, M. A., Frisbie, C. D.: High Open-Circuit Voltage Photovoltaic Cells with a Low Bandgap Copolymer of Isothianaphthene, Thiophene, and Benzothiadiazole Units. J. Phys. Chem. C. 113, 21928-21936 (2009)

[14] Svensson, M., Zhang, F., Inganäs, O., Andersson, M. R.: Synthesis and properties of alternating polyfluorene copolymers with redshifted absorption for use in solar cells. Synth. Met. 135-136, 137-138 (2003)

[15] Halls, J. J. M., Arias, A. C., MacKenzie, J. D., Wu, W. S., Inbasekaran, M., Woo, E. P., Friend, R. H.: Photodiodes based on polyfluorene composites: Influence of morphology. Adv. Mater. 12, 498-+ (2000)

[16] Grell, M., Bradley, D. D. C., Inbasekaran, M., Woo, E. P.: A glass-forming conjugated main-chain liquid crystal polymer for polarized electroluminescence applications. Adv. Mater. 9, 798-& (1997)

[17] Svensson, M., Zhang, F., Veenstra, S., Verhees, W., Hummelen, J., Kroon, J., Inganäs, O., Andersson, M.: High-Performance Polymer Solar Cells of an Alternating Polyfluorene Copolymer and a Fullerene Derivative. Adv. Mater. 15, 988-991 (2003)

[18] Inganäs, O., Svensson, M., Zhang, F., Gadisa, A., Persson, N. K., Wang, X., Andersson, M. R.: Low bandgap alternating polyfluorene copolymers in plastic photodiodes and solar cells. Appl. Phys. A Materials Science & Processing. 79, 31-35 (2004)

[19] Slooff, L. H., Veenstra, S. C., Kroon, J. M., Moet, D. J. D., Sweelssen, J., Koetse, M. M.: Determining the internal quantum efficiency of highly efficient polymer solar cells through optical modeling. Appl. Phys. Lett. 90, 143506 (2007)

[20] Chen, M.-H., Hou, J., Hong, Z., Yang, G., Sista, S., Chen, L.-M., Yang, Y.: Efficient Polymer Solar Cells with Thin Active Layers Based on Alternating

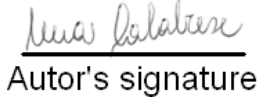

Polyfluorene Copolymer/Fullerene Bulk Heterojunctions. Adv. Mater. 21, 4238-4242 (2009)

Autor's signature

4 CHARACTERIZATION METHODS

4.1 INTRODUCTION

The correlation of physical and chemical properties with structural characteristics, production and preparation conditions is of crucial importance for the development of new materials and the optimization of existing products. Comprehensive knowledge of the material properties of a material under production or application conditions is therefore critical for its success. The dependence of macroscopic product properties on the characteristics of the material on a microscopic level is another important aspect for successful product development and for the solution of production and quality problems. Some of the investigation techniques required for an extended characterization of active materials for organic solar are listed in the **Figure 4.1**.

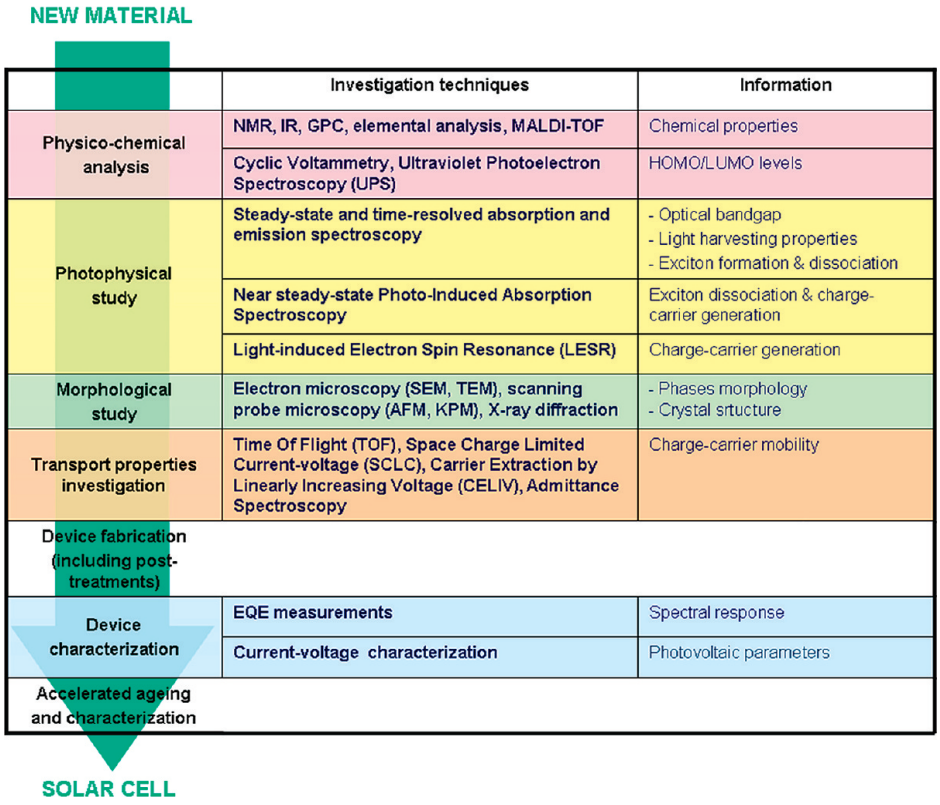

	Investigation techniques	Information
Physico-chemical analysis	NMR, IR, GPC, elemental analysis, MALDI-TOF	Chemical properties
	Cyclic Voltammetry, Ultraviolet Photoelectron Spectroscopy (UPS)	HOMO/LUMO levels
Photophysical study	Steady-state and time-resolved absorption and emission spectroscopy	- Optical bandgap - Light harvesting properties - Exciton formation & dissociation
	Near steady-state Photo-Induced Absorption Spectroscopy	Exciton dissociation & charge-carrier generation
	Light-induced Electron Spin Resonance (LESR)	Charge-carrier generation
Morphological study	Electron microscopy (SEM, TEM), scanning probe microscopy (AFM, KPM), X-ray diffraction	- Phases morphology - Crystal structure
Transport properties investigation	Time Of Flight (TOF), Space Charge Limited Current-voltage (SCLC), Carrier Extraction by Linearly Increasing Voltage (CELIV), Admittance Spectroscopy	Charge-carrier mobility
Device fabrication (including post-treatments)		
Device characterization	EQE measurements	Spectral response
	Current-voltage characterization	Photovoltaic parameters
Accelerated ageing and characterization		

Autor's signature

Figure 4.1 Nonexhaustive list of investigation techniques required for an extended characterization of active materials for polymer (organic) solar.cells.

The methods used in this work are briefly described here in after.

4.2 PHOTOPHYSICAL, CHEMICAL AND STRUCTURAL ANALYSIS

4.2.1 NUCLEAR MAGNETIC RESONANCE SPECTROSCOPY

Nuclear magnetic resonance (NMR) spectroscopy has become a powerful tool for the organic chemist since instruments became easily available in the late 1950s, and developments in instrumentation in the last decade have extended the usefulness of the technique. The technique is only applicable to those nuclei which possess a spin quantum number (I) greater than zero. The most important of such nuclei as far as the organic chemist is concerned are ^{1}H and ^{13}C, both of which have a spin quantum number of ½. Other nuclei with non-zero spin quantum numbers are ^{19}F and ^{31}P, with I = ½**;** ^{14}N and ^{1}D**,** with I = 1; and ^{11}B and $^{35}C1$, with I = 3/2. All of these have been extensively studied by NMR spectroscopy. Nuclei with non-zero spin quantum numbers can be thought of as tiny spinning bar magnets. This spinning magnetic field creates a magnetic dipole, the magnitude of which is given by the nuclear magnetic moment μ. ^{1}H have relatively large magnetic moments and are relatively easily studied by NMR spectroscopy. ^{13}C has a much smaller magnetic moment which has meant that until relatively recently, with the introduction of new instrumental techniques, the ^{13}C nucleus was not easily studied by nuclear magnetic resonance spectroscopy. In the absence of an applied magnetic field the nuclei are randomly orientated. When the nuclei are placed in a magnetic field they align themselves in relation to the applied field. The number of orientations which the nucleus can adopt is limited by the spin quantum number and is equal to (2I + 1). Thus those nuclei with I= ½ have two possible orientations in the magnetic field (+½ and -½). The two orientations are associated with different energy levels, orientation against the magnetic field being of higher energy and thus having a lower population. The difference in energy

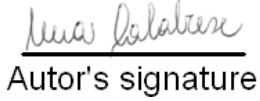

between the two spin states is dependent on the magnitude of the applied magnetic field and the nuclear magnetic moment. The frequency of radiation necessary to effect a transition between the two energy levels is given by the equation:

$$\upsilon = \frac{\mu B_0}{hI}$$

(10)

where v is the frequency of radiation, μ is the magnetic moment of the nucleus, B_0 is the strength of the external magnetic field, h is Planck's constant, and I is the spin quantum number. Thus the larger the applied magnetic field the greater the energy difference between the two levels and the greater the frequency of radiation necessary to effect the transition between the two levels. The basis of the NMR experiment is to subject the nuclei to radiation which will result in a transition from the lower energy state to the higher one. The value of NMR spectroscopy to the organic chemist is that the precise difference in energy levels between the two spin orientations is dependent on the particular location of the atom in the molecule. This is because each nucleus is subject to the differing effects of the magnetic fields of neighbouring nuclei. Only nuclei which are in exactly the same magnetic environment will have exactly the same energy difference between spin orientations when placed in a magnetic field. In NMR spectroscopy these differences in energy are detected and provide information on the variety of locations of the nuclei in the molecule.

4.3 UV-VIS SPECTROSCOPY

Absorption of light regards the interactions between electromagnetic radiation and matter in the ultraviolet-visible (UV-Vis) region. The absorption of UV or visible radiation corresponds to electronic transitions of outer electrons. There are three main types of electronic transition which can be considered:

1. Transitions involving π, σ, and n electrons (organic compounds);
2. Transitions involving d and f electrons (metal complexes);

3. Charge-transfer transitions involving electrons in donor-acceptor system (organic compounds and metal complexes).

When an atom or molecule absorbs energy, electrons are promoted from their ground state to an excited state. In a molecule, the atoms can rotate and vibrate with respect to each other. These vibrations and rotations also have discrete energy levels, which can be considered as being packed on top of each electronic level. The absorption spectrum is the superposition of rotational and vibrational transitions on the electronic transitions gives a combination of overlapping lines; this appears as a continuous absorption band.

Absorption of ultraviolet and visible radiation in organic molecules is restricted to certain functional groups (*chromophores*) that contain valence electrons of low excitation energy.

There are four types of possible electronic transition which can be considered:

1. from a non-bonding orbital (n) an antibonding π -orbital (π*);
2. from a non-bonding orbital (n) to an antibonding σ -orbital (σ*);
3. from a bonding orbital (π) to an antibonding π-orbital (π*);
4. from a bonding orbital (σ) to an antibonding σ-orbital (σ*).

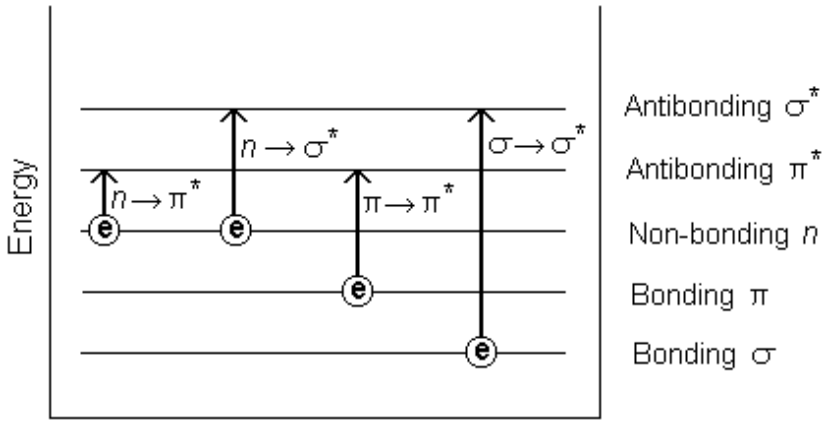

Figure 4.2 Schematic representation of orbital energy level

The energies noted above are sufficient to promote or excite a molecular electron to a higher energy orbital. Consequently, absorption spectroscopy carried out in this region is sometimes called electronic spectroscopy. A diagram showing the various kinds of electronic excitation that may occur in organic molecules is shown on the left. Of the four

Autor's signature

transitions outlined, only the two lowest energy ones are achieved by the energies available in the 200 to 800 nm spectrum. As a rule, energetically favored electron promotion will be from the highest occupied molecular orbital (HOMO) to the lowest unoccupied molecular orbital (LUMO), and the resulting species is called an excited state. When sample molecules are exposed to light having an energy that matches a possible electronic transition within the molecule, some of the light energy will be absorbed as the electron is promoted to a higher energy orbital. An optical spectrometer records the wavelengths at which absorption occurs, together with the degree of absorption at each wavelength. The resulting spectrum is presented as a graph of absorbance (A) versus wavelength. Absorbance usually ranges from 0 (no absorption) to 2 (99% absorption), and is precisely defined in context with spectrometer operation.

Because the absorbance of a sample is proportional to the number of absorbing molecules in the spectrometer light beam (e.g. their molar concentration in the sample tube), it is necessary to correct the absorbance value for this and other operational factors if the spectra of different compounds are to be compared in a meaningful way. The corrected absorption value is called molar absorptivity, and is particularly useful when comparing the spectra of different compounds and determining the relative strength of light absorbing functions (chromophores). Molar absorptivity (ε) is defined by Lambert-Beer law as:

$$\varepsilon = \frac{A}{c \cdot l} \tag{11}$$

where A is the absorbance, c is sample concentration in moles/liter and l is the length of light path through the sample in cm. It is clear that the only molecular moieties likely to absorb light in the 200 to 800 nm region are pi-electron functions and hetero atoms having non-bonding valence-shell electron pairs. Such light absorbing groups are referred to as chromophores. The oxygen non-bonding electrons in alcohols and ethers do not give rise to absorption above 160 nm. Consequently, pure alcohol and ether solvents may be used for spectroscopic studies. The presence of chromophores in a molecule is best documented by UV-Visible spectroscopy, but the failure of most instruments to provide absorption data for wavelengths below 200 nm makes the detection of isolated chromophores problematic. Fortunately, conjugation generally moves the absorption maxima to longer wavelengths, so conjugation becomes the major structural feature identified by this technique.

Autor's signature

Molar absorptivities may be very large for strongly absorbing chromophores (>10,000) and very small if absorption is weak (10 to 100). The magnitude of ε reflects both the size of the chromophore and the probability that light of a given wavelength will be absorbed when it strikes the chromophore.

4.3.1 THE IMPORTANCE OF CONJUGATION

Consider three molecules: ethane, buta-1,3-diene and hexa-1,3,5-triene (**Figure 4.3**). In these cases, there is delocalisation of the pi bonding orbitals over the whole molecule.

Ethene contains a simple isolated carbon-carbon double bond, but the other two have conjugated double bonds. In these cases, there is delocalisation of the π-bonding orbitals over the whole molecule. All of the molecules give similar UV-visible absorption spectra - the only difference being that the absorptions move to longer wavelengths as the amount of delocalisation in the molecule increases. This can be easly understood if consider the energy levels diagram of these compounds (see **Figure 4.3**).

In an isolated double bond (ethane), there is one π-bonding orbital and one π -antibonding orbital. When two double bonds are conjugated (diene), the four π-atomic orbitals combine to generate four π-molecular orbitals (two are bonding and two are antibonding). In a similar manner, the three double bonds of a conjugated triene create six π-molecular orbitals, half bonding and half antibonding. The energetically most favorable π-π* excitation occurs from the highest energy bonding π-orbital (HOMO) to the lowest energy antibonding π-orbital (LUMO). Increased conjugation brings the HOMO and LUMO orbitals closer together. The energy required to effect the electron promotion is therefore less, and the wavelength that provides this energy is increased correspondingly. Thus, extending conjugation generally results in shifts at longer wavelength and in a greater absorbance.

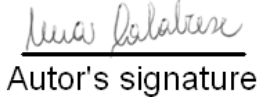

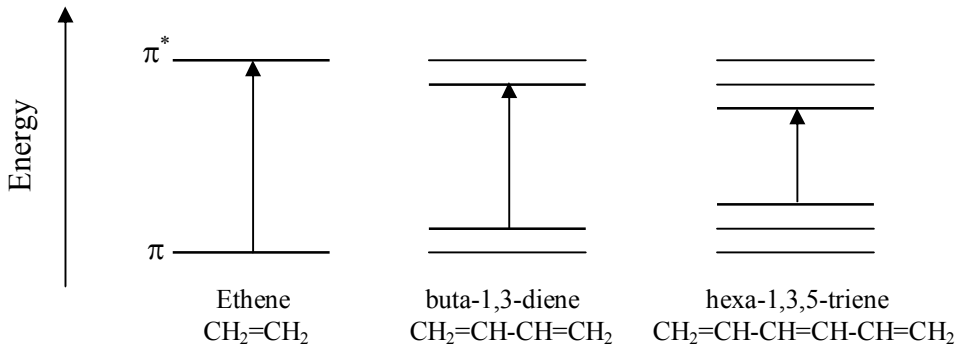

Figure 4.3 Energy levels diagram of ethane, buta-1,3-diene, hexa-1,3,5-triene

Spectroscopists use the terms defined in the **Table 4.1** when describing shifts in absorption.

Table 4.1 Terminology for absorption shifts.

Nature of Shift	**Descriptive Term**
To Longer Wavelength	Bathochromic
To Shorter Wavelength	Hypsochromic
To Greater Absorbance	Hyperchromic
To Lower Absorbance	Hypochromic

The appearance of several absorption peaks or shoulders for a given chromophore is common for highly conjugated systems, and is often solvent dependent. This fine structure reflects not only the different conformations such systems may assume, but also electronic transitions between the different vibrational energy levels possible for each electronic state. Vibrational fine structure of this kind is most pronounced in vapor phase spectra, and is increasingly broadened and obscured in solution as the solvent is changed from hexane to methanol.

Autor's signature

4.4 CYCLIC VOLTAMMETRY

Cyclic voltammetry (CV) is the most widely used technique for acquiring qualitative and quantitative information about electrochemical reactions. The power of cyclic voltammetry results from its ability to rapidly provide considerable information on the thermodynamics of redox processes and the kinetics of heterogeneous electron-transfer reactions, and on coupled chemical reactions or adsorption processes. In particular, it offers a rapid location of redox potentials of the electroactive species, and convenient evaluation of the effect of media upon the redox process. This technique consists of scanning linearly the potential of a stationary working electrode, using a triangular potential waveform. The potential is measured between the reference electrode and the working electrode and the current is measured between the working electrode and the counter electrode by a potentiostat. This data is then plotted as current (i) vs. potential (E). The forward scan produces a current peak for any analytes that can be reduced (or oxidized depending on the initial scan direction) through the range of the potential scanned. The current will increase as the potential reaching the reduction potential of the analyte, but then falls off as the concentration of the analyte is depleted close to the electrode surface. If the redox couple is reversible when the applied potential is reversed, it will reach the potential that will reoxidize the product formed in the first reduction reaction, and produce a current of reverse polarity from the forward scan. This oxidation peak will usually have a similar shape to the reduction peak. As a result, information about the redox potential and electrochemical reaction rates of the compounds are obtained. For instance if the electronic transfer at the surface is fast and the current is limited by the diffusion of species to the electrode surface, then the current peak will be proportional to the square root of the scan rate. The formal potentials of the first oxidation and first reduction of a complex can be correlated to the energies of its highest occupied molecular orbital (HOMO) and lowest unoccupied molecular orbital (LUMO) [1]. Similarly, this HOMO-LUMO energy difference, i.e. the band gap of the system, typically determines the lowest energy electronic transition in the UV-Vis spectrum. However the electrochemical gap is greater than the optical gap calculated from the UV-Vis spectra and this discrepancy is usually related to the charge carriers formation in voltammetric measurements [2].

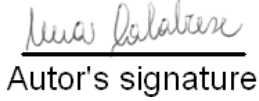

4.5 RAMAN AND FT-IR SPECTROSCOPY

When atoms become attached to each other through a formation of chemical bonds, a molecule or macromolecule is formed. Because all atoms in a molecule possess kinetic energy, they vibrate. Such vibrations can be deconvoluted to so-called normal vibrational modes, and classified into a few classes: some modes may be observed in the Raman spectrum, some in the infrared (IR) spectrum, and some may or may not be seen in either spectrum. When the molecule possesses a high degree of symmetry, there is a rule of mutual exclusion which states that no vibrational mode may be observed in both the IR and Raman spectra. This high symmetry is defined by a center of inversion operation. As the symmetry is reduced, and the molecule no longer contains a center of inversion, some vibrational modes may be seen in both the IR and in the Raman spectra. However, these modes will often have quite different intensity in the two spectra. The quantum mechanical selection rules state that, observation of a vibrational mode in the IR spectrum requires a change in dipole moment during the vibration. The observation of a vibrational mode in the Raman spectrum requires a change in the electron polarizability (change of the dipole moment with distance) resulting from the movement of atoms. The apparent differences in the principles governing both effects have led to the development of two physically distinct, yet complimentary, experimental approaches to obtain IR and Raman spectra. The detection of Raman scattering involves a completely different assemblage of principles. When monochromatic radiation at an opportune frequency ν_0 strikes a transparent sample, the light is scattered. While most of the scattered light consists of radiation at the frequency of the incident light referred to as the Raleigh scattering, typically 1 out of 10^6 photons are scattered inelastically. This portion of the scattering is referred to as Raman scattering. This inelastically scattered fraction of light, composed of new modified frequencies**,** **($\nu_0+\nu_k$)** is referred to anti-Stokes scattering, and **($\nu_0-\nu_k$)** is the Stokes scattering component. This energy diagram shows that the anti-Stokes scattering requires that the molecules start in an excited vibrational state. Because the easiest way to populate these excited vibrational states is by a thermal excitation, the anti-Stokes intensities will be very temperature dependent and typically quite weak at room temperature. Therefore, Stokes scattering is the most common way to record Raman spectra. The absorption process

Autor's signature

observed in IR may, and under certain selection rules, correspond to the vibrational energy levels depicted for the Stokes Raman scattering process.

Since the source of the Raman spectrum is a scattering event, the Scattered Intensity is directly proportional to the concentration of species giving rise to the Raman lines. This is different than in an IR absorption experiment which follows Beer's Law discussed in the previous section.

The wavenumber (energy or frequency) of an IR/Raman Absorption depends on the mass of the atoms connected to a chemical bond, the strength of the chemical bond, and the geometry of the molecule. In particular, higher mass leads to smaller frequencies and stronger bonds lead to higher frequencies of vibration. There are two basic types of vibrations, stretches and bends. Bends require less energy so occur at lower frequencies for the same or similar bonds. There are many types of bends, Twisting, Rocking, Scissoring, Tortional, Breathing (For ring molecules) and other specialized bends. There are generally two types of stretching, symmetric and asymmetric. Symmetric stretches require lower energy than asymmetric stretches.

4.5.1 VIBRATIONAL SPECTROSCOPY ON CONJUGATED POLYMER

Due to the strong electron-phonon coupling in conjugated polymers, Raman spectroscopy and infrared absorption are powerful techniques for the investigation of the doping induced lattice relaxation around the charge carriers. Consequently, the vibrational behaviour of relatively simple conjugated polymers in their pristine and doped states (mostly of the *p*-type) has been the subject of much theoretical and experimental work during the last two decades [3]. The infrared spectra of conjugated polymers in their conductive (chemically-, electrochemically-, or photo-doped) states are characterized by intense infrared absorption bands (infrared active vibrations, IRAV bands), typically ranging from 1600 cm^{-1} to 700 cm^{-1}. These bands originate from the strong electron-phonon coupling mentioned above and thus provide not only structural but also electronic information. In addition, broad IR absorption bands at higher energy usually accompany IRAVs. These bands correspond to

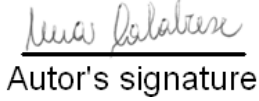

the transitions involving the electronic levels induced in the gap, *via* lattice relaxation, by the doping process. Several theoretical models have been developed in order to explain the spectroscopic signatures of charge carriers in conjugated polymers. For the description of the electronic and vibrational properties of neutral and doped *trans*-polyacetylene, Horovitz *et al*. and Ehrenfreund *et al*. have considered the change in the charge density wave associated to the vibrational motion of the polymer backbone [4]. As quantification of the localization of charge a pinning parameter was introduced. Zerbi *et al*. explained the IRAV bands by the IR activation of the Raman active *A*g modes in the pristine form of the polymer due to the local breaking of the symmetry around the charge carrier. In this model, the high intensity of the IRAV bands is motivated by the large variation of the electric dipole moment associated to the oscillation of the charged defect. An effective conjugation coordinate (ECC) describes the changes in geometry going from the ground- to the excited-state of the polymer as an alternating stretching-shrinking of carbon-carbon bonds. The higher the contribution of a given mode to the ECC, the higher is the intensity of the corresponding IRAV band. This origin of the IRAV bands shows that both Raman spectroscopy and IR spectroscopy as complementary techniques are necessary for understanding the vibrational spectra of pristine and doped conjugated polymers. By the use of models [5] has been established a link between the electronic absorption bands and the IRAV bands of doping induced spectra. All of the models correlate intensity, width and position of the IRAV bands to the delocalization of charge carriers along the polymer chain. These theories, developed for relatively simple systems like *trans*-polyacetylene and extended to few polyheteroaromates, do not account for possible differences in the IRAV signatures of positive and negative charge carriers. In addition, since the pinning in absence of counterions should be lower, photoinduced IRAV bands should appear at lower wavenumbers than chemically induced bands. Experimental work has confirmed that these models rationalize the spectroscopic behavior of conjugated polymers, providing a self-consistent description of the vibrational properties of many and relatively simple systems like, for instance, poly(alkylthiophene)s [3]. However, some complex conjugated polymers show a more complex behavior. These materials are often promising candidates for applications since they may combine low band gap, outstanding optical properties and high stability in either the *p*- and *n*-doped states. The large number of atoms in a polymer chain makes the possible number of IR/Raman bands enormous. Synthetic polymer chains are

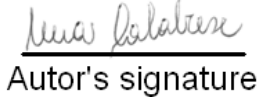

composed of repeated chemical groups, monomer units, which are arranged about the chain axis in a similar fashion for all of these groups. The simplest approach to considering the IR/Raman absorption patterns from synthetic polymers is to identify characteristic chemical groups which give rise to absorptions. This approach, of identifying chemical groups as independent contributions to a complex IR/Raman pattern, is called the group contribution method. The basic assumption of the group contribution method is that vibrations from most chemical species are little effected by their bonding to the polymer chain. This approach is accurate in the sense that absorptions for most chemical groups will fall in a limited range which can be distinguished from other absorptions due to the strength of the absorption, for example polar bonds have strong absorptions in IR, combined with the range of wavenumbers where the absorptions occur.

4.6 MOLECULAR WEIGHT DETERMINATION

Because virtually all polymers are mixtures of many large molecules, one must resort to averages to describe molecular weight. Among many possible ways of reporting averages, three are commonly used: the number average (M_n), weight average (M_w), and z-average (M_z) molecular weights described by the follow formulas:

$$M_n = \frac{\sum_{i=1}^{\infty} N_i M_i}{\sum_{i=1}^{\infty} N_i} \tag{12}$$

$$M_w = \frac{\sum_{i=1}^{\infty} N_i M_i^2}{\sum_{i=1}^{\infty} N_i M_i} \tag{13}$$

$$M_z = \frac{\sum_{i=1}^{\infty} N_i M_i^3}{\sum_{i=1}^{\infty} N_i M_i^2} \tag{14}$$

where N_i be the number of polymers with molecular weight M_i.

Autor's signature

The weight average is probably the most useful of the three, because it fairly accounts for the contributions of different sized chains to the overall behavior of the polymer, and correlates best with most of the physical properties of interest. The ratio of M_w to M_n is known as the *polydispersity index* (PDI), and provides a rough indication of the breadth of the distribution. The PDI approaches 1.0 (the lower limit) for special polymers with very narrow molecular weight distributions, but, for typical commercial polymers, is typically greater than 2 (occasionally much greater).

4.6.1 GEL PERMEATION CHROMATOGRAPHY

Gel permeation chromatography (GPC) is by far the most versatile technique for the determination of molecular weight in a polymer sample. GPC involves passing a dilute polymer solution through a tubular column packed with polymeric gel (crosslinked) beads. Under high pressure flow some of the polymer chains are forced into the pores of the gel, while others pass by the gel beads. The residence time of a given polymer chain in the packed column depends on the path it takes through the gel. For instance, a low molecular weight oligomer will easily be force into the pores of the gel and will take a circuitous path through the column, traveling a distance equivalent to hundreds of the column length. High molecular weight species can not fit into the pores of the gel, i.e. they are excluded, and can pass more directly to the exit of the column traveling a distance roughly equivalent to the column length. The selectivity of this process for molecular weight is outstanding and the range of molecular weights which can potentially be characterized by this technique is only limited by the ability to produce controlled spaced gels.

4.7 ELECTRON PARAMAGNETIC RESONANCE

Electron paramagnetic resonance (EPR) or electron spin resonance (ESR) spectroscopy is a technique for studying chemical species that have one or more unpaired electrons, such as organic and inorganic free radicals or inorganic complexes possessing a transition metal

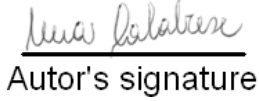

ion. The basic physical concepts of EPR are analogous to those of nuclear magnetic resonance (NMR), but it is electron spins that are excited instead of spins of atomic nuclei. Because most stable molecules have all their electrons paired, the EPR technique is less widely used than NMR. However, this limitation to paramagnetic species also means that the EPR technique is one of great specificity, since ordinary chemical solvents and matrices do not give rise to EPR spectra. Every electron has a magnetic moment and spin quantum number I = 1/2, with magnetic components $m_s = \pm 1/2$. In the presence of an external magnetic field with strength B_0, the electron's magnetic moment aligns itself either parallel ($m_s = -1/2$) or antiparallel ($m_s = +1/2$) to the field, each alignment having a specific energy (Zeeman effect). The parallel alignment corresponds to the lower energy state, and the separation between it and the upper state is:

$$\Delta E = g_e \mu_B B_0 \tag{15}$$

where g_e is the electron's so-called g-factor and μ_B is the Bohr magneton. This equation implies that the splitting of the energy levels is directly proportional to the magnetic field's strength, as shown in the Figure XX. An unpaired electron can move between the two energy levels by either absorbing or emitting electromagnetic radiation of energy $\varepsilon = h\nu$ such that the resonance condition, $\varepsilon = \Delta E$, is obeyed. Substituting in $\varepsilon = h\nu$ and $\Delta E = g_e \mu_B B_0$ leads to the fundamental equation of EPR spectroscopy:

$$h\nu = g_e \mu_B B_0$$

Experimentally, this equation permits a large combination of frequency and magnetic field values, but the great majority of EPR measurements are made with microwaves in the 9 - 10 GHz region, with fields corresponding to about 3500 G (0.35 T).

In principle, EPR spectra can be generated by either varying the photon frequency incident on a sample while holding the magnetic field constant, or doing the reverse. In practice, it is usually the frequency which is kept fixed. A collection of paramagnetic centers, such as free radicals, is exposed to microwaves at a fixed frequency. By increasing an external magnetic field, the gap between the $m_s = +1/2$ and $m_s = -1/2$ energy states is widened until

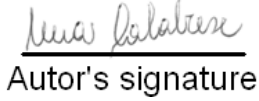

it matches the energy of the microwaves, as represented by the double-arrow in the diagram above. At this point the unpaired electrons can move between their two spin states. Since there typically are more electrons in the lower state, due to the Maxwell-Boltzmann distribution, there is a net absorption of energy, and it is this absorption which is monitored and converted into a spectrum. Important information can be obtained by analysis of ESR spectra. The main is the registration of appearance of cation/anion radicals after light excitation and hence, the charge separation processes with the estimation of charge carriers concentration. The analysis of spectroscopic Zeeman splitting factor (*g*-factor) gives information about the symmetry of the paramagnetic centre and the average *g*-factor value on the deviation from free electron *g*-factor $\Delta g = g - g_e = \lambda/\Delta E_g$, where λ is the spin-orbit coupling constant and ΔE_g is the polymer band gap, and hence about the most probable position (spin density maximum) of polaron localization on the polymer chain. This is really possible because of the significant difference of λ magnitude for main chain atoms of conjugated polymer and ΔE_g may be directly estimated by the light absorption experiment. Furthermore, the EPR signal linewidth analysis gives essential information about: (a) spin-lattice and spin-spin relaxations, (b) exchange and dipole–dipole interactions, (c) anisotropic broadening, connected with the anisotropy of *g*-factor components and slow molecular rotational motion, (d) inhomogeneous broadening connected with unresolved hyperfine EPR signal structure. The time dependence of the signal amplitude gives information on the charge separation kinetics after light on and intrinsically charge recombination kinetics after light off. This type of study has the aim of compare of the microscopic properties of the different systems prepared on identical conditions. This is a first step to estimate the suitability and perspective of polymer types components of solar cell devices.

4.8 MORPHOLOGICAL STUDY

In organic solar cells, the charge generation and charge transport depend strongly on the nanoscale morphology, defined as the arrangement of the donor and acceptor networks throughout the bulk. At the heart of improving solar cell efficiency is engineering the

photoactive morphology to get large interface areas for exciton dissociation and, at the same time, to form continuous donor and acceptor networks for charge transport. **Figure 4.4** provides a schematic drawing of device structure and typical solar cell morphology. The optimal phase of each component should have a domain size between 10 nm and 20 nm, similar to the exciton diffusion length.

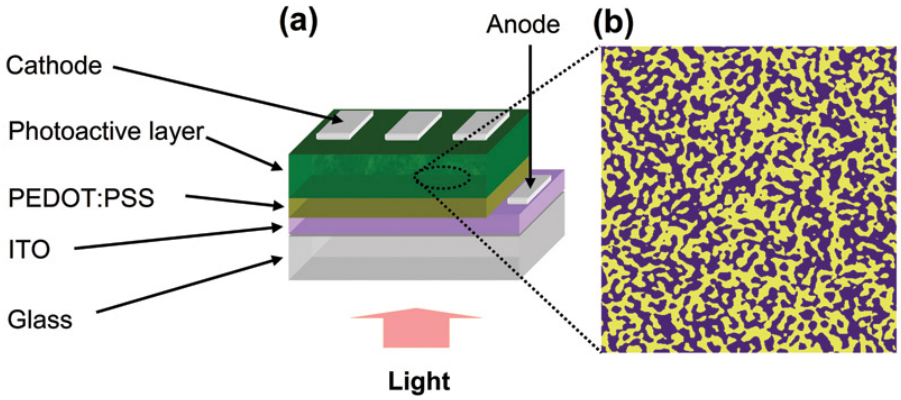

Figure 4.4 (a) A typical solar cell structure consisting of PEDOT:PSS deposited onto a glass/ITO substrate. The photoactive layer is spun cast atop the PEDOT:PSS film, followed by the aluminum cathode electrode evaporation. (b) Topographic image obtained using atomic force microscopy showing phase separation where yellow and purple areas are donor and acceptor phases, respectively. A nanoscale phase separation of donor and acceptor materials in the active layer is needed to achieve efficient exciton dissociation and charge transport.

To better understand how nanoscale morphology affects charge generation and transport, one needs powerful tools to visualize the phase separation of the two components, as well as to understand the optoelectronic processes occurring in the devices at the nanometer scale. For this purpose, many techniques such as high resolution transmission electron microscopy (TEM) and scanning probe microscopy (SPM) have been deployed. With its wide variety of scanning and measurement modes such as atomic force microscopy (AFM), conductive AFM, transient-resolved electrostatic force microscopy (trEFM), and Kevin probe microscopy (SKPM), SPM can enable simultaneous local probing of morphology, electrical and optoelectronic properties of solar cell materials, establishing a direct correlation of local heterogeneity in nanostructure and photocurrent generation with bulk device performance. AFM is extremely useful for studying the local surface molecular composition and mechanical properties of a broad range of polymer materials, including block copolymers, bulk polymers, thin-film polymers, polymer composites, and polymer blends. The photoconductive AFM (pcAFM) is based on a conductive AFM setup

Autor's signature

equipped with a light source. The light is focused on the device through the ITO (indium tin oxide) using an inverted optical microscope and a sample (e.g. a film or device) is loaded in a air-cell. The AFM probe can either sit on a specific point on a sample surface to record the current as a function of an applied bias or the probe can be scanned with a fixed applied bias to provide a current map. Metal-coated silicon probes with varying work functions can be employed as the top nanoelectrode for either hole or electron collection. Due to the small radius of the probe used in pcAFM measurements, solar cell performance at the nanoscale can be examined and correlated to the bulk measurements, thus providing a comprehensive picture of phase separation, charge generation, charge transport and collection. When the pcAFM is equipped with a tunable monochromatic light source, it can reveal not only spatially, but also spectrally the complexity of the morphology and photocurrent generation.

Nanoscale phase separation of donor and acceptor molecules in the photoactive layer is elucidated by imaging electron and hole collection networks at the same location. Due to the high work function of the gold-coated silicon probe (~5.1 eV), photogenerated holes are collected by the AFM probe and electrons are collected by the ITO electrode when a bias above open-circuit voltage is applied. This process is reversed when a bias below the open-circuit voltage is applied to the substrate; the photogenerated holes then travel toward the cathode, while the probe tip collects electrons. The applied bias must be small enough so that no charge is injected from the electrodes. Therefore, the photocurrent structure collected at positive and negative biases reveals hole and electron collection networks corresponding to the donor and acceptor phases at the film surface, respectively. Contributing to the low efficiency of the bulk device is the large phase separation of donor and acceptor materials in the blend films, which leads to the reduction of interface areas for exciton dissociation and interruption of charge collection pathways.

The pcAFM technique also offers a great opportunity to study nanoscale photophysics using light intensity dependence measurements. The heterogeneity in nanostructure and optoelectronics of the photovoltaic materials can be a reason for low performance of bulk devices. Analyzing short-circuit current (I_{sc}) as a function of light intensity sheds light on local variation in photocurrent generation and recombination. A better understanding of the relationship between nanostructure and optoelectronic properties will help improve the device efficiency. The I_{sc} increases with incident light intensity (P), according to a power-

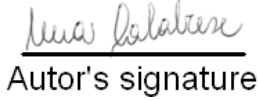

Autor's signature

law behavior $I_{sc} \sim P^{\alpha}$. The α value is suggestive of the degree of recombination processes. The free carrier loss due to charge recombination increase with increasing α. Further study, such as external quantum efficiency measurements, can examine the blend composition which results in high photogenerated carrier recombination. Comparing this investigation to processing conditions would be the best way for enhancing the efficiency of photovoltaics.

4.9 TRANSPORT PROPERTIES INVESTIGATION

When trying to improve and develop electronic devices made of π-conjugated polymers, it is crucial to understand the charge carrier transport and recombination processes in these materials. Charge carrier mobility techniques in organic materials can be classified according to *e.g.,* the mode of charge generation (photogenerated, doping induced, electrostatic, or injected by electrical contacts) or as transient or (quasi-) steady state (see **Figure 4.5**)

		Transient	*(Quasi-) Steady State*
Mode of charge generation	***Photo-induced***	Time of Flight (ToF) Photo-CELIV	Photoconductivity Photo-impedance
	Doping-induced	CELIV	Conductivity
	Electrostatic		Field Effect Transistor
	Injected (from contacts)	DI SCLC tr-EL	SCLC Time-resolved optical detection

Figure 4.5 Experimental techniques used to determine charge carrier mobility. CELIV: charge extraction by linearly increasing voltage; DI SCLC: dark injection space charge limited current; tr-EL: transient electroluminescence.

The time of flight technique (ToF), and the complimentary technique of charge extraction by linearly increasing voltage (CELIV) are used in this study to measure charge carrier mobility in conjugated polymers. The measurement principles and the schematic responses of these transient conductivity techniques are illustrated in **Figure 4.6**

Autor's signature

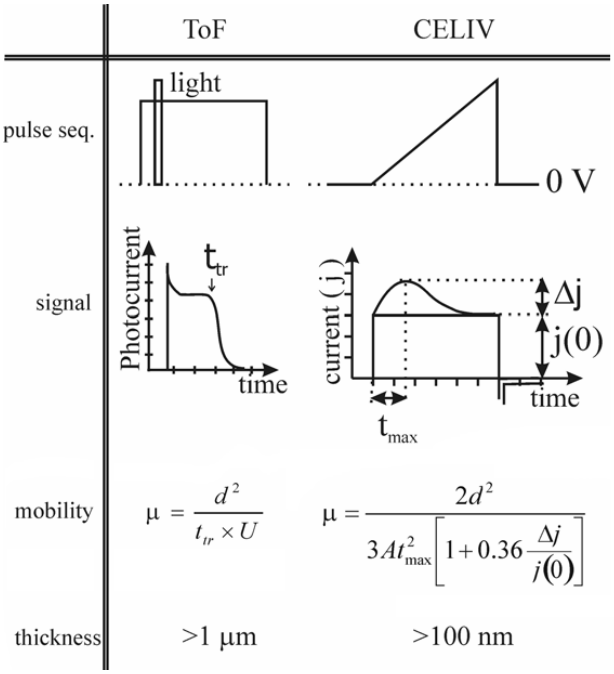

Figure 4.6 The pulse sequence and schematic response of the ToF, CELIV and photo-CELIV technique. The calculation of mobility and the typical thickness of the device are also displayed for comparison.

In the time of flight technique, the transit time (t_{tr}) of a two dimensional sheet of photogenerated charge carriers drifting through a sample of know thickness (d) is determined under an applied external electric field (E=U/d). The ToF mobility is then calculated as $\mu=d^2/(U\times t_{tr})$. The condition of surface photogeneration of charge carriers in a ToF technique requires large film thicknesses with high optical density (>10). Photocurrent transients can be characterized as non-dispersive exhibiting a well developed plateau, in which case the transit time is defined as the intersect of the plateau with the tail of the photocurrent transient as it is shown in **Figure 4.6**. In the presence of strong dispersion, the recorded photocurrent transients do not exhibit a plateau, but decrease constantly. In dispersive cases the transit time is defined as the intersect of the two linear regimes in the log photocurrent versus log time plots. The field is assumed to be uniformly distributed over the sample, which condition is maintained by:

- limiting the number of photogenerated charge carrier to less than 10% of the capacitive charge,

Autor's signature

- making that the dielectric relaxation time (τ_σ) is larger than the transit time $\tau_\sigma = \varepsilon\varepsilon_0 / \sigma_c >> t_{tr} = \frac{d^2}{\mu V}$, where σ_c [Ω cm^{-1}]is the conductivity.

Otherwise the number of equilibrium or doping induced charge carriers (ep_0d, where p_0 is the charge carrier concentration) are sufficient to screen and redistribute the electric field prior to the arrival of the photoexcited charge carriers at the electrode.

In conductive samples with short τ_σ, the complementary technique of CELIV can be used. In the CELIV technique the equilibrium charge carriers are extracted from a dielectric under a reverse bias voltage ramp. The mobility of extracted charge carriers is calculated from the time when the extraction current reaches its maximum (t_{max}). The CELIV measurement is most conveniently performed when the current due to the capacitance displacement current equals to the extraction current at its maximum Δj. This experimental condition is achieved by *e.g.,* selecting the proper thickness of the sample. In contrary to ToF, the CELIV technique can be used to determine charge carrier mobility in samples with only a few hundred nanometer thickness.

4.10 DEVICE CHARACTERIZATION

Solar or photovoltaic (PV) cells are made up of semiconductor materials that absorb photons from sunlight and then release electrons, causing an electric current to flow when the cell is connected to a load. A variety of measurements are used to characterize a solar cell's performance, including its output and its efficiency. This electrical characterization is performed as part of research and development of photovoltaic cells and materials, as well as during the manufacturing process.

Some of the electrical tests commonly performed on solar cells involve measuring current and capacitance as a function of an applied DC voltage. Capacitance measurements are sometimes made as a function of frequency or AC voltage. Some tests require pulsed current-voltage measurements. These measurements are usually performed at different light intensities and under different temperature conditions. A variety of important device parameters can be extracted from the DC and pulsed current-voltage (I-V) and capacitance-

Autor's signature

voltage (C-V) measurements, including output current, conversion efficiency, maximum power output, doping density, resistivity, etc. Electrical characterization is important in determining how to make the cells as efficient as possible with minimal losses.

The most common method for electrical characterization in the laboratory involves recording the electrical response of the organic photovoltaic device in the dark and under illumination. The electrical response is measured using a source-measure unit (SMU), also called a source meter. The source meter has the capacity to apply a voltage to a two-terminal device under test (DUT), such as a solar cell, and measure the current. Alternatively, a current can be passed through the device and the voltage can be measured. Most commonly and practically, the voltage is applied and the current is measured. The reason for this lies in the fundamental nature of the OPV device, which is a thin film. It is rather unpredictable what current range a given device will respond in and the passage of a particular current set by the experimenter may require unrealistic voltages, leading to breakdown and destruction of the device. Therefore, it is almost exclusively the voltage that is swept. Typical voltage ranges for single devices are from −1 V to +1 V, vice versa.

4.11 REFERENCES

[1] Hwang, S.-W., Chen, Y.: Synthesis and Electrochemical and Optical Properties of Novel Poly(aryl ether)s with Isolated Carbazole and p-Quaterphenyl Chromophores. Macromolecules. 34, 2981-2986 (2001)

[2] Johansson, T., Mammo, W., Svensson, M., Andersson, M. R., Inganas, O.: Electrochemical bandgaps of substituted polythiophenes. J. Mater. Chem. 13, 1316-1323 (2003)

[3] Zerbi, G.: Vibrational Spectroscopy of Conducting Polymers: Theory and Perspective. John Wiley & Sons, Ltd, (2006)

[4] Ehrenfreund, E., Vardeny, Z., Brafman, O., Horovitz, B.: Amplitude and phase modes in trans-polyacetylene: Resonant Raman scattering and induced infrared activity. Phys. Rev. B. 36, 1535 (1987)

Autor's signature

[5] Girlando, A., Painelli, A., Soos, Z. G.: Electron--phonon coupling in conjugated polymers: Reference force field and transferable coupling constants for polyacetylene. J. Chem. Phys. 98, 7459-7465 (1993)

Autor's signature

5 RESULTS AND DISCUSSION

5.1 SYNTHESIS OF POLYMERS

Three pseudo-random copolymers (**P1**, **P2**, **P3**) based on Fluorene (F), Thiophene (T) and Benzothiadiazole (B) units were synthetized by Suzuki cross-coupling polymerization [1] from dibromides and boronic diacids or diesters. The chemical structures are reported according in Scheme 5.1.

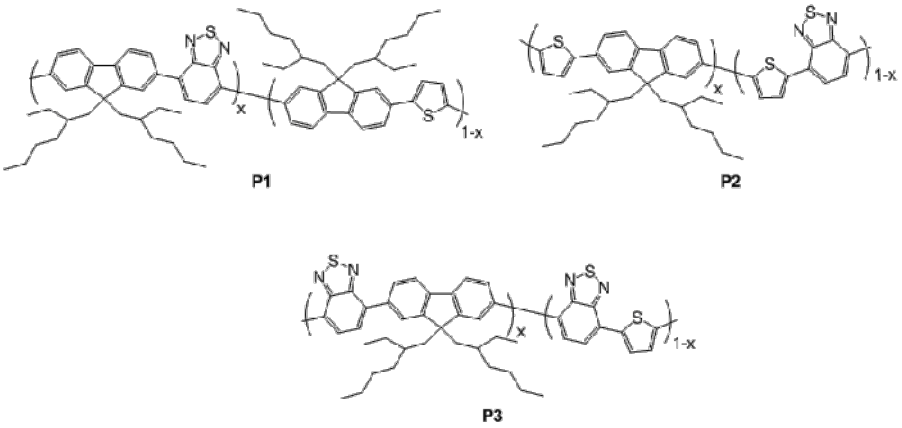

Scheme 5.1 Structures of random copolymers **P1-P3**.

As a result of the adopted procedure, in all copolymers in turn each F, T, B monomer unit is alternated to the other two units, which are randomly distributed (Scheme 5.2).

Autor's signature

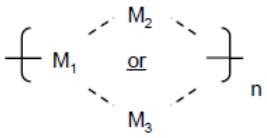

	M_1	M_2	M_3
P1	F	B	T
P2	T	F	B
P3	B	T	F

Scheme 5.2 Structure of pseudo-random copolymers

P1 and **P3** were obtained from 9,9-bis(2-ethylhexyl)fluorene-2,7-diboronic acid and 2,1,3-benzothiadiazole-4,7-bis(4,4,5,5-tetramethyl)-1,3,2-dioxaborolane, respectively, reacted with an equimolar mixture of the complementary dibromides. The synthesis of **P2** from thiophene-2,5-diboronic acid and 1:1 mixture of 2,7-dibromo-9,9-bis(2-ethylhexyl)fluorene and 4,7-dibromo-2,1,3-benzothiadiazole was also attempted, but no polymer was recovered. A possible explanation for this might be that deboronation side-reaction prevents the aryl-aryl coupling and the polymerization [2]. This problem was already observed before in the case of polymerization with thiophene-2,5-diboronic acid as starting monomer [3, 4]. Thus, **P2** was prepared from 2,5-dibromothiophene and an equimolar mixture of boronic derivatives of the two other monomers, affording a dark brown product in fairly good yield. To study the effect of the molecular weight on the photophysical properties and photovoltaic performance of fullerene-based bulk heterojunction solar cells, these copolymers were prepared into two different version: low molecular weight and high molecular weight. As reference a copolymer based on the same monomeric units but having a strictly alternate structure was synthetized in according to Scheme 5.3

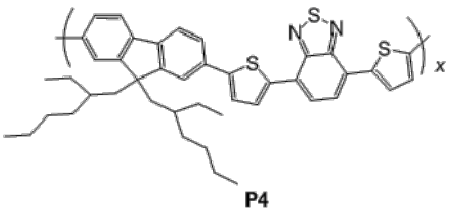

P4

Autor's signature

Scheme 5.3 Chemical structure of the alternating copolymer **P4**

For comparison, the F-T and F-B alternating binary copolymers were also synthesized and the chemical structures are shown in **Scheme 5.4** Chemical structure of the alternating copolymers $(F\text{-}B)_n$ and $(F\text{-}T)_n$.

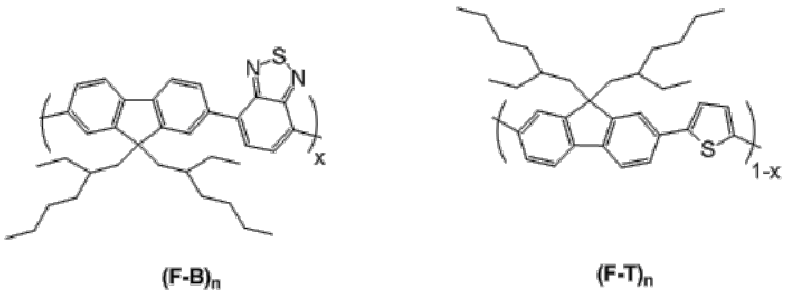

Scheme 5.4 Chemical structure of the alternating copolymers $(F\text{-}B)_n$ and $(F\text{-}T)_n$.

The weight-average molecular weight (Mw), and polydispersity indices (PDIs) were measured by GPC and the data are summarized in **Table 5.1**.

The properties of conjugated polymers are remarkably sensitive to the presence of impurities, which might act as uncontrolled dopants, traps of charge carriers, quenchers of excited states, etc. To improve the performance the copolymers solution was treated by ammonia and EDTA to remove contaminants such as catalyst residue and side-products from copolymers synthesis (see **Table 5.2**).

Table 5.1 Weight-average molecular weight (Mw), and polydispersity indices (PDIs) of all copolymers.

Entry	GPC			
	Low MW		High MW	
	Mw (g/mol)	PDI	*Mw* (g/mol)	PDI
P1	2300	1.7	34600	3.00
P2	1400	1.6	3200	1.80
P3	1600	2.6	--	--
P4	--	--	13600	2.5

Autor's signature

Table 5.2 Elemental analysis of copolymers at different stages of purification.

Entry	Before purification		After purification	
	Pd (ppm)	P (ppm)	Pd (ppm)	P (ppm)
P1	3400	800	10	700
P2	1100	800	100	800
P3	30000	9000	5000	900
P4	--	--	30	520

5.2 STRUCTURAL PROPERTIES

The structure of all investigated copolymers was verified by Nuclear Magnetic Resonance spectroscopy. The NMR analysis of copolymers was limited by poor spectral resolution due to the repeating structure of the monomers in the polymer backbone and the relatively low molecular weight. Furthermore, resonances from defects or other microstructures were frequently not resolved from the primary polymer signals, and were been difficult to detect and analyze. Thanks to the increase of the molecular weight and to the analysis of a large number of model compounds, as monomers, trimers and alternating copolymers, it was possible to attribute a part of the signals in the aromatic area of the random copolymers where was observed a high overlap of signals. A detailed study of the polymers microstructure and monomer sequence distribution by NMR is currently under way. In this work only the monomer composition is reported. The experimental compositions of **P1** and **P2** (with high MW) determined by nuclear magnetic resonance are near to the nominal ratio expected on the basis of the monomers feed (1: x ~ y ≈ 0.5); the discrepancies arise from the partial overlapping of some peaks. For **P1** the experimental F:T:B monomer ratio is 0.47:0.27:0.25, while for **P2** is 0.28:0.51:0.21 (the accuracy is estimated around ± 5%). On the other hand, **P3,** the less soluble polymer with a marked tendency to aggregate, exhibits broad NMR signals that cannot be accurately integrated.

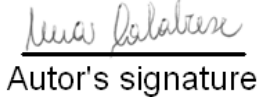

Autor's signature

5.3 VIBRATIONAL PROPERTIES

IR and Raman spectroscopy are powerful tools for studying the structure of doped and pristine conjugate copolymers. The charge carriers such as charged solitons, polarons and bipolarons can be identified by IR and Raman spectroscopy. In particular, IR is very useful for detecting the photogenerated and injected carriers give rise to very intense IR bands. Raman instead give us information about the crystalline/amorphous state of hole transport materials. Therefore, using together these technique can be obtained important information about the spectra/structure correlations. However, in the analysis of the vibrational spectra of conjugated systems, the classical spectra/structure correlations (in infrared or Raman) may fail and may be misleading. Indeed the delocalization of π electrons strongly affects the dynamics and the optical properties of the molecule and consequently the derived IR and Raman spectra, in terms of frequencies and intensity of the bands. The reason are the following [5]:

5. Because of π delocalization the equilibrium geometry of the molecule (overall or local) may change drastically, thus shifting vibrational frequencies from the tradition group frequencies used by chemists;
6. Because of the existence of long range forces the normal modes may not only determined by short range forces but also by longer range force originating many units away from the central repeat unit;
7. Because of the high mobility and large polarizability of the delocalizated π orbitals, the transition moments (which determine IR and/or Raman intensities) are modulated by the extent of delocalization of the π electrons along the molecular skeleton, thus generating seemingly strange and unexpected effects in the vibrational spectra.

The physics which follows is that when electron delocalization takes place in a molecule, a coupling between vibrations and electrons (e/ph coupling) may take place. In other words the motion of the nuclei along specific normal modes in the ground electronic state tends to carry the molecule to the first dipole allowed electronic excited state. The vibrational coordinates, strongly involved in e/ph coupling, are Я modes that describe a totally symmetric collective mode where all C=C bonds stretch in phase while all C-C bonds

shrink in phase. These modes identify a dimerization amplitude oscillation or a vibrational displacement, which traces the trajectory that nuclei must follow to move from the ground electronic state (aromatic) to the first excited state (quinoidic). Я modes show dispersion in frequency with conjugation length namely they decrease when delocalization increases. Within a homologous series of polymers, the shift to lower frequencies indicates an increase in effective conjugation length, or rather the vibronic coupling, in turn, generally associated with a decrease of the energy gap. The physical relevance of this observations is that while intra-molecular in phase force constants change with delocalization length, out of plane motions turn out to be almost independent of delocalization. The Я vibrations appearing in IR spectra with negligible intensity. As a consequence, information on π electrons delocalization can be only derived from the Raman spectrum (very strong Я modes). For this reason, while the IR spectroscopy for conjugated polymers is particularly informative on the charge carriers generated by photoexcitation and/or doping (IRAV: Activated Infrared Vibrations), Raman spectroscopy is essential in the characterization of conjugated polymers.

All these considerations have been well identified and rationalized for the linear conjugated polymers such as polyacetylene and polyenes. In these system there is a downward shift of the strong Raman lines with increasing conjugation lengths. The Raman spectrum of these materials shows a frequency and intensity dispersion with the wavelength of the exciting laser line. While the frequency depends on the effective conjugation length through the Я mode, the intensity depends on many parameters and primarily on the frequency of the exciting line, which determines the resonance conditions. In the linear polyaromatic chains, that consist of a linear chain of aromatic units linked to each other by single or quasi single CC bonds, the coplanarity and structural rigidity of the aromatic ring maximizes intra-ring delocalization, while the torsional flexibility about the inter-ring CC bond modulates the conjugation between aromatic units, strongly conformation dependent. It follows that for such systems (e.g. polythiophene), although there are still Я modes particularly intense in Raman, their position may be less affected by the length of the polymer chain than is observed for linear conjugated polymers (e.g. polyacetylene) just because the π electrons are more confined and the effective conjugation as well as the vibronic coupling are less extend along the polymer backbone [6]. Further evidence of the confinement of π electrons (pinning [7]) is also shown by the

Autor's signature

superimposition of the IR spectrum of photoexcitation to the IRAV bands due to doping, generally observed in such systems [8].

The IR spectra are more complex than Raman spectra due to the presence of much more bands. For this reason, the Raman spectra were used for all possible correlation. The polymers with high and low molecular weight shown different spectra. The high MW copolymer shown a more clear spectra of the one acquired for low Mw copolymer.

After a detail study of the spectra and thanks to comparison with reference monomer, trimers and alternating copolymer, have been possible to obtain the follow correlation:

Raman *(cm^{-1})*	***Structural unit***
1450	T (F-T-F)
1444	T (F-T-B)
1430	T (B-T-B)
1610	F (B-F-B)
1605	F (T-F-T)
1547	B (F-B-F)
1540	B (T-B-T)

5.4 OPTICAL PROPERTIES

The optical properties of all copolymers were studied by measuring UV-Vis and photoluminescence (PL) spectra in chloroform solution ($CHCl_3$) and in thin film. A red shifted by 15-25 nm were observed in films compared with those in solutions suggesting that significant solid intermolecular interactions were present in the solid state [9]. The data in solution allow a homogeneous comparison of the copolymers because eliminating variations due to interactions inter-chain caused by stacking polymers in solid form. Instead, data on thin film reproduce the operating conditions of the devices.

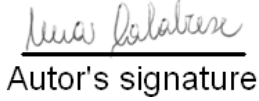

The optical energy gap of **P1-P4** copolymers with high and low MW was estimated from the onset of absorption and the data are summarized in **Table 5.3**. For convenience, are tabulated only the data for the copolymers with high molecular weight.

The UV-Vis absorption spectra of the alternating copolymer used as reference **P4** are shown in **Figure 5.1** in $ChCl_3$ solution and in thin film.

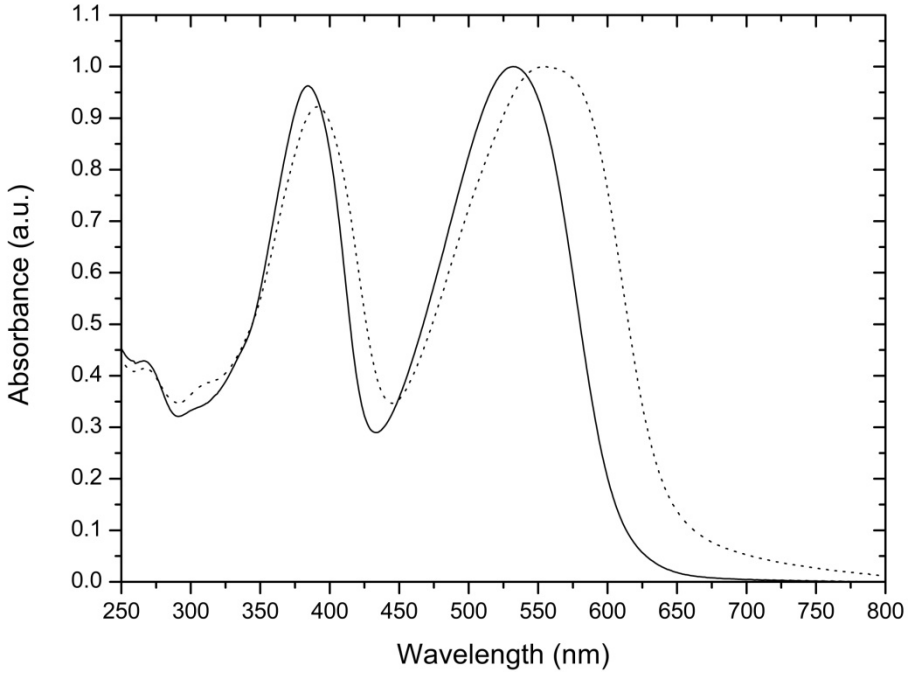

Figure 5.1 Normalized UV-Vis absorption spectra of **P4** copolymer in $CHCl_3$ solution (solid) and in thin film (dot).

The spectrum of alternating copolymer **P4** exhibited two bands respectively (called *camel-back bands*) typical of the push-pull systems which contain the F, T, B units [6]. The nature of the two distinct peaks are theoretically ascertained by semi-empirical quantum chemistry calculations. They suggest that the absorption peak at high energy (low

wavelength) is due to optical transitions between delocalized π-electron states, $\pi \rightarrow \pi^*$,

Autor's signature

extending on the all chain, while the second absorption peak, found at lower energies (high

wavelength), is due to intrachain charge transfer (iCT), where the absorption of incident radiation leads to formation of an excited electronic state where the negative charge densities resides on the benzothiadiazole acceptor unit while the positive charge densities remains delocalized on fluorene and thiophene units in the π-conjugated backbone. The shape of the peaks and the trend of the absorption wavelength were generally similar to that in solution (see **Table 5.3**). The absorption maxima in the films were red shifted by 7-23 nm compared with that in solution. For **P4** was found an optical energy gap of 2.05 eV in solution and 1.94 eV in thin film.

In **Figure 5.2** the emission spectra are shown when exciting either transition. The photoluminescence yield is higher for the ultraviolet (384 nm) excitation channel (solid line) compared to that of the green (532 nm) excitation channel (dot line). However, apart from this difference in photoluminescence yield, the emission spectra are identical and centered around 640 nm. This suggests that one dominant channel for emission is reached irrespective of what transition is excited. The excitation spectrum of **P4** copolymer, is presented in **Figure 5.2** and compared with the absorption spectra. The spectrum is taken from backward emission at 640 nm corresponding to the wavelength of maximum photoluminescence. The spectrum is corrected for the instrument response and the wavelength dependency of the light source. It reveals a severe reduction of emission from the green band, at lower excitation energies, compared to the absorption spectrum. Hence the photoluminescence is predominantly obtained from the ultraviolet spectral region. Deviations from absorption spectra are often attributed to alternative decay channels such as intersystem crossing, generation of charged species, or other non radiative decay.

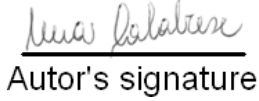

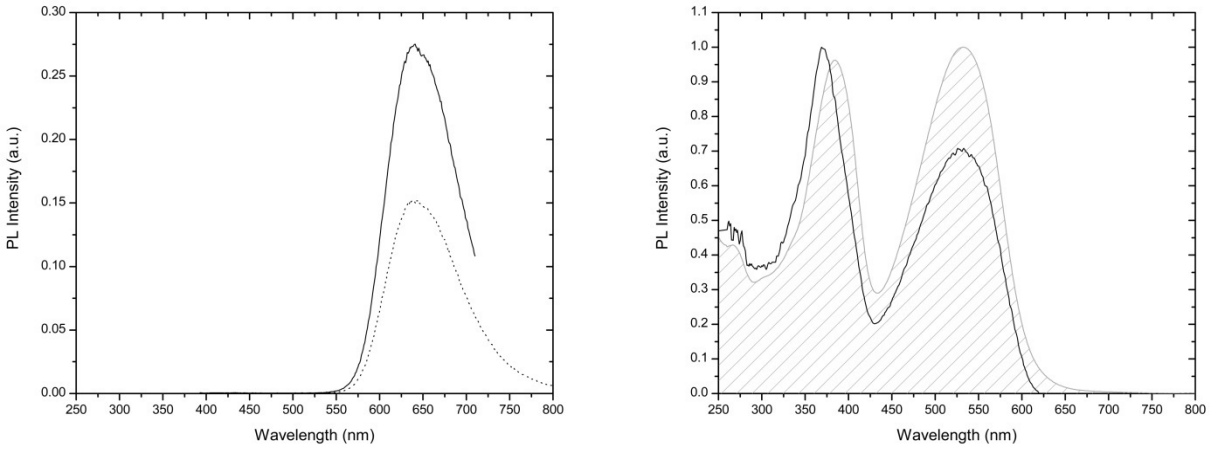

Figure 5.2 *Left*: Normalized PL spectra of **P4** with λ_{exc}=384 nm (solid line) and λ_{exc}=532 nm (dot line). *Right*: Normalized PL spectrum of **P4** measured at maximum photoluminescence yield (λ_{max}=640 nm). Grey patterned area represents the absorption spectrum in arbitrary units.

For comparison, the UV-Vis and photoluminescence spectra of $(F\text{-}T)_n$ and $(F\text{-}B)_n$ alternating binary copolymers (**Scheme 5.4** Chemical structure of the alternating copolymers $(F\text{-}B)_n$ and $(F\text{-}T)_n$**Scheme 5.4**) were also registered and the spectra are reported in **Figure 5.3**. The F-B copolymer contain alternating electron-donating (F) and electron-withdrawing (B) units and exhibits the properties of the donor-acceptor systems. The absorption spectra of F-B, both in solution and in the solid, display two well separated bands. The absorption band centered at higher energy can be attributed to a π-π* transition while the absorption band centered at lower energy can be attributed to a intrachain charge transfer (iCT) transition [6]. The F-T copolymer contain only electron-donating (F, T) units and exhibits no donor-acceptor properties. Indeed, the F-T copolymer spectrum exhibits a single absorption at due to a π-π* transition extending on the all chain; the structure is completely conjugated thanks to alternation of five- and six-membered rings.

Autor's signature

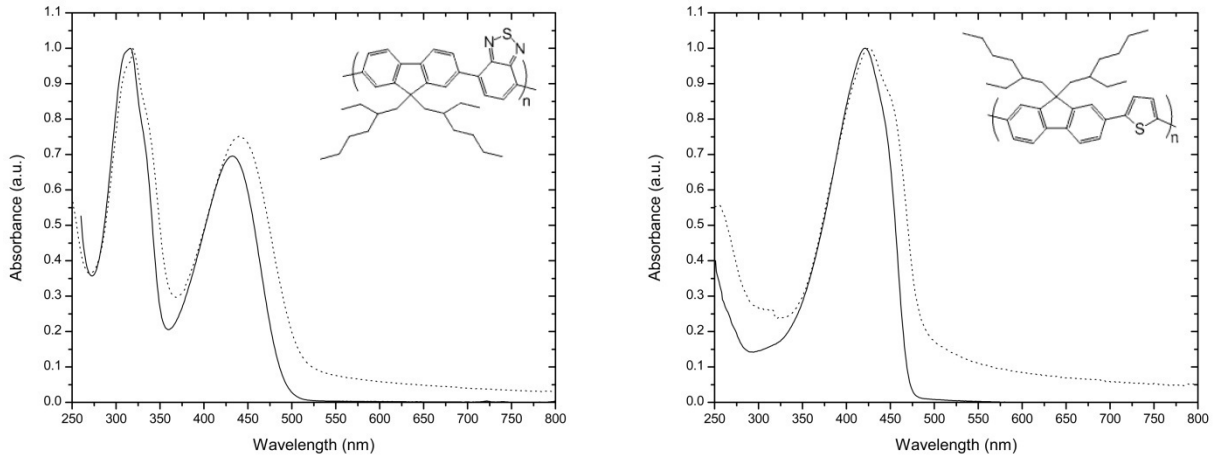

Figure 5.3 Normalized UV-Vis absorption spectra of $(F\text{-}B)_n$ (*Left*) and $(F\text{-}T)_n$ (*Right*) copolymers in $CHCl_3$ solution (solid line)and as thin film (dot line).

The $(F\text{-}T)_n$ emission spectra (**Figure 5.4**) show a low stokes shift (difference in), indicating a low distortion of the excited state (lower energy) compared to the fundamental electronic state. The spectrum displays a structured form that indicates a rigid ground state that confirm the complete flatness of the copolymer. The $(F\text{-}B)_n$ emission spectra (**Figure 5.4**) is not structured and show a greater stokes shift than the copolymer F-T.

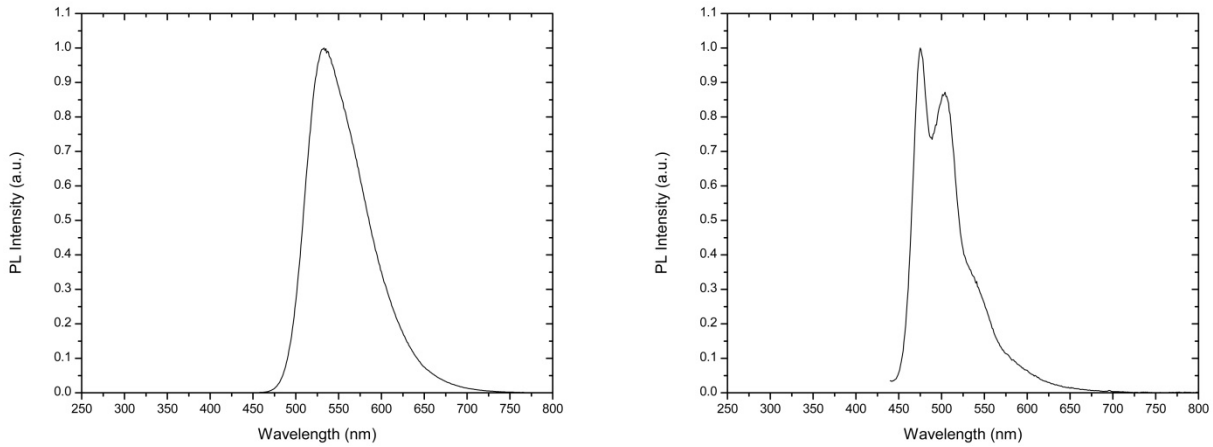

Figure 5.4 *Left*: Normalized PL spectrum of F-B copolymer in thin film with λ_{exc}=440 nm. *Right*: Normalized PL spectrum of F-T copolymer in thin film with λ_{exc}=425 nm.

P1 $((FT)_x\text{-}(FB)_y)$ contains long electron rich F-T sequences interrupted by B electron poor units; on average, there are on average more electron rich rings (in the calculations

Autor's signature

fluorene counts for two rings) than electron poor group. In other words, electron poor units are somewhat too sporadic along the chain to lead to a low bandgap structure [10]. The UV-Vis spectra of the copolymer **P1** with low and high molecular weight (in $CHCl_3$ solution and in thin film) are shown in **Figure 5.5** and the data are summarized in **Table 5.3**. The shape of the peaks and the trend of the absorption wavelength were generally similar to those in solution. Both copolymers exhibited two major absorption bands. The peak at longer wavelength could be attributed to the intramolecular charge transfer (iCT) transition, and the other at shorter wavelength was the result of a higher energy transition. It is interesting to notice that there is a band gap decrease with increasing molecular weight due to the shift at lower energy of the band at higher wavelength. Take into account the highest number of repeat units in the high Mw copolymer, the shift could be attributed to a better conjugation of the polymer backbone. The lower energy band remains in the same position in either case, indicating that the transition is not influenced by the extent of the conjugation. Furthermore, the copolymer **P1** with high Mw exhibits an intensity variation between the two bands, probably due to the intensity increase of the band related to the conjugation.

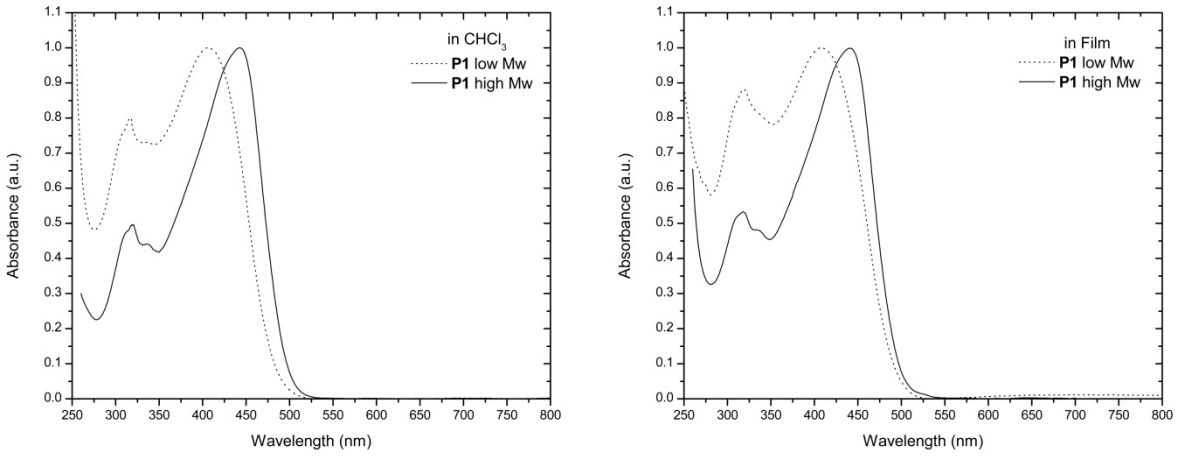

Figure 5.5 Normalized UV-Vis absorption spectra of copolymer P1 in $CHCl_3$ solution (*Left*) and in thin film (*Right*).

Interestingly, from **Figure 5.6** that the spectrum of **P1** (both with low and high molecular weight) is quite well approximated by a linear combination (l.c.) of the spectra of alternating polymer $(F\text{-}T)_n$ and $(F\text{-}B)_n$:

Autor's signature

$A(\lambda)_{P1} = A(\lambda)_{F\text{-}T} + k * A(\lambda)_{F\text{-}B})$

where k is a constant dependent on molar absorptivity of F-T and F-B polymers and relative abundance of corresponding monomers in **P1**. Apparently, the iCT band of the F-B portion at lower energy of **P1** is totally hidden by the π-π* band attributed to the F-T sequences. The fact that the ternary random copolymer appears to be a combination of the two parent binary copolymers suggests that the conjugation of the molecular chain is imperfect, otherwise the resulting delocalized system would exhibit very different features, with significant shifts in the peak positions.

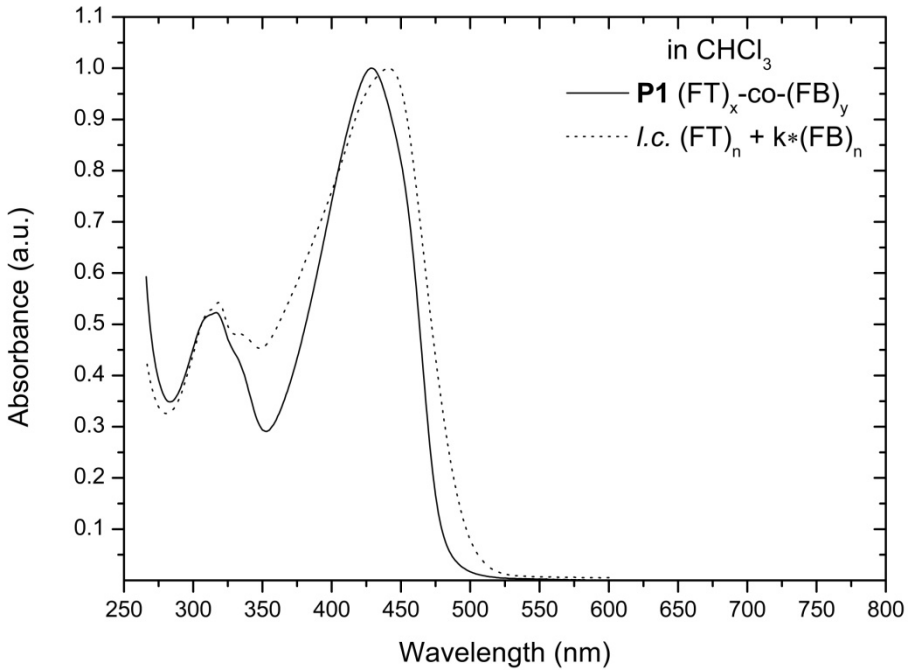

Figure 5.6 Normalized UV-Vis spectrum of random copolymer **P1** (solid line)compared to the spectrum of the linear combination of alternating polymer F-B and F-T spectra (dot line), both registered in $CHCl_3$ solution.

In **Figure 5.7** are reported the PL spectra of the low and high Mw copolymer **P1**. Unlike the shift of the absorption maximum, the emission maximum remains exactly in the same position. The emission is however less extended in the case of the polymer with a higher weight than the lower weight copolymer. This may be due to partial reduction of impurities that can quench the emission and/or different packing due to different molecular weights.

Autor's signature

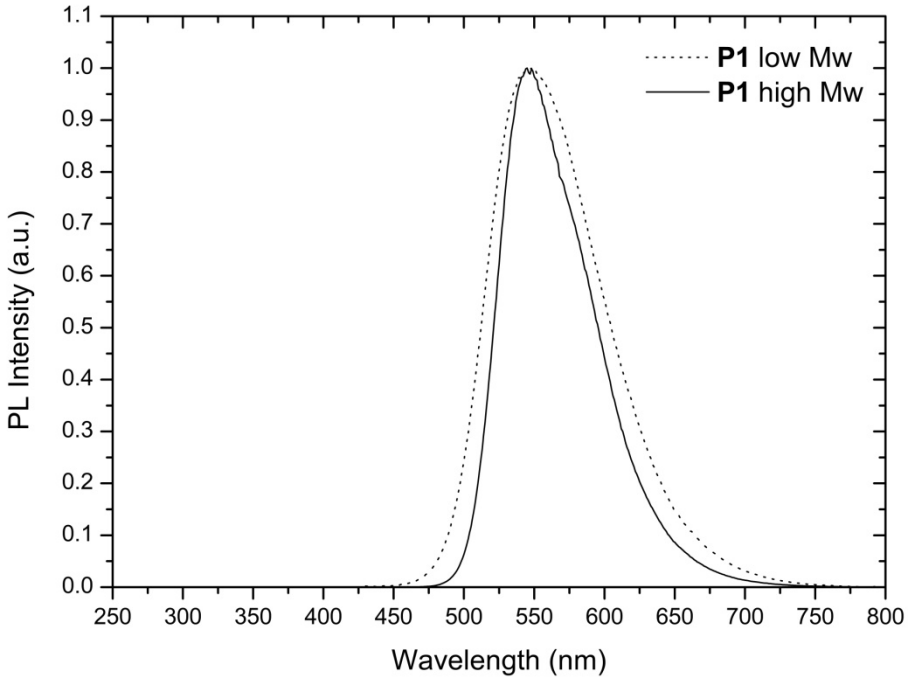

Figure 5.7 Normalized PL spectra of low Mw **P1** in thin film with λ_{exc}=415 nm (dot line) and high Mw P1 in thin film with λ_{exc}=450 nm (solid line).

The UV-Vis spectra of **P2** ($(TB)_x$-co-$(TF)_y$) (with low and high Mw) are shown in **Figure 5.8** in $CHCl_3$ solution and in thin film. All spectra displayed two distinct bands. The lower energy band is possibly due to a transition to a charge transfer state where the excited electron are localized on the benzothiadiazole electron-poor unit and the hole remains delocalized on fluorene and thiophene units, the higher energy band is associated to a delocalized excitonic π-π* transition showing exchange of double and single bonds.

Autor's signature

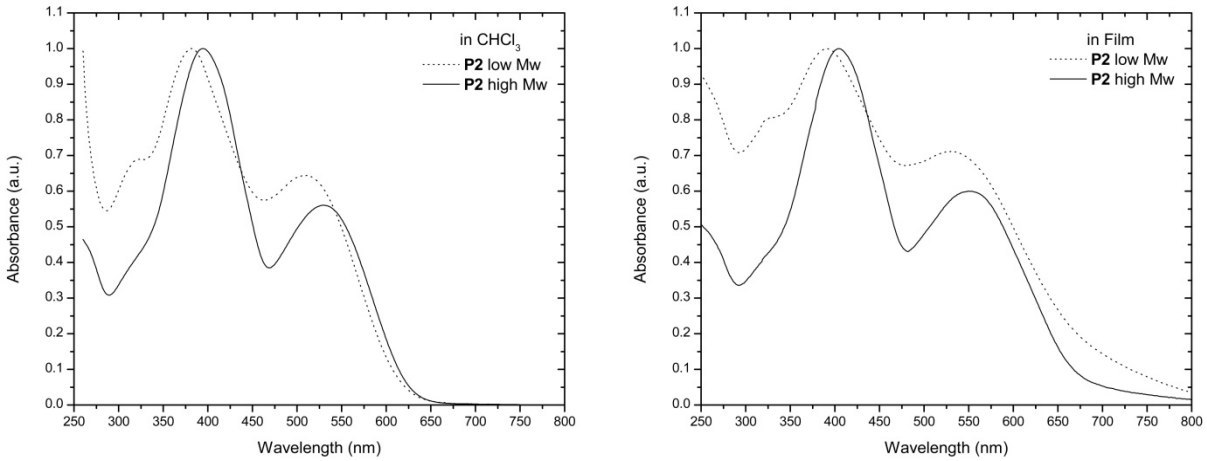

Figure 5.8 Normalized UV-Vis absorption spectra of copolymer **P2** in $CHCl_3$ solution (*Left*) and in thin film (*Right*).

The random copolymer **P2** in a strictly alternation of repeating units can be considered as the random version of the alternating copolymer **P4**. Indeed, **P2** compared to **P4** (see **Figure 5.9**) exhibits the same spectroscopic features. However, while the red band and the blue band of the alternating copolymers (**P4**) are similar in intensity, in **P2** the blue band is much more intense than the red one. Moreover, the blue band of the random copolymer is broader and slightly red-shifted. It can be speculated that these features of the conjugation band might arise from the large variety of structural situations present in the random structure compared to the alternating one.

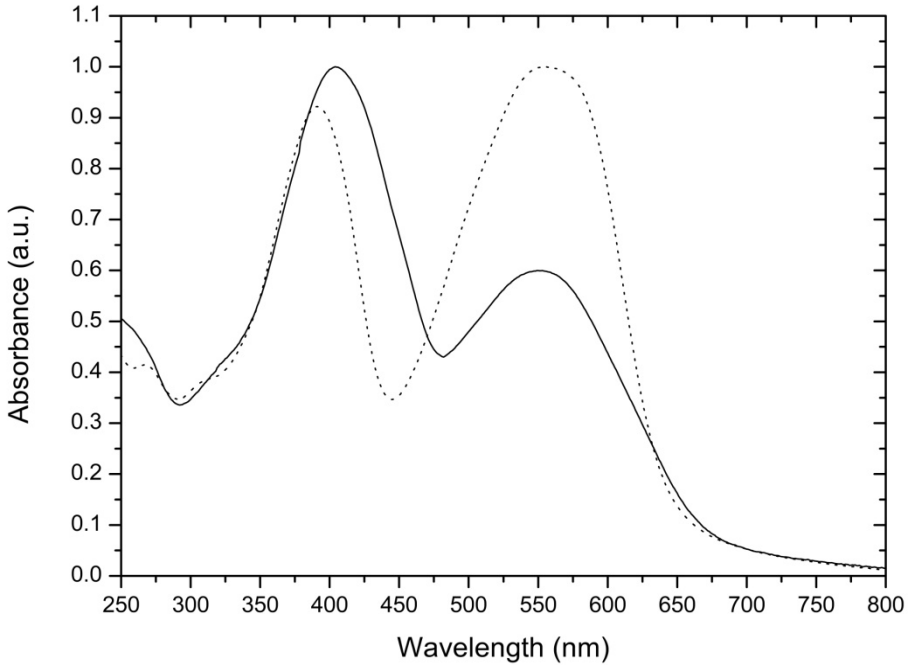

Figure 5.9 Normalized UV-Vis spectrum of high Mw **P2** compared to the UV-Vis spectrum of P4, both acquired on thin film.

P2 has a lower molecular weight than **P1**, and the ratio between electron rich/electron poor rings in the chain is comparable to **P1**. However, the perfect alternation between five- and six-membered rings along the chain favors the planarity of the structure. As a consequence, the absorption is shifted to lower energy.

In **Figure 5.10** is shown the PL spectra of the **P2** copolymer with high Mw compared to the PL spectrum of **P4**. This comparison is meaningful only in qualitative and not quantitative terms due to the difficulty to obtain two films, homogeneous and with the same absorption, from different copolymers. In this case only a blue-shift was observed in the random copolymer (**P2**) compared to the alternating copolymer (**P4**).

Autor's signature

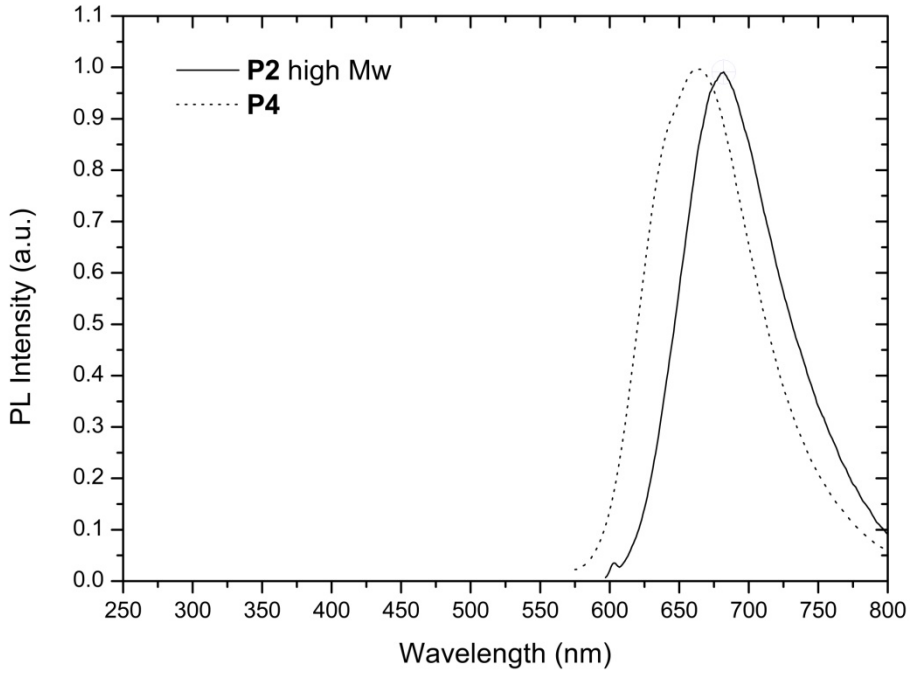

Figure 5.10 Normalized PL spectrum of high Mw **P2** with λ_{exc}=550 nm (solid line) compared to the PL spectrum of **P4** λ_{exc}=532 nm (dot line), both acquired on thin film.

The random copolymer **P3** ($(BT)_x$-co-$(BF)_y$) showed many problems for spectroscopy analysis due to very low solubility, the difficult to obtained a good film and the tendency to agglomerate. Different solvents were tested in order to obtain a good sample for optical analysis: Chloroform, orto-DiChloroBenzene and Cyclohesane. All films have a poor quality and exhibit a broad absorption band and a tail extending up to 1500 nm. As an example, in **Figure 5.11** are shown the spectra of **P3** copolymer in thin films. The scattering of the films makes difficult the estimation of the optical band gap. It's interesting to know the great difference of energy gap between all films. This can be attributed to the scattering of the samples or to stacking copolymer effect. The absorption peak at lower energy change shape with the change of solvent deposition. For this reasons, in **Table 5.3** are reported only the data on thin film from chloroform.

Autor's signature

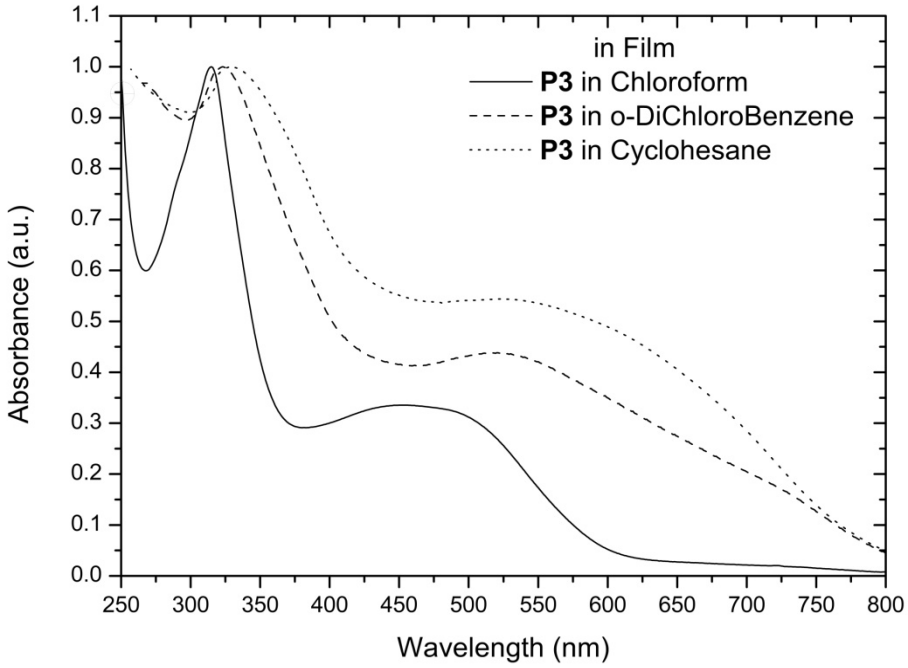

Figure 5.11 Normalized UV-Vis spectra of **P3** in thin film from Chlorofrom (solid line), o-DichloroBenzene (dash line), Cyclohesane (dot line).

A synthesis of a copolymer with a longer chains should lead to the deposition of a better film and hence eliminate the scattering allowing a precision estimation of the optical band gap.

The purification process not affected the UV-Vis spectra of all copolymers.

Table 5.3 UV-Vis data of **P1-P4** copolymers with high molecular weight, in $CHCl_3$ solution and in thin film.

Entry	UV-Vis absorption			
	Solution		Thin Film	
	Eg^{opt} (eV)	λ_{max} (nm)	Eg^{opt} (eV)	λ_{max} (nm)
P1	2.51	310/443	2.38	320/449
P2	1.99	394/530	1.86	404/549
P3	--	--	1.40	315/451
P4	2.05	384/532	1.94	391/557

Autor's signature

5.5 DETECTION OF CHARGE TRANSFER BY PHOTOLUMINESCENCE QUENCHING

The quenching of photoluminescence of an appropriate donor copolymer by a suitable acceptor gives a first indication of an effective donor-acceptor charge transfer as described by Sariciftci et al. [11] for composite of p-conducting polymers and fullerene derivates.
The **Figure 5.12** contains the PL spectra of the alternating copolymer **P4** and blends of **P4** with PCBM in three different weight ratio. The spectra show a clear photoluminescence quenching effect. Indeed, the PL intensity of **P4** is sharply reduced (30 times) by addition of about 10% w/w of PCBM, and almost two order of magnitude by addition of about 50% w/w of PCBM; a further increase in PCBM quantities (100% w/w) leads to no significant changes in PL quenching. This finding demonstrates that the electron transfer efficiency from the photoexcited copolymer to the fullerene acceptor, and thus the photoluminescence quenching, increases with the PCBM concentration, suggesting that **P4** might be an effective copolymer donor for solar cells.

Autor's signature

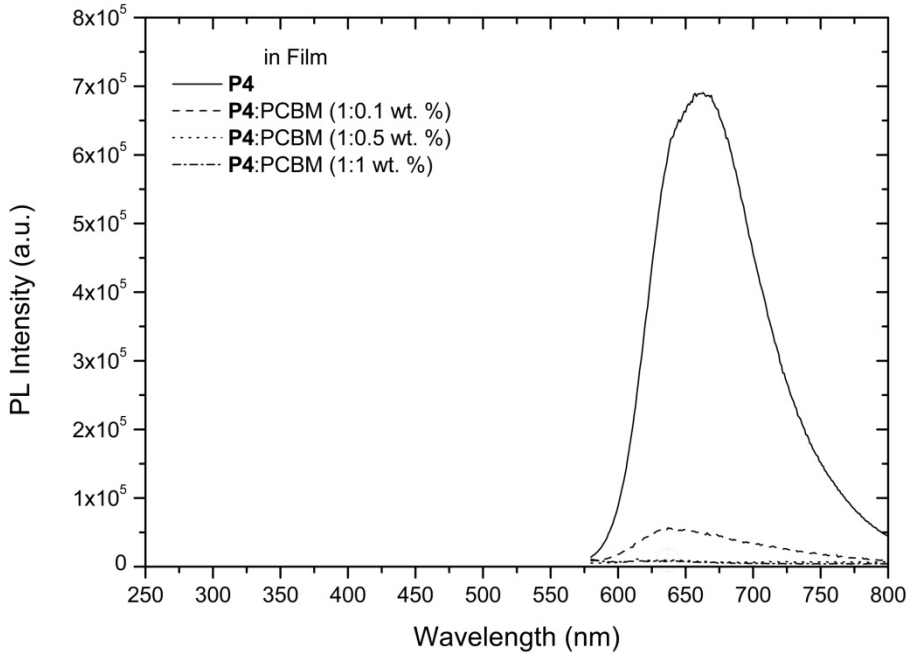

Figure 5.12 PL spectra of pristine film **P4** (solid line) and of **P4** blends with PCBM (1:0.1 w/w) (dash line), (1:0.5 w/w) (dot line), (1:1 w/w) (dash dot line) with λ_{exc}=460 nm. For convenient, the intensity of blends is amplified of a factor 5.

The same behavior was found for **P1**/PCBM (**Figure 5.13**) and **P2**/PCBM (**Figure 5.14**), which is even more promising than **P1** for photovoltaic applications, thanks to its lower energy gap.

Autor's signature

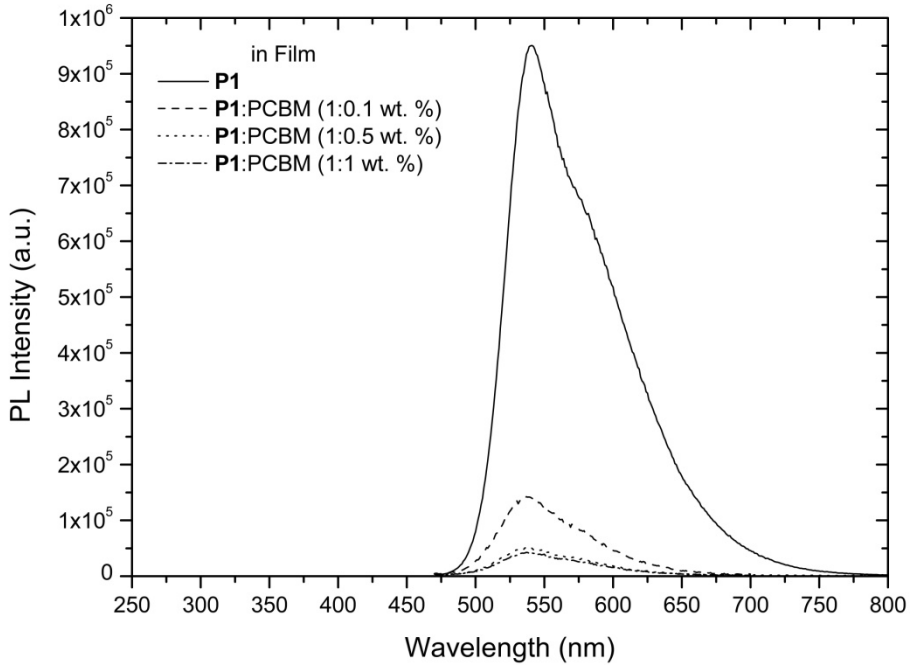

Figure 5.13 PL spectra of pristine film **P1** (solid line) and of **P1** blends with PCBM (1:0.1 w/w) (dash line), (1:0.5 w/w) (dot line), (1:1 w/w) (dash dot line) with λ_{exc}=460 nm. For convenient, the intensity of blends is amplified of a factor 5.

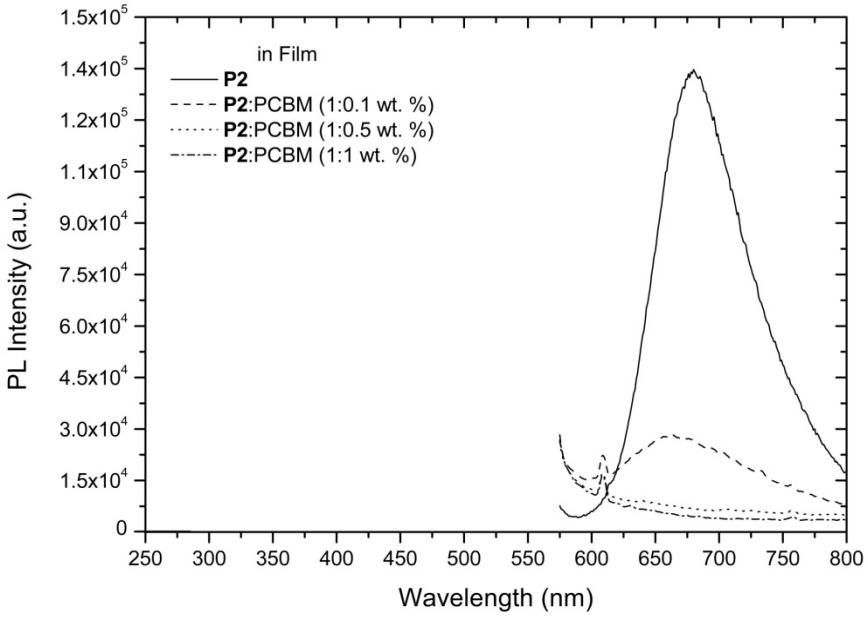

Figure 5.14 PL spectra of pristine film **P2** (solid line) and of **P2** blends with PCBM (1:0.1 w/w) (dash line), (1:0.5 w/w) (dot line), (1:1 w/w) (dash dot line) with λ_{exc}=460 nm. For convenient, the intensity of blends is amplified of a factor 5.

Autor's signature

P3 is photoluminescent only in solution. This can be attributed to intermolecular interaction or aggregates formation, which are strongly dependent on type of solid material considered, that promotes non-radiative decay of photoexcited state.

5.6 ELECTROCHEMICAL PROPERTIES

Cyclic voltammetry (CV) was employed to determine redox potentials of polymers and to estimate their HOMO and LUMO energy. Electrochemical data of **P1**-**P4** with low and high molecular weight, were calculated from the onsets of oxidation and reduction potentials according to the semi empirical equation [12]:

$$E_{HOMO/LUMO} = [-e\,(E_{onset(vs.SCE)} - E_{onset(Vreference\ vs\ SCE)})]-4.8\ [eV]$$

Electrochemical data of low (spectra not showed) and high molecular weight copolymers are tabulated in are reported in **Table 5.4**. The voltammograms of **P1**-**P4** copolymers with high MW after purification process are shown in **Figure 5.15**.

Table 5.4 Electrochemical data of **P1-P4** copolymers.

Entry	Cyclic Voltammetry								
	Low MW			High MW			After purification		
	HOMO (eV)	LUMO (eV)	Eg^{cv} (eV)	HOMO (eV)	LUMO (eV)	Eg^{cv} (eV)	HOMO (eV)	LUMO (eV)	Eg^{cv} (eV)
P1	-5.59	-2.99	2.60	-5.42	-2.49	2.93	-5.61	-2.87	2.74
P2	-5.41	-3.31	2.10	-5.29	-3.21	2.08	-5.31	-3.26	2.05
P3	-5.32	-3.31	2.01	--	--	--	-5.01	-3.40	1.61
P4	--	--	--	--	--	--	-5.38	-3.21	2.17

While, the optical measurements are not substantially affected of the purification process, the electrochemical measurements shown a pronunced difference expecially in the case of **P2** (see **Table 5.4**). Thus, there is a decrease of the energy gap with the conjugation length as a consequence of the molecular weight increase, like for UV-Vis measurements, but, in this case, this decrease is more pronounced after the purification process.

Autor's signature

In the cathodic zone, **P1**-**P2** voltammetric curves exhibit a chemically reversible reduction behaviour. The reduction onsets decrease in the order **P3**>**P2**>**P1**, a trend accounting for the fact that the polymer (**P3**) with the higher content of electron poor units (B) has the highest electron affinity, while the copolymer (P1) with the higher content of electron rich units (F) has the lowest electron affinity. In the anodic zone, the oxidation behavior of **P1** and **P2** is chemically reversible, while the electron transfer in **P3** shows a tendency to irreversibility. The oxidation potentials are high for **P1** and **P2** (> 0.9 vs Fc+/Fc), according with the donor character of this class of conjugated polymers. The oxidation onsets decrease in the order **P1**>**P2**>**P3** consistently with the ionization potentials expected on the basis of the balance of electron rich/electron poor groups. The distance between first oxidation and reduction peak is not rigid, but increase in the series **P3**<**P2**<**P1** with the introduction of electron rich groups**.** This evidence suggests that the incipient radical cation and anion are differently delocalized on the conjugated system. Furthermore, molecular geometry and conjugation affect the electrochemical bandgap. In **P1** the loss of planarity, and consequently the loss in conjugation, could be another reason of difficult oxidation and reduction.

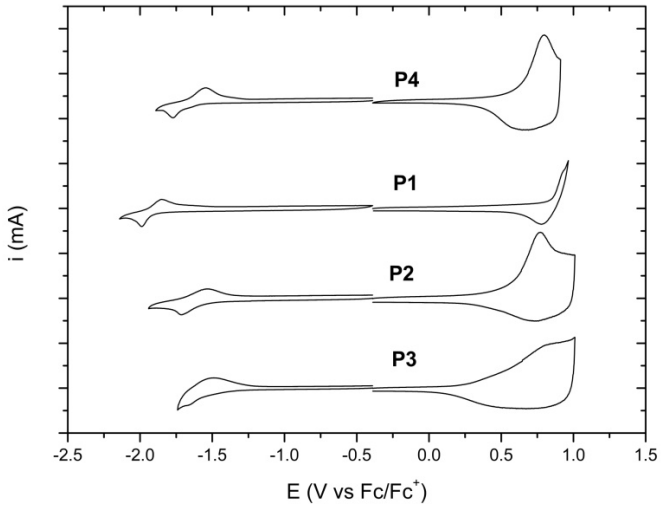

Figure 5.15 Voltammograms of **P1-P4** copolymers with high MW after purification process.

For all investigated polymers the electrochemical gap is greater than the optical gap calculated from the UV-Vis spectra (see **Table 5.3**). This discrepancy is usually related to the

Autor's signature

charge carriers formation in voltammetric measurements [13]. These conclusion are valid for both copolymers with low and high molecular weight.

5.7 INVESTIGATION OF CHARGE TRANSFER BY EPR SPECTROSCOPY

In polymer solar cells the dominating processes are the generation of charge carriers by absorption of light, the separation of charge carrier pairs, and the motion of charge carriers to the electrodes. An effective method for investigation of the light induced charge carrier generation, of the separation and the recombination of charge carrier pairs is the electron paramagnetic resonance (EPR). The EPR methods can be subdivide in light-induced EPR (LEPR) and Time resolved-EPR (TR-EPR). The TR EPR methods may be classified in terms of the methods of detection as continuous wave (CW) and Fourier transform (FT) methods. The CW and FT methods are expected to differ somewhat in terms of sensitivity and resolution due to differences in the technical aspects of data acquisition and analysis.
In the follow sections are discussed the TR-EPR and LEPR spectra of the pristine copolymers and of the mixture of copolymers/PCBM. All measurements are made on low molecular weight random copolymers.

5.7.1 TR-EPR SPECTRA ANALYSIS PERFORMED ON PRISTINE POLYMERS

All TR-EPR spectra were acquired on samples in frozen solution at low temperature, typically 120K, for obtained a rigid matrix in which material molecules are dispersed and not interacting with each other. All spectra can be attributed to transient molecular states of triplet (S = 1), photogenerated by pulsed laser. These transient species have lifetimes of typically few microseconds at 120K. For spectral simulation and analysis in EPR was used EasySpin, a comprehensive software package based on Matlab [14].
The triplet species are characterized by follow parameters: the Zero Field Splitting (ZFS), the values of the g tensor and the initial populations of the sublevels of spin (denoted by Px, Py, Pz), which are different from those of equilibrium (spin-polarized triplets).

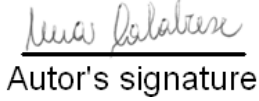

Analysis of these spectra was based on the spectral simulation from EPR spectra calculated for the spin-polarized triplet. ZFS and the populations parameters that better simulate the experimental spectra are the result of the spectra eleboration.

The spectra of the alternating copolymer **P4** in o-Dichlorobenzene solution at 120K, excited with the second harmonic of a Nd:YAG laser (λ=532 nm), is shown in **Figure 5.16**.

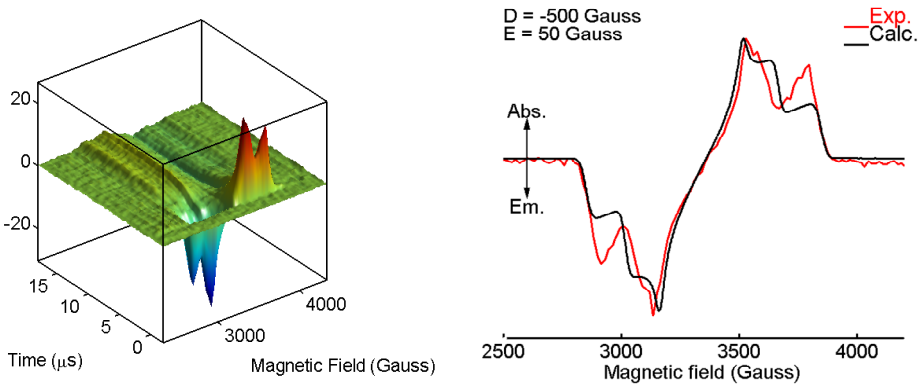

Figure 5.16 *Left:* TR-EPR dataset (intensity vs. Field / time) of **P4** in o-DCB solution. *Right*: TR-EPR spectrum extracted at time t = 0.5 microseconds (red curve) and its spectral simulation (black curve).

The TR-EPR spectrum of **P4**, assigned to the triplet excited state, has a great intensity, and this indicates an effective ISC mechanism from the singlet excited state. The spectrum has been simulated with ZFS parameters very similar to those obtained in frozen solution (reported in **Table 5.5**). However, attempts to fit the shape of the spectrum using populations px , py , pz for the three Cartesian triplet levels were not successful. Indeed, the simulation doesn't reproduce faithfully the experimental spectrum. Probably in the experimental spectrum there is the presence of more than one triplet state, with different values of ZFS and populations. **Table 5.5** shows the ZFS parameters and the populations obtained from the simulation of the spectrum as a single triplet state. As regards the mechanism of population of the sublevels of the triplet, the Px, Py and Pz values indicate the preferential population of a single sublayer of spin (Tz).

Autor's signature

Table 5.5 ZFS values and populations of the triplet of the alternating copolymer P4.

	P4
D (Gauss)	-500
E (Gauss)	50
Px : Py : Pz	0.1 : 0.1 : 1.0

The spectra of the random copolymer **P1** in o-Dichlorobenzene solution at 120K, excited with the second harmonic of a Nd:YAG laser (λ=532 nm), is shown in **Figure 5.17**.

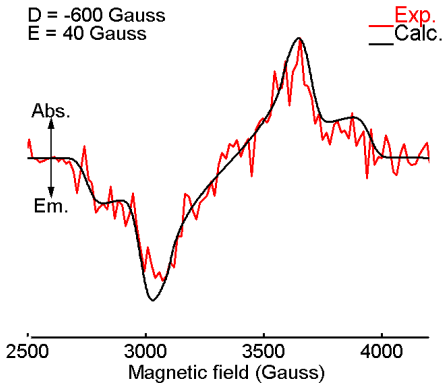

Figure 5.17 TR-EPR spectrum of **P1** extracted at time t = 0.5 microseconds (red curve) and its spectral simulation (black curve).

The TR-EPR spectrum of the polymer **P1**, assigned to the triplet excited state, is weak showing a reduction of the efficiency of the mechanism of ISC. The low value of signal/noise ratio does not permit to suppose the presence of different triplet signals. **Table 5.6** shows the ZFS parameters and the populations obtained from the simulation as a single triplet state. As regards the mechanism of population of the sublevels of the triplet, the values of Px, Py and Pz indicate a splitting of population between two levels (Ty and Tz).

Table 5.6 ZFS values and populations of the triplet of the random copolymer **P1.**

	P1
D (Gauss)	-600

Autor's signature

E (Gauss)	40
Px : Py : Pz	0.2 : 0.6 : 1.0

The spectra of the random copolymer **P2** with low molecular weight in o-Dichlorobenzene solution at 120K, excited with the second harmonic of a Nd:YAG laser (λ=532 nm), is shown in **Figure 5.18**.

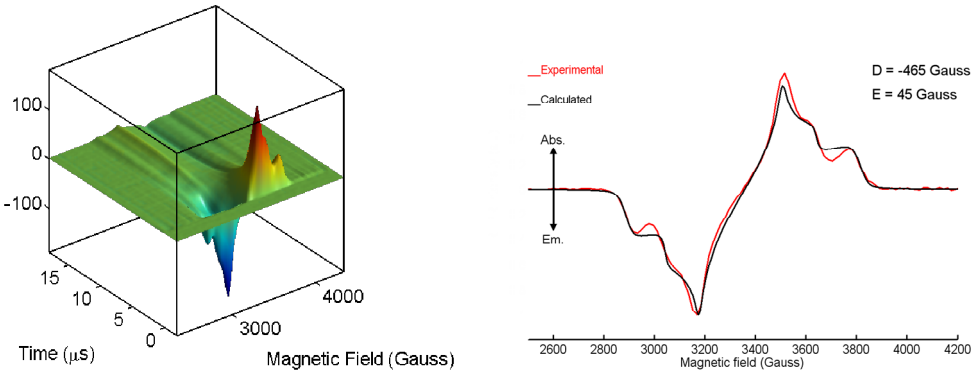

Figure 5.18 *Left:* TR-EPR dataset (intensity vs. Field / time) of **P2** in o-DCB solution. *Right*: TR-EPR spectrum extracted at time t = 0.5 microseconds (red curve) and its spectral simulation (black curve).

The TR-EPR spectrum of the random copolymer **P2**, is intense (efficient ISC). Even in this case the simulation not reproduces well the experimental spectrum for the presence of more than one triplet state, with different values of ZFS and different populations. **Table 5.7** shows the ZFS parameters and the populations obtained from the simulation of the spectrum as a single triplet state. As regards the mechanism of population of the sublevels of the triplet, the values of Px, Py and Pz indicate the preferential population of a single sublayer of spin (Tz).

Table 5.7 ZFS values and populations of the triplet of the random copolymer **P2.**

	P2
D (Gauss)	-465
E (Gauss)	45
Px : Py : Pz	0.2 : 0.0 : 1.0

Autor's signature

The spectra of the random copolymer **P3** with low molecular weight in o-Dichlorobenzene solution at 120K, excited with the second harmonic of a Nd:YAG laser (λ=532 nm), is shown in **Figure 5.19**.

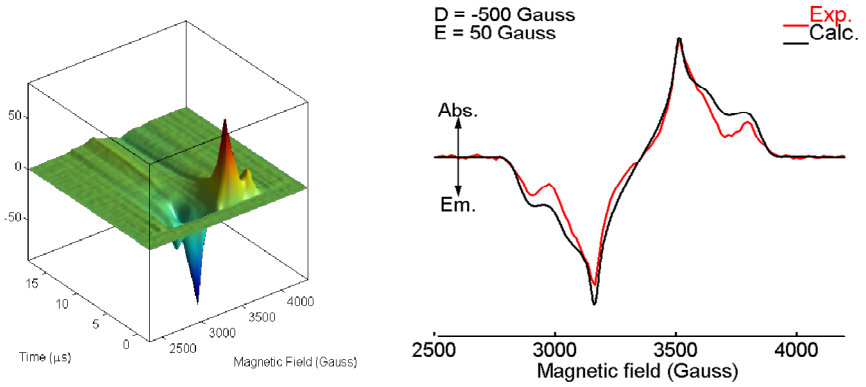

Figure 5.19 *Left*: TR-EPR dataset (intensity vs. Field / time) of **P3** in o-DCB solution. *Right*: TR-EPR spectrum extracted at time t = 0.5 microseconds (red curve) and its spectral simulation (black curve).

The TR-EPR spectrum of the random copolymer **P3**, is intense (efficient ISC). The simulation doesn't reproduce faithfully the experimental spectrum, perhaps because of the presence of more than one triplet state, with different values of ZFS and populations. **Table 5.8** shows the ZFS parameters and the populations obtained from the simulation of the spectrum as a single triplet state. As regards the mechanism of population of the sublevels of the triplet, the values of Px, Py and Pz indicate the preferential population of a single sublayer of spin (Tz).

Table 5.8 ZFS values and populations of the triplet of the random copolymer **P3.**

	P3
D (Gauss)	-500
E (Gauss)	50
Px : Py : Pz	0.2 : 0.0 : 1.0

The TR-EPR measurements on the series of copolymers indicate, in all cases examined, the formation of triplet states with different efficiencies as a conseguence of the

Autor's signature

photoexcitation. The Jablonsky diagram describing the experimental observations is shown in **Figure 5.20**.

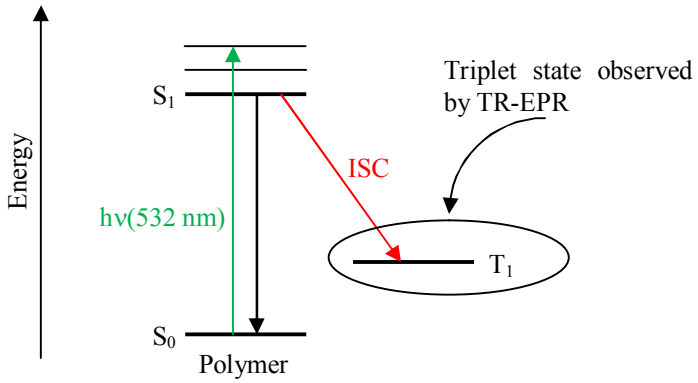

Figure 5.20 Jablonsky diagram describing the excited state observed by TR-EPR.

5.7.2 TR-EPR SPECTRA ANALYSIS ON POLYMERS BLENDED WITH FULLERENE

The TR-EPR spectra recorded in solid mixtures of polymer/PCBM indicate the presence of a variety of molecular species generated by impulse laser excited:

a) triplet state, localized or mobile

b) Pairs of interacting radicals (spin-correlated radical pair, SCRP)

c) non-interacting radicals (free radical pair, RP)

The analysis of the spectra is therefore dependent on the sample: for spectra that exhibit characteristics of type a), the analysis was performed in the same manner describe in the previous section.

The spectra of the blend **P4**/PCBM on film from o-Dichlorobenzene at 120K, excited with the second harmonic of a Nd:YAG laser (λ=532 nm), is shown in **Figure 5.21**. At the wavelength used for this experiment both species are photoexcited, but the absorption coefficient is higher for the alternating copolymer **P4**.

Autor's signature

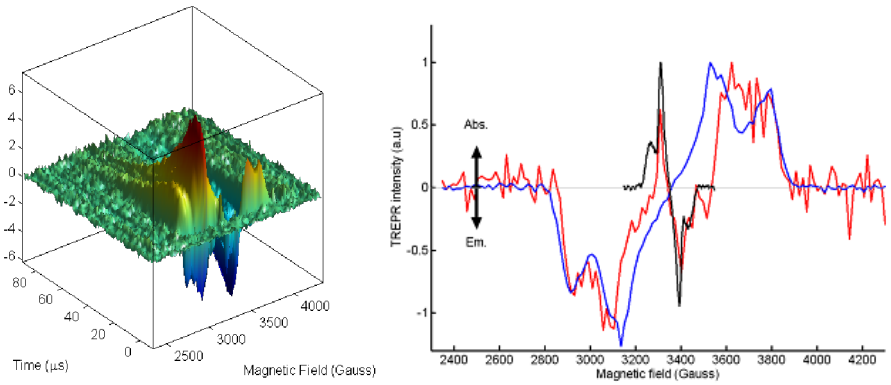

Figure 5.21 *Left* TR-EPR dataset (intensity vs. Field / time) of the blend **P4**/PCBM (1:1 w/w) on film from o-DCB. *Right* : TR-EPR spectrum extracted at time t = 0.5 microseconds of PCBM (black curve), **P4** (red curve) and **P4**/PCBM (red curve).

The interpretation of the blend spectrum is based on a comparison with the spectrum of the pristine copolymer and PCBM both in frozen matrix. The spectrum of the mixture is the sum of two this two contributions. This means that the photoexcitation produces the triplet state both in the PCBM and in the copolymer. Additional information can be obtained by examining the spectrum of the mixture at delays greater than 0.5 microseconds after the laser pulse. This spectrum is shown in **Figure 5.22**.

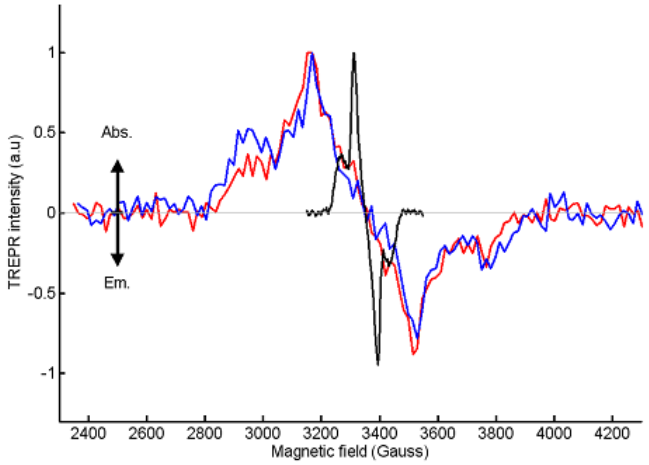

Autor's signature

Figure 5.22 TR-EPR spectrum extracted at time t = 10 microseconds of PCBM (black curve) and **P4** (red curve) in frozen matrix and **P4**/PCBM (red curve) on film (*Right*).

After 10 microseconds the PCBM component has completely disappeared, which is unusual considering that the TR-EPR spectrum of PCBM in frozen matrix persists for hundreds of microseconds at T = 120K. This phenomena can be explained considering that the energy was transferred from the triplet of PCBM to the triplet of the polymer. The triplet state of copolymer (**P4**) is greater in intensity (but with reversed polarity) compared to the value of 0.5 microseconds. In order that the Triplet-Triplet energy transfer from PCBM to copolymer occur it is necessary that the PCBM triplet energy is higher. The Jablonski diagram of this mixture is shown in **Figure 5.23**.

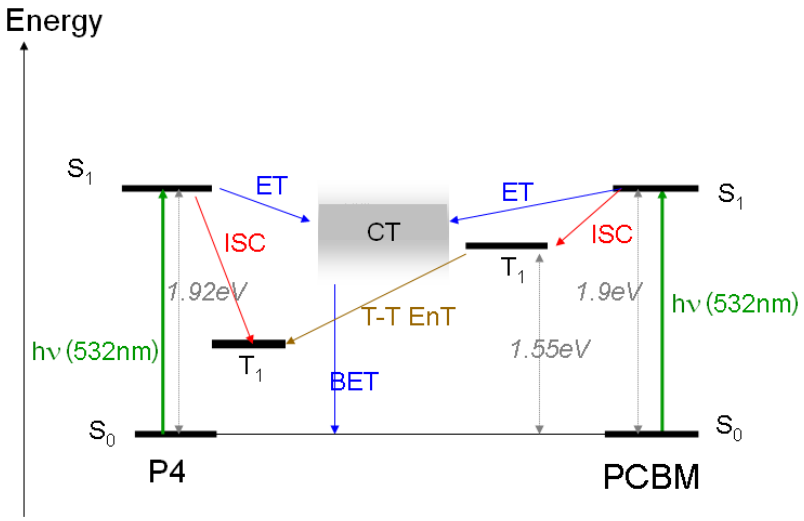

Figure 5.23 Jablonski diagram describing the blend P4/PCBM photophysics.

The spectra of the blend **P1**/PCBM on film from o-Dichlorobenzene at 120K, excited with the second harmonic of a Nd:YAG laser (λ=532 nm), is shown in **Figure 5.24**. At the wavelength used for this experiment the absorption coefficient of random copolymer **P1 is** very low.

Autor's signature

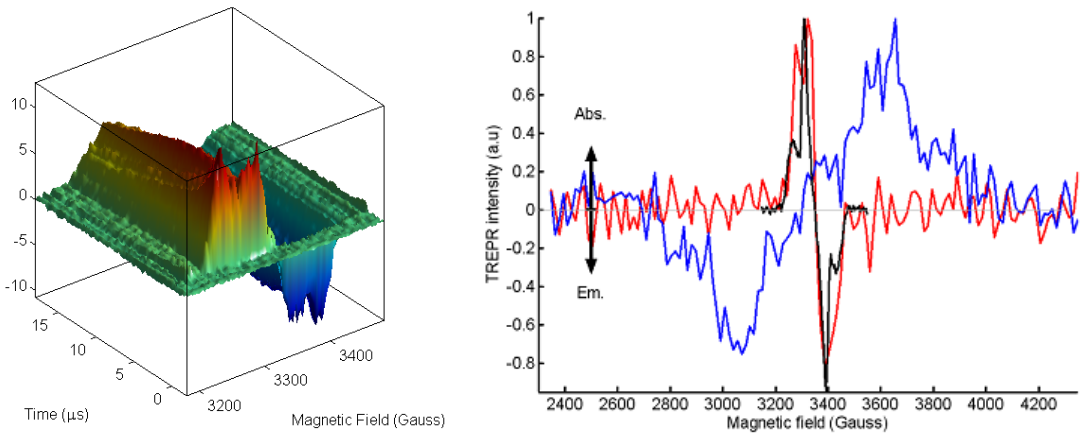

Figure 5.24 *Left*: TR-EPR dataset (intensity vs. Field / time) of the blend P1/PCBM (1:1 w/w) on film from o-DCB. *Right*:TR-EPR spectrum extracted at time t = 0.5 microseconds of PCBM (black curve), **P4** (red curve) and **P4**/PCBM (red curve).

In this case, the TR-EPR spectrum shows only the presence of the PCBM triplet, with anomalous polarization and a weak presence at the center of radical pair states, which are more visible in the spectra recorded at higher temperatures (see **Figure 5.25**).

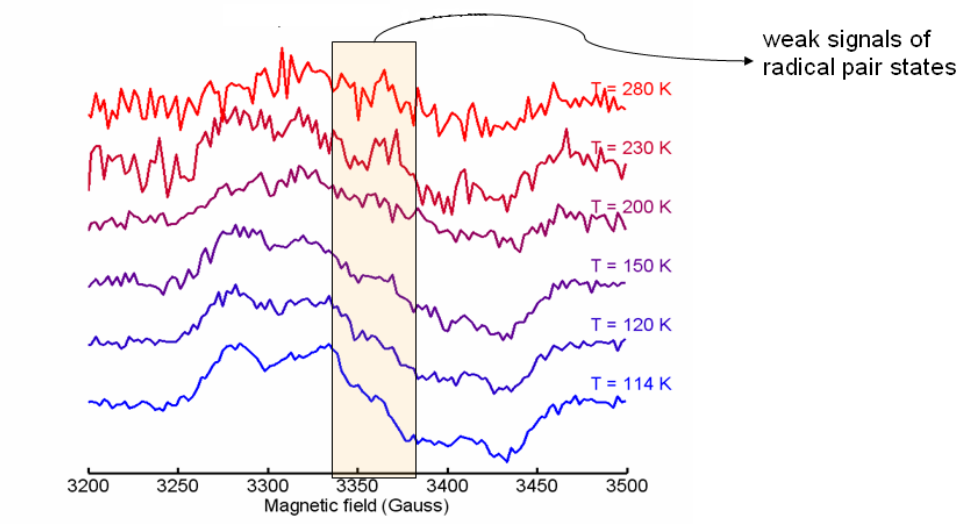

Figure 5.25 EPR spectrum extracted at time t = 0.5 microseconds of the blend **P1**/PCBM (1:1 w/w) on film from o-DCB at different temperatures.

Even in this case (as in the case of polymer blend **P4**/PCBM) was observed, in part, the CT (generated by electron transfer from copolymer to PCBM) and especially the product of

Autor's signature

recombination of the CT state, that is the PCBM triplet state, which is therefore the excited state to lower energy. The Jablonski diagram of the mixture is shown in **Figure 5.26**.

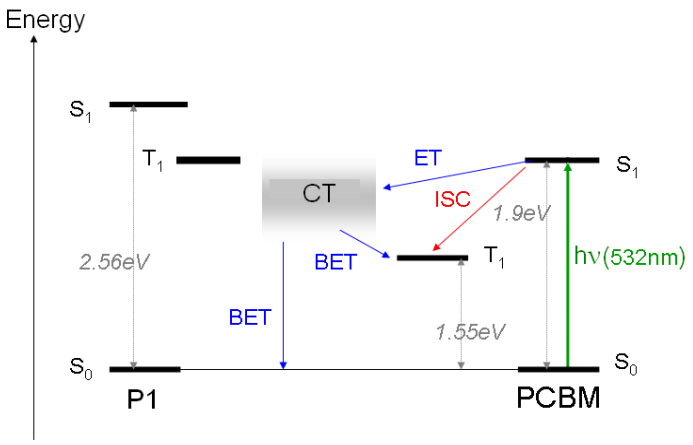

Figure 5.26 Jablonski diagram describing the blend **P1**/PCBM photophysics**.**

The spectra of the blend **P2**/PCBM on film from o-Dichlorobenzene at 120K, excited with the second harmonic of a Nd:YAG laser (λ=532 nm), is shown in **Figure 5.27**. At this wavelength the absorption of the copolymer is predominantly compared to PCBM.

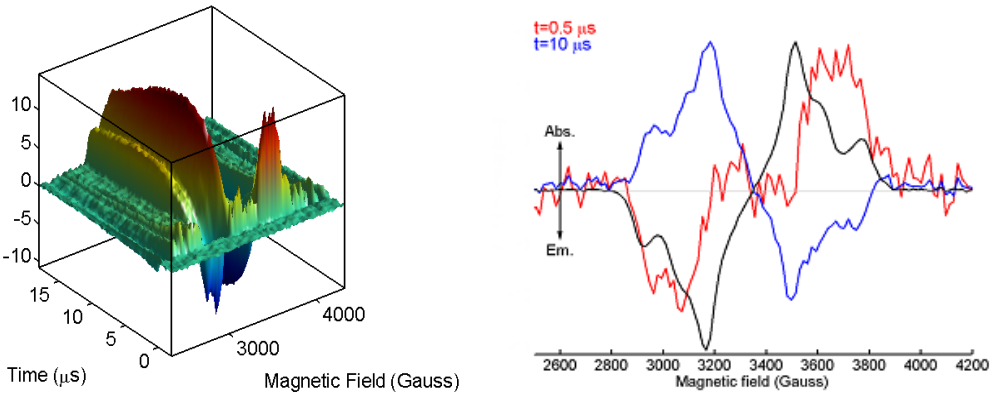

Figure 5.27 *Left*: TR-EPR dataset (intensity vs. Field / time) of the blend **P2**/PCBM (1:1 w/w) on film from o-DCB. TR-EPR spectrum extracted at time t = 0.5 microseconds (red curve), at time t = 10 microseconds (blue curve) and the spectrum of **P2** in frozen matrix (black curve).

The pattern of energy levels of spin and its photophysical processes is shown in **Figure 5.28**.

Autor's signature

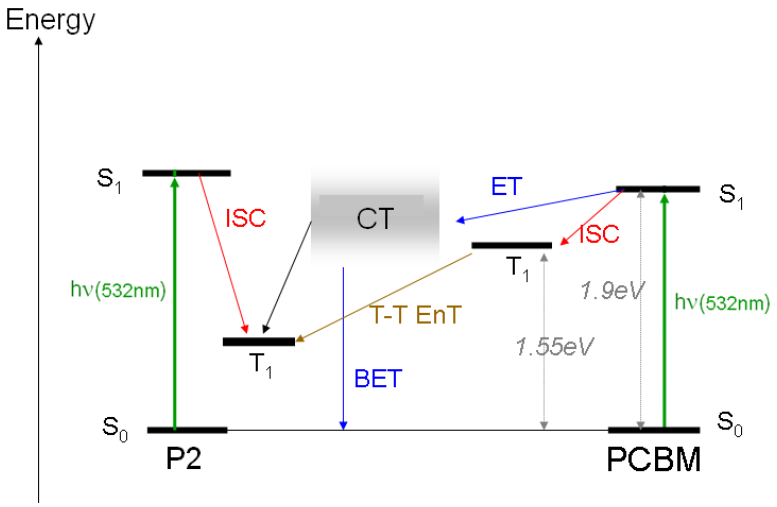

Figure 5.28 Jablonski diagram describing the blend **P2**/PCBM photophysics**.**

The spectra of the blend **P3**/PCBM on film from o-Dichlorobenzene at 120K, excited with the second harmonic of a Nd:YAG laser (λ=532 nm), is shown in **Figure 5.29**. At this wavelength the absorption of the copolymer is predominantly compared to PCBM.

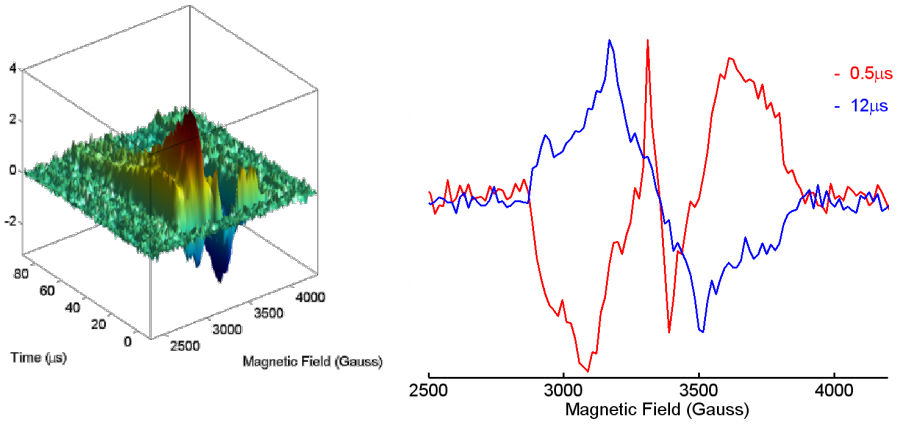

Figure 5.29 *Left*: TR-EPR dataset (intensity vs. Field / time) of the blend **P3**/PCBM (1:1 w/w) on film from o-DCB. *Right*:TR-EPR spectrum extracted at time t = 0.5 microseconds (red curve), at time t = 12 microseconds (blue curve) and **P3**/PCBM (black curve).

Also for this copolymer is observed initially (at 0.5 microseconds), the characteristic spectrum of the triplet of the copolymer (**P3**) with the presence of the triplet spectrum of

Autor's signature

PCBM in the center. At longer times (12 microseconds) the polarization spectrum is reversed and the signal of the PCBM triplet disappears. So this situation is similar to that already observed for the copolymer **P4** and described by the Jablonski diagram in **Figure 5.30**.

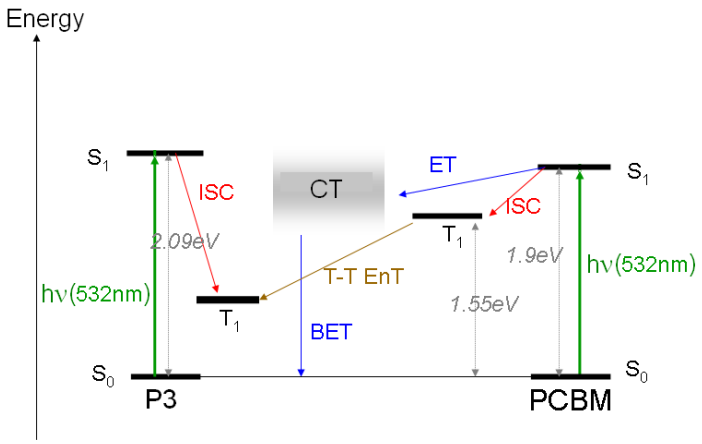

Figure 5.30 Jablonski diagram describing the blend **P3**/PCBM photophysics**.**

The TR-EPR measurements of the blend copolymer/PCBM showed at least two different types of behavior:

1. Blends of **P2, P3** and **P4**with PCBM showed the formation of independent states of the polymer and the PCBM triplet. However PCBM triplet energy is transferred quickly to the triplet state of the copolymer, which then is the excited at lower energy. Also in this case the charge separation can occur and immediate charge recombination can occur with production of the triplet state of the copolymer.
2. Blend of **P1** with PCBM showed only the triplet state of PCBM, which gets the state to lower energy.

Considering the simplified scheme introduced by Janssen [15], the cases examined fall into a category B (see **Figure 5.31**), where, however, the state T can be either the triplet state of PCBM (in the case of the blend **P1**/PCBM) or the triplet state of the copolymer (in the case of the blends **P2, P3, P4**/PCBM).

Autor's signature

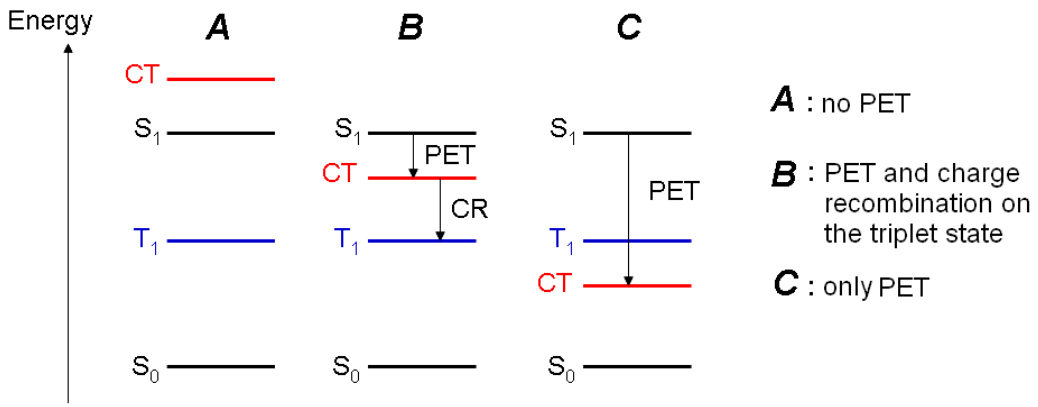

Figure 5.31 Schematic diagram of possible arrangements of energy levels of a polymer/PCBM and related efficient photophysical processes (electron transfer PET and / or recombination) in this system depending on the energy involved. S1 and T1 in the diagram represent the excited singlet and triplet of the polymer and / or PCBM, CT is the torque generated by electronic transfer.

5.7.3 LEPR SPECTRA ANALYSIS ON SOLID MIXTURES OF POLYMERS/PCBM

The LESR experimental procedure consisted of the following sequence:

1. scan the spectrum of the sample before illumination (Dark);
2. scan the ESR spectrum of the no-illuminated sample (Light OFF);
3. scan the ESR spectrum under light illumination (Light ON).

For all samples tested were found two EPR signals which were attributed to the positive polaron (P^+) or radical cation on the copolymer chain and the radical anion on the fullerene ($PCBM^-$) The assignment was made on the basis of the g factors of the lines observed in the LEPR spectra. ($g_{PCBM} \cong 1.9999$), $g_{P^+} \cong 2.0020\text{-}2.0040$). The experimental errors on the g factors are about $\Delta g = \pm 0.0005$.

The spectra of the copolymers **P4** doped with PCBM in 1:1 w/w proportion are shown in **Figure 5.32**.

Autor's signature

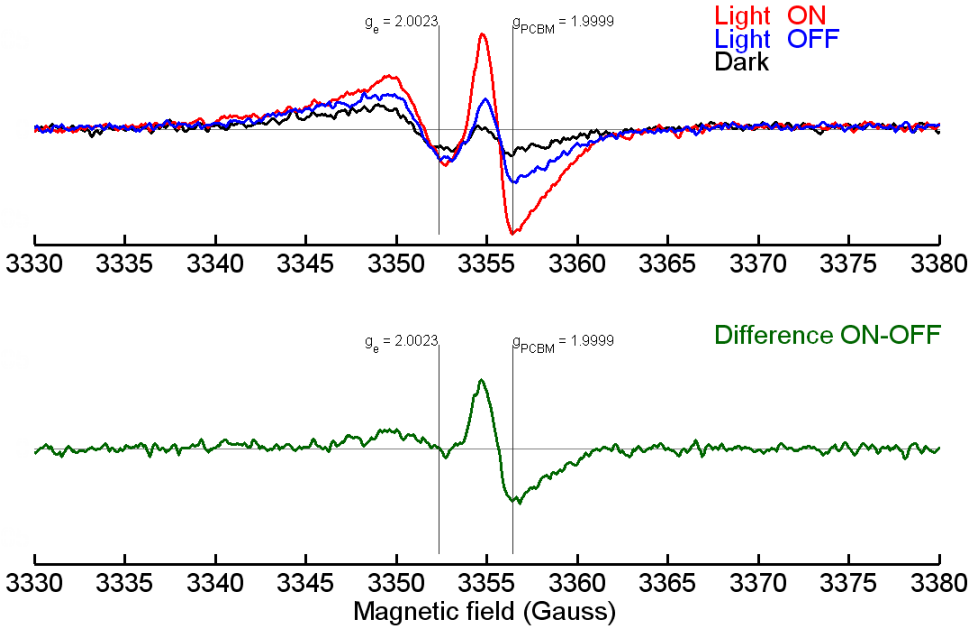

Figure 5.32 LESR spectra of the blend **P4**/PCBM (1:1 w/w) on film from o-DCB, T=120K, $\lambda_{exc.}$= 532 nm.

LESR spectra of the blend **P4**/PCBM shows:

- the presence of the positive polaron (P^+) on the copolymer chain and the radical anion on the fullerene ($PCBM^-$) in the dark;
- the increase of intensity of both signals when light is switch ON;
- slow decrease of both signals when light is switch OFF.

This means that the charge transfer, namely the main process in the blends, has occurred. Since it is much more likely that charge transfer occurs between adjacent molecular species (copolymer (**P4**) and PCBM), can be concluded that there is a rapid spatial separation between the photoinduced charges, which is proposed to be responsible of long lifetime of the charge separated state in these systems, that allows their spectroscopical observation. The signals of polarons P^+ and of $PCBM^-$ decay approximately equal rapidity. The spectra of the copolymers **P1** doped with PCBM in 1:1 w/w proportion are shown in **Figure 5.33**.

Autor's signature

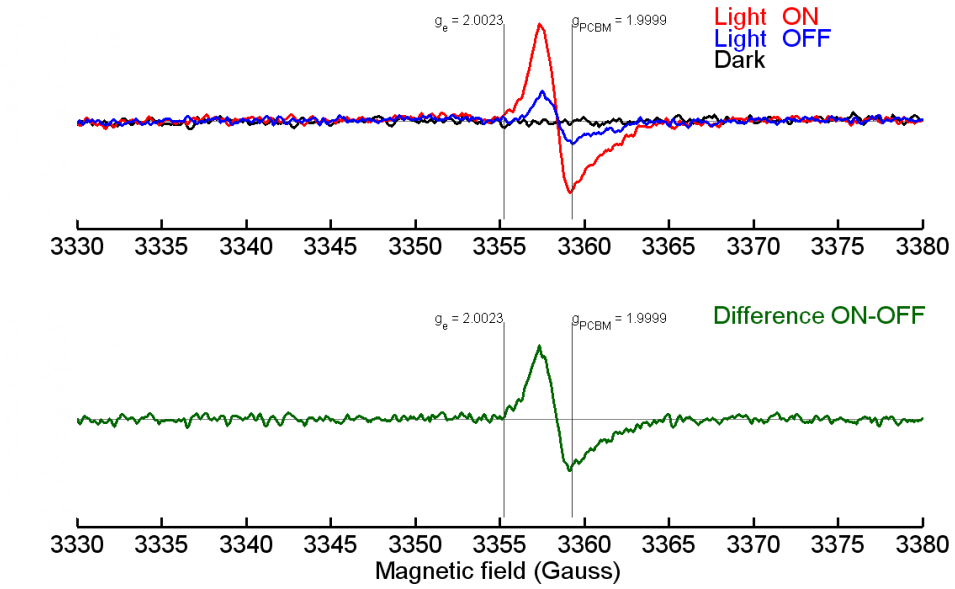

Figure 5.33 LESR spectra of the blend **P1**/PCBM (1:1 w/w) on film from o-DCB, T=120K, $\lambda_{exc.}$= 532 nm.

LESR spectra of the blend **P1**/PCBM shows:

- the absence of the positive polaron (P^+) on the copolymer chain and the radical anion on the fullerene ($PCBM^-$) in the dark;
- the presence of the only radical anion signal on the fullerene ($PCBM^-$) when light is switch ON;
- fast decrease of the radical anion signal when light is switch OFF.

In this case the positive polaron (P^+) on the copolymer (**P1**) has a lower lifetime than the radical anion on the fullerene ($PCBM^-$).

The spectra of the copolymers **P2** doped with PCBM in 1:1 w/w proportion are shown in **Figure 5.34**.

Autor's signature

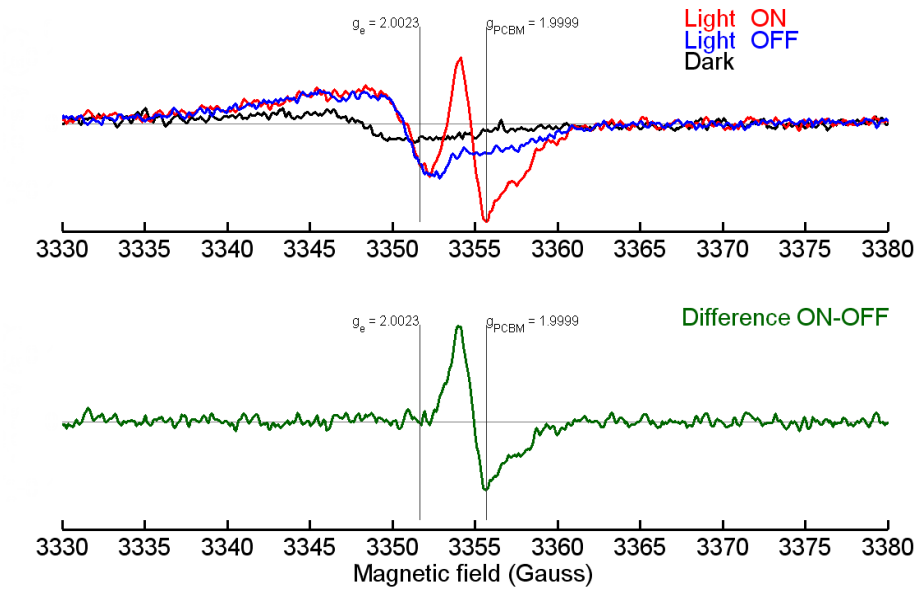

Figure 5.34 LESR spectra of the blend P2/PCBM (1:1 w/w) on film from o-DCB, T=120K, $\lambda_{exc.}$= 532 nm.

LESR spectra of the blend **P2**/PCBM shows:

- the presence of the weak positive polaron (P^+) on the copolymer chain in the dark;
- the presence of the positive polaron (P^+) on the copolymer chain and the radical anion on the fullerene ($PCBM^-$) when light is switch ON;
- the persistence of the positive polaron (P^+) signal on the copolymer and fast decrease of the radical anion signal when light is switch OFF;
- in the spectrum difference remains only the signal of the PCBM anion

In this case the traps in the copolymer (**P2**) are at deeper energy than those of the PCBM anion.

The spectra of the copolymers **P3** doped with PCBM in 1:1 w/w proportion are shown in **Figure 5.35**.

Autor's signature

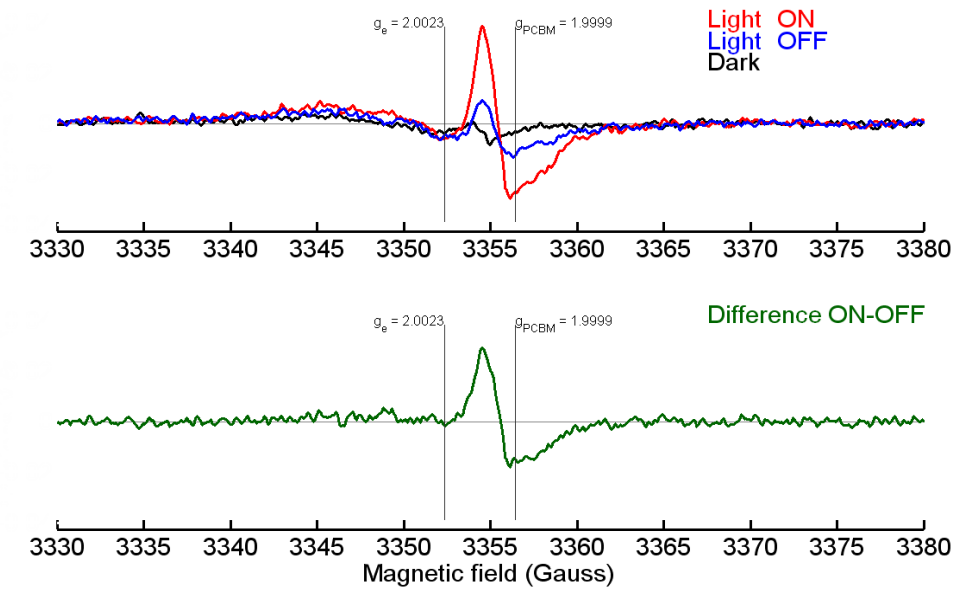

Figure 5.35 LESR spectra of the blend **P3**/PCBM (1:1 w/w) on film from o-DCB, T=120K, $\lambda_{exc.}$= 532 nm.

LESR spectra of the blend **P3**/PCBM shows:

- the presence of the weak positive polaron (P^+) signal on the copolymer chain and the weak radical anion signal on the fullerene ($PCBM^-$) in the dark;
- the presence of a weak positive polaron (P^+) signal and an intense radical anion signal ($PCBM^-$) when light is switch ON;
- the persistence of the positive polaron (P^+) signal on the copolymer and a pronounced decrease of the radical anion ($PCBM^-$) signal when light is switch OFF;
- in the spectrum difference remains only the signal of the PCBM anion

For the study of recombination of separated charges only the decay curves of the PCBM radical anions were measured by monitoring the LESR signal after switching light off. This is sufficient because it is assumed, as relatively probable, that in such systems charge neutrality exists in larger scales, that means the number of positive and negative charges is always equal. Moreover, in the case of a MDMO-PPV/PCBM composite it was proved by Schultz et al. [16] that the signals of polarons P^+ and of $PCBM^-$ decay approximately equally rapid. In **Figure 5.36** was reported the result for the ESR signal at the position of the PCBM anion as a function of time, in presence/absence of light. The switching off of the excitation light does not lead to the disappearance of the ESR signal at low temperatures.

Autor's signature

To eliminate the ESR spectrum completely, the sample had to be warmed up to room temperature (annealing).

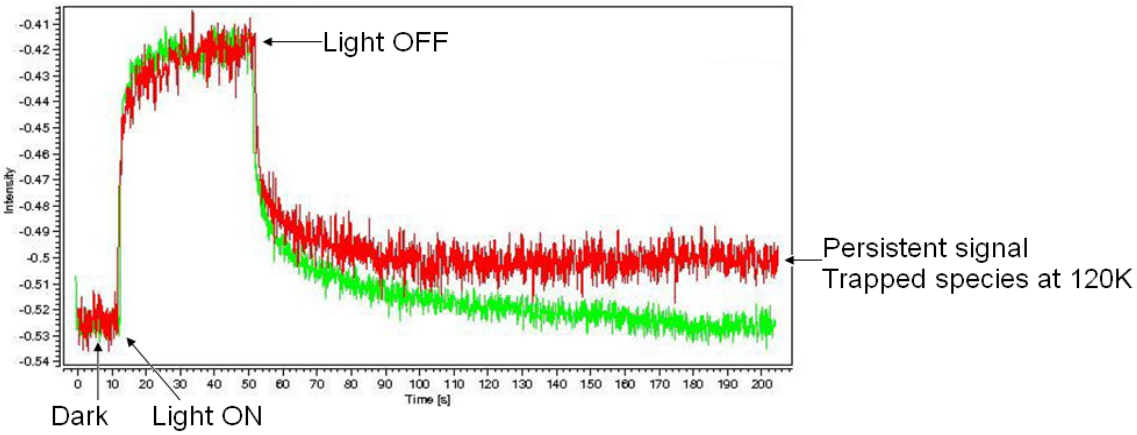

Figure 5.36 Rise and decay of PCBM radical anion (T= 120 K, λ_{exc}= 488 nm). Annealing (red line): after the measurement at 120 K the sample is warmed to room temperature and then measured at 120 K. No annealing (green line): the measurement was carried out without annealing.

The first level is the dark signal, then, when the sample is photoactivated the signal increases first abruptly and then more slowly until equilibrium is reached. A dramatic decrease of the signal is observed when the light switching off but it can be observed that the dark signal after light excitation is different from the one before light excitation hence there is a persistent signal that represented long lived species trapped in to material. The intensity of the residual signal decreases with temperature, because the trapped charges have enough thermal energy to dropout from the potential barriers.

This is shown in **Figure 5.37**.

Autor's signature

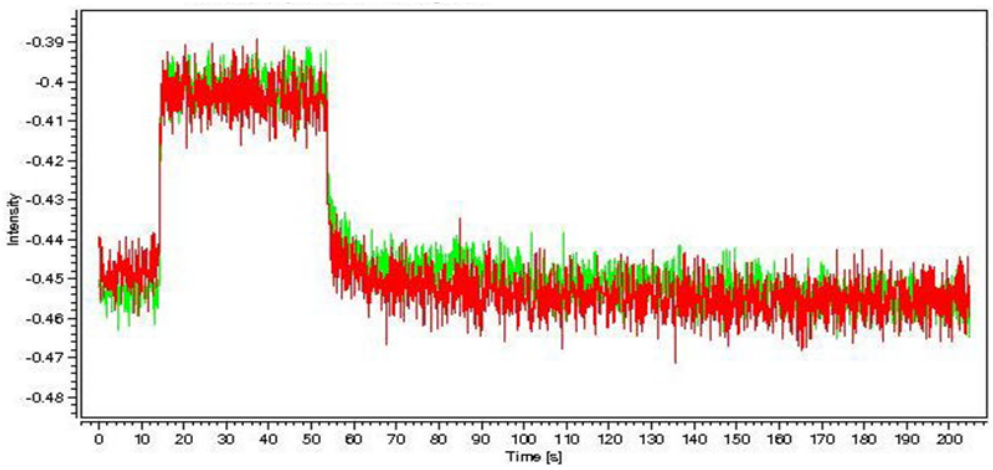

Figure 5.37 Rise and decay of PCBM radical anion (λ_{exc}= 488 nm).. Annealing (red line): after the measurement at 120 K the sample is warmed to room temperature and then measured at 140 K. No annealing (green line): the measurement was carried out without annealing .

The LESR of films of the pristine polymers with high molecular weith and blends with PCBM are reported in **Figure 5.38**

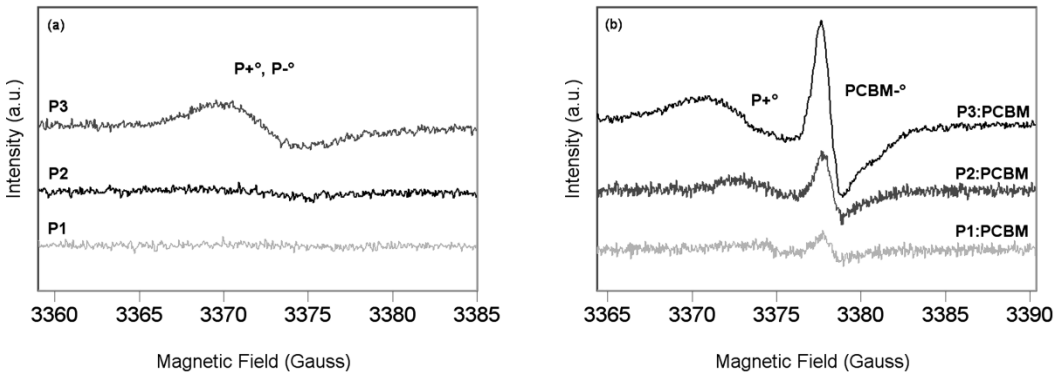

Figure 5.38 *Left*: LEPR of pristine copolymers with high molecular weight. *Right:* LEPR of copolymers blended with PCBM.

Concerning the pure copolymer films a photoinduced signal at g = 2 is observable **P3**, and, only in traces, in **P2**, and is assigned to photoinduced polarons P^+ on the base of comparison with g (P^+) = 2.002 in PAT [17] and at g (P^+) = 2.003 in PFO [35]. Polaron formation is presumably due to charge transfer occurring between adjacent polymer chain or also in an intramolecular process, between electron rich and electron pure moieties,

Autor's signature

favoured in P3 where they are present with the same abundance. No polaron signal is observed in polymer **P1**, where photoexcitation is more likely relaxed through an intramolecular radiative decay, as shown by its strong fluorescence. It is possible that the observed lack of fluorescence in the pure **P3** film is due on the opposite to the efficiency of a non radiative decay pathway through charge transfer. In spectra registered on all blend films both the $P^{+\circ}$ (g =2.002 (**P1**); g= 2.002 (**P2**) ; g = 2.003 (**P3**)) and $PCBM^{-\circ}$ (g= 1.9995 signals are observed, indicating the occurrence of some charge transfer towards the fullerene molecule, but with different relative intensity. The highest concentration of photoinduced charges is observed in **P3**, confirming the ability of this polymer to stabilize the ionic radical, observed also on the pristine polymer, and is lowest in **P1**. Note however that the ESR signal is due to the equilibrium population over 10 μs integration due to the ESR detection at 100 KHz modulation, so that the contribution of very quickly recombining charges is lost. Therefore the failure in observing an intense LESR spectrum of trapped charge species does not mean that charge transfer has not occurred, but that the equilibrium population of charge transfer state is low, either because of weak generation or as an effect of strong recombination. From this point of view there is not any contradiction with fluorescence quench results on this same system, showing that charge transfer occurs efficiently also in **P1**; evidences from fluorescence and LESR suggest that in **P1**:PCBM there is a strong charge recombination. In addition, the LESR spectrum shows that charge transfer can be photoinduced also in **P3**:PCBM blend, even if the pristine polymer is not fluorescent in the solid state, yielding a more stable population of separated charges than **P2** or **P1**. The polaron g value in **P3** is the furthest from the free-electron value 2.0023, pointing to a higher interaction of the unpaired electron spin with heteroatom nuclei spins, or a higher localization, as suggested also by the large ΔH (5 Gauss) significantly higher than observed in P3AT systems (≈ 3 Gauss). Moreover, a comparison of relative intensities shows that in all the examined materials the photo-excited spin concentration is much lower than in reference PAT:PCBM systems , similarly to what is reported also for PFO:PCBM blend [18], and explained with a higher charge recombination rate.

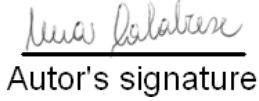

5.8 MODELLING

The modelling activity related to this task has involved a detailed study of chosen series of model oligomers representative of all the copolymers under examination.

Modelling analysis was started before experimental data related to the real copolymers was available, in particular, at that time, the analysis of their polydispersity and the distribution of individual components within the copolymer was still missing. Therefore, we opted for a purely statistical analysis of all possible combinations of copolymers consisting of three different monomer units one of which, in turn, was prepared in the copolymer in an alternate ("spacer") while the other two were distributed randomly in the positions vacated by the spacer.

Therefore, were constructed all possible chains of type: $\mathbf{(-\alpha\text{-}X\text{-})_n}$ where **X** may be **β** or **γ** and where: **{α, β,γ}**={Fluorene**(=F),**BenzoTiaDiazole**(=B),**Thiophene**(=T)}**

We think it's important to emphasize that this approach assumes that, during the synthesis of the copolymers, the real affinity for the growing chain of one or the other of the monomers available in solution is identical**.**

Due to the fact that information about the average length and polydispersity of copolymers was not available at the beginning of the theoretical work, all possible copolymers have been systematically constructed in accordance with the rule $\mathbf{(-\alpha\text{-}X\text{-})_n}$ with $\mathbf{n=2^m}$ and where **m={0,…,3}.**

Given the rapid increase with N, of all the possible combinations, as far as the copolymers of length $\mathbf{n=2^4=16}$ were concerned, the analysis has been limited to the investigation of a subset consisting of copolymers of type:: $\mathbf{-(-\alpha\text{-}\beta\text{-}\alpha\text{-}X)_n-}$ where **X=β** or **X=γ** and, obviously: **{α,β,γ}={F,B,T}**.

5.8.1 COMPUTATION METHOD

Modelling of the molecular structures object of this study was obtained by quantum mechanical Hartree Fock methods (for the initial preparation of the monomeric units) and

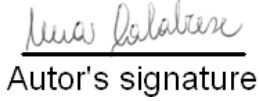

with methods based on density functional theory approach (for the geometric optimization of monomer and of oligomeric models). More specifically, the geometric data necessary to obtain the initial structure of the monomers under examination was derived from the library of models we have developed over the years with the Hartree Fock method based on STO-3G basis set [19]. This approach allows to perform geometrical optimizations of structures obtaining models reasonably close to the real conformational energy minimum in a reasonable amount of time. Subsequently, the conformers obtained, were submitted to the more rigorous (and therefore more computationally expensive) Density Functional method. The Amsterdam Density Functional program (ADF) from SCM was applied on our High Power Scientific Computing System (146 processing units, AMD Opteron and Athlon-based Linux RH Enterprise, with 432 GB RAM and 6TB storage).

The base functions adopted for all the models are Slater-type orbitals Type TZP (Triple Zeta - more accurately a Double Zeta for the core and Triple Zeta for the valence level - with the addition of a further additional polarization function). In order to decrease the computational complexity inherent to SCF calculations Small Core functions have been implemented. Here, atomic internal levels below the valence shell are kept "frozen", and these are orthogonalized independently from the higher levels that are treated without any other approximation. "Core Small" is the smallest of the available basis sets with inner frozen shell. The DFT calculations are performed with two Generalized Gradient Approximations (GGA): the BP-86 method in which the exchange function developed by Becke is combined with the correlation functional developed by Perdew, and the hybrid method B3-LYP [8]. The latter method is an extension of the three-parameters method proposed by Becke employing the correlation functional developed by Lee, Yang and Parr and ensures one of the best accuracies obtainable with the DFT method. The parameterizations used are listed in Append A.

5.8.2 MODEL OPTIMIZATION

Calculation methods discussed in the previous section were adopted in order to create and optimize the molecular models. First of all, geometry of the three base monomers has been optimized **F**, **B**, **T**. As far as the fluorene model is concerned, it has been optimized both

Autor's signature

the model with two Methyl groups substituents in position 9 and the one in which the two hydrogen atoms in position 9 are replaced with 2 ethyl-hexyle. For the latter a series of simulations which allowed the identification and study of the conformational minimum for the molecule have been carried out. Prior analysis of the distribution of frontier orbitals related to this and for the fluorene substituted with two methyl groups showed that, as expected, the presence of alkyl substituents does not significantly alter the energy of the orbitals, so it was decided to pursue our task adopting the dimethyl substituted fluorine instead of the fully substituted moiety, with obvious advantages in terms of computational complexity needed to optimize a single model both in the number of degrees of conformational freedom that should have been systematically explored for the substituted one. In this regard, see the data in **Table 5.9**.

Table 5.9 Calculated energy levels of substituted fluorene.

MONOMER	HOMO (eV)	LUMO (eV)	Eg (eV)
Fluorene_dimethyle	-5.3648	-1.8148	3.55
Fluorene_alchilated	-5.3453	-1.7833	3.562

Once obtained the nuclear geometry and the electronic properties for each monomer (the most significant data are reported in **Table 5.10**) three dimers F-B, B-T and T-F were investigated.

Table 5.10 Calculated energy levels of B, T and F monomer unit.

MONOMER	HOMO (eV)	LUMO (eV)	Eg (eV)
Benzothiadiazole	-6.2538	-3.3312	2.9226
Thiophene	-5.8589	-1.4038	4.4551
Fluorene	-5.3648	-1.8148	3.55

The extra degree of freedom (the σ bond with the partial π character that joins each pair of monomer units) was explored in its entirety, allowing us to detect an absolute minimum for each pair of structures. The structural data and energy of the dimers are shown in **Table 5.11**.

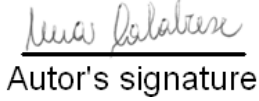

Table 5.11 Calculated structural data and energy levels of dimers.

	Optimized dihedral	Starting dihedral	HOMO (eV)	LUMO(eV)	Eg (eV)
TF	25,73	90	-5,054	-2,242	2,812
	156,5	110	-5,052	-2,248	2,804
	0	0	-4,998	-2,303	2,6949
	180	180	-5,002	-2,302	2,6999
BF	34,31	45	-5,306	-3,31	1,996
	146,66	90	-5,312	-3,299	2,013
	0	0	-5,253	-3,369	1,8835
	180	180	-5,269	-3,353	1,9163
TB	172,37	135	-5,456	-3,424	2,032
	180	180	-5,45	-3,424	2,0263
	2,84	90	-5,403	-3,419	1,984
	0	0	-5,402	-3,419	1,9832

An identical approach was undertaken for the tetrameters. Systematical analysis shows that these are 12 in all **α-β-α-β, α-β-α-γ, α-γ-α-β, α-γ-α-γ** where of course: **{α,β,γ}={F,B,T}**. The energy data related to tetrameters is presented in **Table 5.12**.

Table 5.12 Calculated energy levels of tetramers.

TETRAMER	HOMO (eV)	LUMO (eV)	Eg (eV)
BFBF	-5.08	-3.399	1.681
BTBT	-5.095	-3.714	1.381
BFBT	-5.106	-3.475	1.631
BTBF	-5.067	-3.644	1.423
TBTB	-5.095	-3.714	1.381
TBTF	-4.87	-3.507	1.363
TFTB	-4.958	-3.42	1.538
TFTF	-4.757	-2.622	2.135
FTFT	-4.757	-2.622	2.135
FBFT	-4.967	-3.344	1.623
FTFB	-4.831	-3.332	1.499
FBFB	-5.08	-3.399	1.681

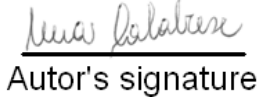

Autor's signature

Expanding the combinatorial analysis, 48 octamers were obtained. The energy data of these latter models is reported in **Table 5.13**.

Table 5.13 Calculated energy levels of octamers.

OCTAMER	HOMO (eV)	LUMO (eV)	Eg (eV)
BTBTBTBT	-4.921	-3.929	0.992
BTBTBTBF	-4.909	-3.907	1.002
BTBTBFBT	-4.96	-3.833	1.127
BTBTBFBF	-4.954	-3.826	1.128
BTBFBTBT	-4.957	-3.746	1.211
BTBFBTBF	-4.944	-3.717	1.227
BTBFBFBT	-5.002	-3.685	1.317
BTBFBFBF	-4.997	-3.678	1.319
BFBTBTBT	-4.905	-3.843	1.062
BFBTBTBF	-4.891	-3.812	1.079
BFBTBFBT	-5.002	-3.685	1.317
BFBTBFBF	-4.938	-3.68	1.258
BFBFBTBT	-4.948	-3.717	1.231
BFBFBTBF	-4.936	-3.65	1.286
BFBFBFBT	-4.998	-3.491	1.507
BFBFBFBF	-4.99	-3.467	1.523
TBTBTFTB	-4.844	-3.755	1.089
TBTBTBTF	-4.805	-3.822	0.983
TBTBTBTB	-4.928	-3.927	1.001

OCTAMER	HOMO (eV)	LUMO (eV)	Eg (eV)
FTFTFTFT	-4.655	-2.804	1.851
FTFTFTFB	-4.669	-3.352	1.317
FTFTFBFT	-4.701	-3.371	1.33
FTFTFBFB	-4.709	-3.422	1.287
FTFBFTFT	-4.751	-3.368	1.383
FTFBFTFB	-4.781	-3.384	1.397
FTFBFBFT	-4.817	-3.368	1.449

OCTAMER	HOMO (eV)	LUMO (eV)	Eg (eV)
TFTFTFTF	-4.65	-2.803	1.847
TFTFTFTB	-4.712	-3.434	1.278
TFTFTBTF	-4.697	-3.519	1.178
TFTFTBTB	-4.783	-3.697	1.086
TFTBTFTF	-4.696	-3.522	1.174
TFTBTFTB	-4.771	-3.573	1.198
TFTBTBTF	-4.729	-3.7	1.029

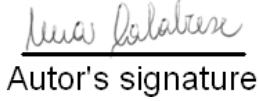

Autor's signature

FTFBFBFB	-4.805	-3.449	1.356
FBFTFTFT	-4.689	-3.356	1.333
FBFTFTFB	-4.734	-3.359	1.375
FBFTFBFT	-4.809	-3.381	1.428
FBFTFBFB	-4.825	-3.427	1.398
FBFBFTFT	-4.776	-3.417	1.359
FBFBFTFB	-4.836	-3.413	1.423
FBFBFBFT	-4.949	-3.441	1.508
FBFBFBFB	-4.991	-3.462	1.529

TFTBTBTB	-4.842	-3.832	1.01
TBTFTFTF	-4.699	-3.528	1.171
TBTFTFTB	-4.785	-3.549	1.236
TBTFTBTF	-4.746	-3.581	1.165
TBTFTBTB	-4.855	-3.733	1.122
TBTBTFTF	-4.748	-3.718	1.03
TBTBTFTB	-4.844	-3.755	1.089
TBTBTBTF	-4.805	-3.822	0.983
TBTBTBTB	-4.928	-3.927	1.001

Autor's signature

Continuing up to the exadecamer, we would get around 256 models. So, the more the 12 more representative sequences:

α-β-α-β-α-γ-α-γ-α-β-α-β-α-γ-α-γ ,

α-γ-α-γ-α-β-α-β-α-γ-α-γ-α-β-α-β ,

α-β-α-γ-α-β-α-γ-α-β-α-γ-α-β-α-γ ,

α-γ-α-β-α-γ-α-β-α-γ-α-β-α-γ-α-β ; always with: **{α,β,γ}={F,B,T}**.

The data for these models is presented in **Table 5.14**.

Table 5.14 Calculated energy levels of the esadecamers.

ESADECAMER	HOMO (eV)	LUMO (eV)	Eg (eV)
BFBFBTBTBFBFBTBT	-4.881	-3.83	1.051
BTBTBFBFBTBTBFBF	-4.884	-3.843	1.041
BFBTBFBTBFBTBFBT	-4.899	-3.757	1.142
BTBFBTBFBTBFBTBF	-4.896	-3.762	1.134
TFTBTFTBTFTBTFTB	-4.688	-3.672	1.016
TBTBTFTFTBTBTFTF	-4.704	-3.747	0.957
TBTFTBTFTBTFTBTF	-4.717	-3.646	1.071
TFTFTBTBTFTFTBTB	-4.708	-3.732	0.976
FBFTFBFTFBFTFBFT	-4.758	-3.402	1.356
FTFBFTFBFTFBFTFB	-4.755	-3.406	1.349
FBFBFTFTFBFBFTFT	-4.725	-3.441	1.284
FTFTFBFBFTFTFBFB	-4.702	-3.433	1.269

5.8.3 TERMINAL SEQUENCES

The copolymer chains obtained by Suzuki reaction may be as end-groups -Br, -$B(OH)_2$ or -H. Simulation of each possible end-groups for all set of simulated polymer would have been an enormous task. Thus, chosen octamer, was verified the influence of the end groups variation on the HOMO and LUMO. In particular, was found that the HOMO/LUMO

Autor's signature

values are substantially unchanged. Consequently in all simulations the chains wer terminated with -H, obtaining a reduction in term of computational cost.

5.8.4 SPECULATIONS ON THE THEORETICAL RESULTS

The calculations performed have allowed us to formulate two considerations: the first of general applicability on push-pull polymers applied to photovoltaics, the second specific to random conjugated polymers. From the distribution of HOMO and LUMO orbital densities on the molecule (**Figure 5.39**) is clearly seen as the last occupied orbital is localized primarily on the electron-rich units of the molecule (Fluorene and Thiophene) while the first empty orbital is essentially localized on the Benzothiadiazole.

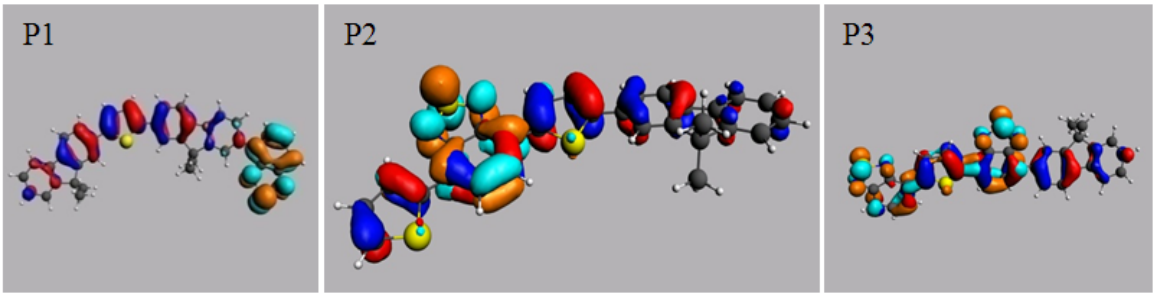

Figure 5.39 HOMO/LUMO Distribution on the repeating unit of the copolymers P1-P3. Red-Blue: HOMO, Orange-Cyan: LUMO

This means that, unlike what can be observed in a conjugate homopolymer as the P3HT, the molecular orbitals are not extended to the whole molecule, but are confined in a defined region of space. This has important implications both for the exciton formation and for the charge transfer. The excited electron cannot find itself anywhere on the molecule but must necessarily be localized on a benzothiadiazole unit and in turn if it would migrate within the polymer domains it must meet another LUMO or two B units must be found at adequately close distance, because otherwise or the transfer cannot occur or, even worse, a intra-or intermolecular hole-electron recombination will happen. It therefore seems that in this type of polymers the hopping can be regarded as the main or only allowable transport

Autor's signature

mechanism, with all the limitations already discussed, and this could significantly reduce the charge mobility. Moreover, in order to obtain an electronic transfer between the polymer and the PCBM, the latter should be close to a B unit. On the other hand, the fact that they already substain a partial charge separation and segregation within the chain may promote the formation of exciton and extend its lifetime. The fluorene-thiophene polymer deserves specific considerations, because, lacking a continuous alternation of electron-rich and electron-poor units, shows more extended molecular orbitals. This leads to a significant hole mobility, as shown by consolidated experimental data. This behaviour is so pronounced that, despite the high Eg number, some researchers bet on this material with the aim to develop high efficiency cells. From literature results that the speed of an electron transfer between a polymer chain and the fullerene is about one order of magnitude higher than that of a polymer-polymer transfer. So regardless the chain that is present at the donor-acceptor interface, transfer occurs only from polymer to fullerene. In the core of the material, instead, polymeric chains are in contact with other chains with various composition and the electron transfer could occur from a chain with relatively high LUMO to a chain with a lower one. Stressing here the point that this consideration must be confirmed by further experiments it can be suggested to extensively investigate this property in the future in order to gain a better control of the polymer morphology and to extend the exciton life.

To make the comparison between the experimental and calculated data obtained, it is necessary to consider what has been measured. The optical energy gap has been estimated by measuring the absorption edge corresponding to the transition from the highest energy level occupied to lowest energy level unoccupied of the polymeric chain at lowest energy gap. Instead, the electrochemical energy gap obtained with cyclic voltammetry technique, has been estimated by the difference between HOMO and LUMOs measured separately. In a solution of random polymer there are several different HOMO and LUMO, which differ depending on the length and composition of the chain. This means that the value of energy gap does not correspond necessarily to the difference between the frontier orbitals of a given compound but the HOMO level is the highest among all those present and the LUMO level the lowest, though belonging to different molecules (**Figure 5.40**).

Autor's signature

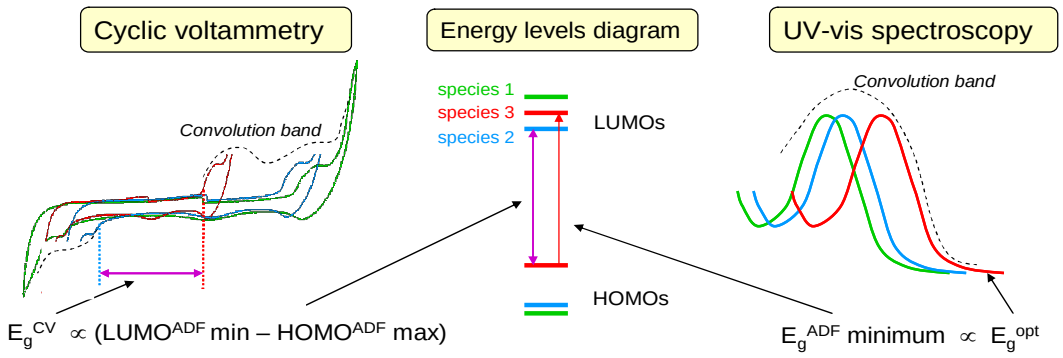

Figure 5.40 CV versus UV-Vis Spectroscopy

Another element to consider is that all possible copolymers have been systematically constructed and simulated during the synthesis of the copolymers, assumes that the real affinity for the growing chain of one or the other of the monomers available in solution is identical**.** In fact the situation is different because putting three monomers in solution is possible to form a number of polymer chains consisting of only two of these three, leading to different results. Considering what wrote above, has been compared the experimental optical and electrochemical data with simulation data referred to chains with four and eight monomeric units in according with weight data and the NMR spectroscopy data. In **Table 5.15** are compared the optical data with the calculate data for copolymer with low molecular weight. The trend is displayed in **Figure 5.41**. To better understand the correlation between experimental and calculated data, for all copolymers was explained the structure, P1: FB-co-FT, P2: TF-co-TB, P3: TB-co-TF.

Table 5.15 Optical energy gap versus calculated energy gap.

Polymer structure	Eg^{opt} (eV)	OCTAMER	Eg^{ADF}_{min} (eV)
TF-co-TB	1.85	TBTBTBTF	0.983
FB-co-FT	2.56	FTFTFBFB	1.287
BT-co-BF	1.58*	BTBTBTBT	0.992

* This is an estimate due to scattering

Autor's signature

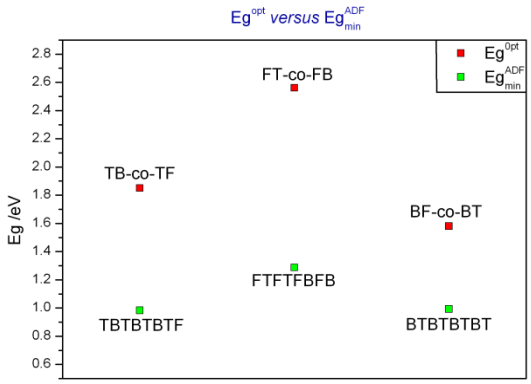

Figure 5.41 Eg^{opt} versus Eg^{ADF}_{min}

The trend is quite respected even if the value of energy gap of the BT-co-BF copolymer is difficult to compare with others due to scattering. Also the copolymer theoretically representative of the energy gap optical is a copolymer of thiophene-benzothiadiazole, in which there isn't the presence of the third comonomer, fluorene. The octamer of these two comonomers is not very soluble and, if it was really formed, may explain the low solubility of the compound.

The electrochemical provides an energy gap value given by the difference between the highest HOMO and the lowest LUMO among all those present (considering the possible co-presence of chains of different lengths), even if they belong to different molecules.

Therefore, the energy gap calculated must be compared with those values both by octamers (**Table 5.16**) and by tetramers (**Table 5.17**).

Table 5.16 Calculated energy gap from the more representative set of octamers and comparison with the electrochemical data.

SPACER	OCTAMER	$LUMO^{ADF}_{min}$ (eV)	OCTAMER	$HOMO^{ADF}_{max}$ (eV)
T	TBTBTBTB	-3,927	TFTFTFTF	-4,65
B	BTBTBTBT	-3,929	BFBTBTBF	-4,891
F	FBFBFBFB	-3,462	FTFTFTFT	-4,655

Polymer structure	Eg^{ADF}=$LUMO^{ADF}_{min}$-$HOMO^{ADF}_{max}$ (eV)	Eg^{cv} (eV)
TB-co-TF	0.723	2.1
FB-co-FT	1.193	2.6

Autor's signature

BT-co-BF	0.962	2.01

HOMO values are always higher calculated and LUMO always lower than experimental. Unexpectedly, however, there is no difficulty in calculating an orbital rather than another, as would be expected given that the HOMO orbital is full, while the LUMO is a theoretical abstraction. Repeating the same comparisons with tetramers can be obtained data reported in **Table 5.17**.

Table 5.17 Calculated energy gap from the more representative set of tetramers and comparison with the electrochemical data.

SPACER	TETRAMER	$LUMO^{ADF}_{min}$ (eV)	OCTAMER	$HOMO^{ADF}_{max}$ (eV)
T	TFTF	-4,757	TBTB	-3,714
B	BTBF	-5,067	BTBT	-3,714
F	FTFT	-4,757	FBFB	-3,399

Polymer structure	$Eg^{ADF}=LUMO^{ADF}_{min}-HOMO^{ADF}_{max}$ (eV)	Eg^{cv} (eV)
TB-co-TF	1.043	2.1
BT-co-BF	1.358	2.6
FB-co-FT	1.353	2.01

It is clearly how the values of tetramers are certainly closer to the measured values.

It is necessary consider that the simulation program gives intrinsically lower values than those measured experimentally since the simulation is performed in a vacuum at 0 K and does not take into account a number of parameters in the bulk. It is clear both theoretical calculations and experimental measurements the random copolymer with fluorene spacer having characterized by a high energy gap due to the low conjugation resulting from the twist in the FB coupling and lack of alternating electron-rich and electron poor units in the FT pair.

Autor's signature

5.9 MOBILITY

Mobility measurement are still under way. In this section is reported the charge carriers mobility of the copolymer **P1** with high molecular weight before and after the purification process. The determination of transit times has been much more difficult to perform for the copolymer not purified than it was for the copolymer purified. This can be attributed to two reasons: (i) the polymeric film of purified **P1**was thinner than the one obtained with not purified **P1** (ii) in the purified polymer the charge carriers mobility is significantly higher with respect to the not purified material. As a consequence, the applied voltage needed to be lower, which hampers the collection of the TOF signal when they are dispersive, as in this case (see Figure 5.42 and Figure 5.43). The transit times (τ_t) were estimated from the photocurrent signals plotted in bi-logarithmic scale.

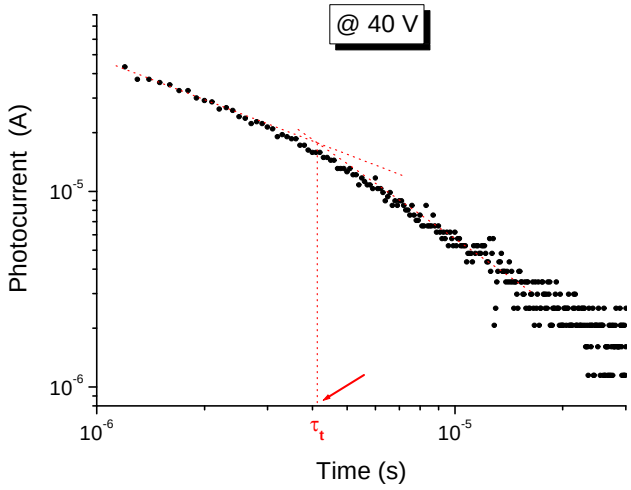

Figure 5.42 TOF signal for the sample ITO/purified **P1**/CGL/Al in bi-logarithmic scale; applied voltage is 40 V. In the figure the procedure to extract transit time is shown. Polymeric film thickness: 1.14 μm.

Autor's signature

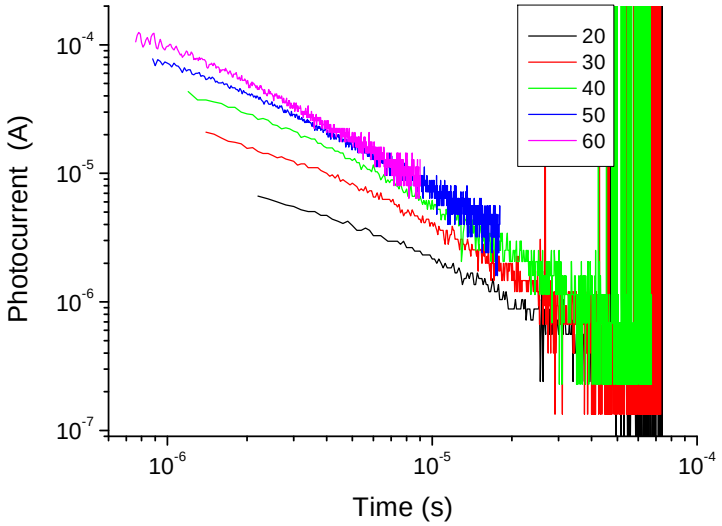

Figure 5.43 TOF signals for sample ITO/purified **P1**/CGL/Al in bi-logarithmic scale, at several values of applied voltage (they are expressed in V units in the legend). Polymeric film thickness: 1.14 mm.

The holes mobility values (μ_h), calculated from the transit times, are reported in Figure 5.44 as function of the square root of the electric field (E). Also in this case, the trend is quite linear, indicating a Poole-Frenkel like behaviour for the mobility of purified polymer.

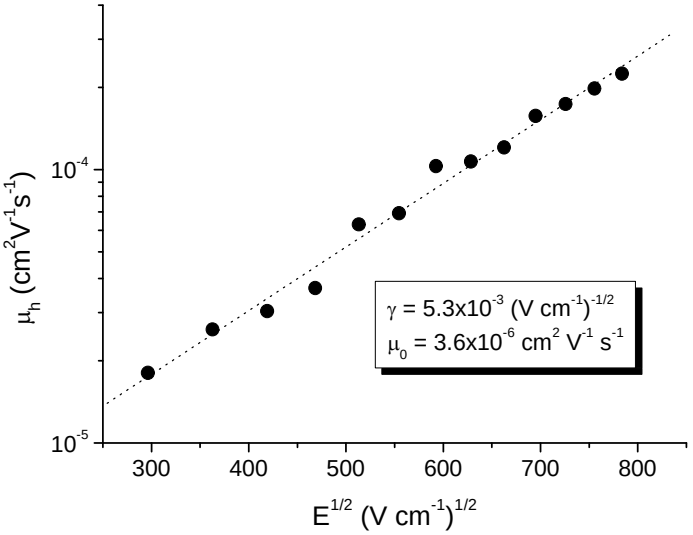

Autor's signature

Figure 5.44 Holes mobility values (μ_h), calculated for sample ITO/purified **P1**/CGL/Al as function of the square root of the electric field (E). The Pool-Frenkel parameters, deduced from the linear fitting procedure, are reported in the figure.

As for γ parameter that describes the strength of the mobility dependence on the electric field, the value is similar to both copolymers, while the value of the mobility extrapolated at zero field, μ_0, is higher than the one of the less purified sample: 3.6×10^{-6} cm^2 V^{-1} s^{-1} vs 9.4×10^{-7} cm^2 V^{-1} s^{-1}. Holes mobility in the purified polymer is higher, as appears logic: comparing the holes mobility values at the same field, there is about a factor 4 between the two compounds, as can be deduced from the graph in Figure 2.2.4.

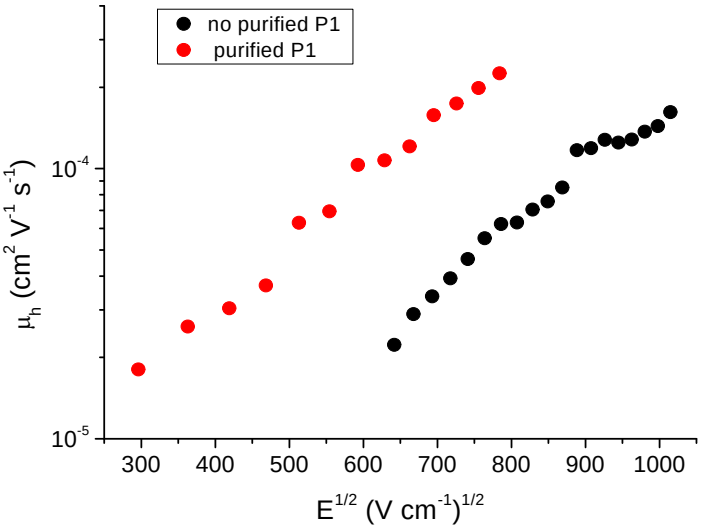

Figure 5.45 Comparison between TOF mobilities calculated for both samples with 1.14 μm in thick for purified **P1** and 1.50 μm in thick for not purified **P1**.

Also in this case the trend of transit times vs electric field has been analyzed, obtaining for purified copolymer a higher value of the dispersion parameter α than for not purified copolymer (0.42 vs 0.32, Figure 2.2.5). This means that the dispersion in the holes transport in the less pure polymer is higher, as expected, although the TOF experimental curves do not seem to confirm this behaviour (as already stressed, this could be attributed

Autor's signature

to the not favourable experimental conditions for the device prepared with purified copolymer).

In conclusion, impurities show two main effects: they increase dispersion in the holes transport, probably acting as charge-trapping centres, and they reduce holes drift velocity.

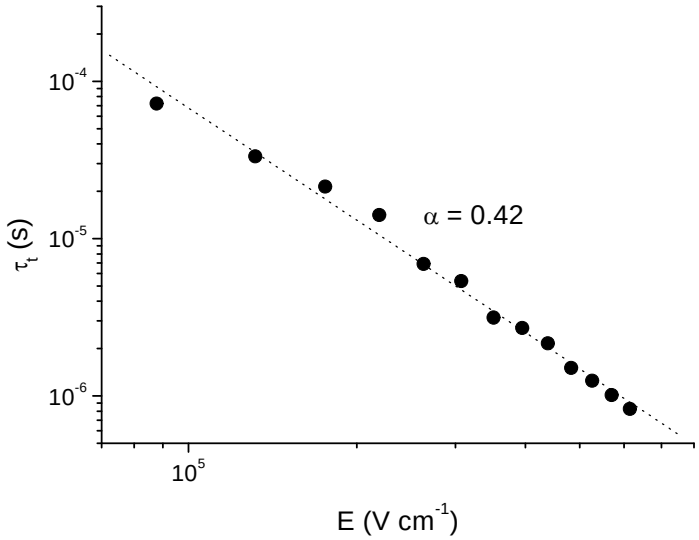

Figure 5.46 Transit times as deduced from TOF as function of the electric field for the sample ITO/30207-69P/CGL/Al (polymeric film thickness: 1.14 μm).

5.10 PHOTOVOLTAIC APPLICATIONS

Photovoltaic devices were fabricated in a typical sandwich structure of glass-ITO/PEDOT:PSS/Copolymer:PCBM/Al, using copolymers as electron donors and the PCBM as electron acceptor. Photovoltaic characterization includes different approaches to optimize the efficiency of the devices.

The parameters taken into account were: selection of the best solvent, optimization of D:A weight ratio, optimization of the active layer thickness and analyzing annealing effects. The effects of three different solvents on the photovoltaic performance were investigated:

Autor's signature

Chloroform, Chlorobenzene and orto-DiChloroBenzene, individually and in a mixture form_ENREF_19. According to the literature the CB and o-DCB are good solvents for PCBM [20]_ENREF_19. The copolymer with low molecular weight showed a medium solubility in all solvents examinated but the photovoltaic devices obtained from them (not reported) have showed very low FF and efficiency. With the increase of molecular weight the copolymers solubility improve For this reason, in the present work, are reported only the devices based on copolymer with high molecular weight. The copolymer **P2** showed very low solubility and the tendency to agglomerate in all solvents; this made difficult to obtain a good film and accordingly devices. It was found that the best solvent is a mixture of chloroform and clorobenzene (1:1 v/v) for **P1**, CB for **P2** and clorobenzene or o-Dichlorobenzene for **P4**.

This results were confirmed by AFM analysis.

The electrochemical data of high MW copolymer before and after purification are displayed in Figure 5.47.

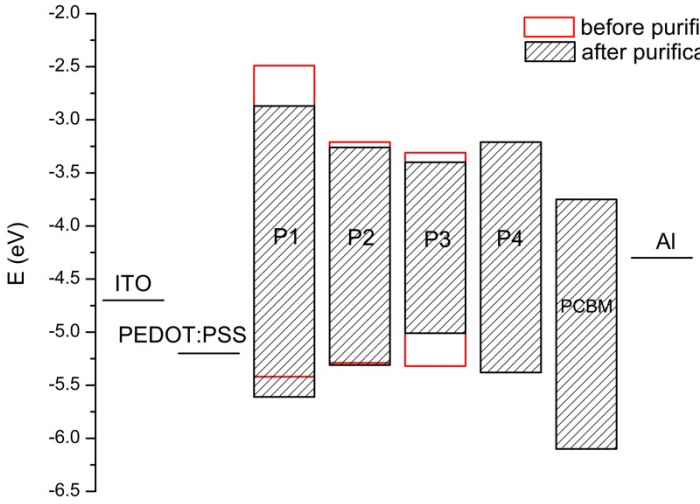

Figure 5.47 Energy level diagram of P1-P4 before and after purification process from voltammetric data.

All the polymers have HOMO and LUMO levels higher than the commonly used [6,6]-phenyl-C_{61}-butyric acid methyl ester (PCBM) acceptor [21]. **P1** is the polymer with the highest $E_{HOMOdonor}$-$E_{LUMOacceptor}$ difference. On this basis **P1** is expected to lead to photovoltaic devices with the better Voc [22]. The $E_{HOMOdonor}$-$E_{LUMOacceptor}$ difference of **P2**

Autor's signature

is lower, but the smaller energy gap could compensate the expected lower Voc with a higher Jsc in designing an efficient solar cell. **P3**, is the polymer with the lower energy gap and this would makes it the best candidate for solar cell applications. Unfortunately, it has a very low solubility and a marked tendency to aggregate.

In order to choose the best blend composition, active layers with D:A w/w ratios 1:1, 1:2, 1:3, and 1:4 were studied. The best efficiencies were observed with P1:PCBM (1:2 w/w) in the mixture of solvent described above, **P2**:PCBM (1:4 w/w), **P4**:PCBM (1:4 w/w) both in Clorobenzene. In order to improve the photovoltaic performance, the active layer thickness was optimized. The best efficiency was found approximately 100 nm for devices based on **P1** and **P2** and about 130 nm for devices based on **P4.** The devices based on purified copolymers have showed the best efficiency and the effects of all parameters take into account on the photovoltaic performances are shown in Figure 5.48 and Figure 5.49**.**

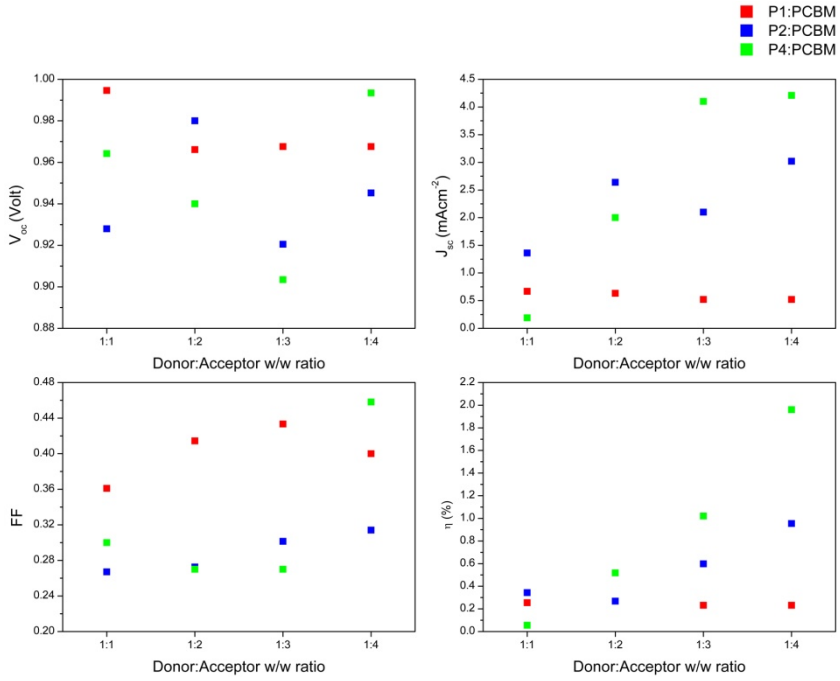

Autor's signature

Figure 5.48 Photovoltaic parameters as a function of the D/A ratio for solar cells besed on P1:PCBM (1:2 w/w) in mixture of solvents (1:1 v/v) (red), P2:PCBM (1:4 w/w) in Chlorobenzene (blue), P4:PCBM (1:4 w/w) in Cholobenzene (green).

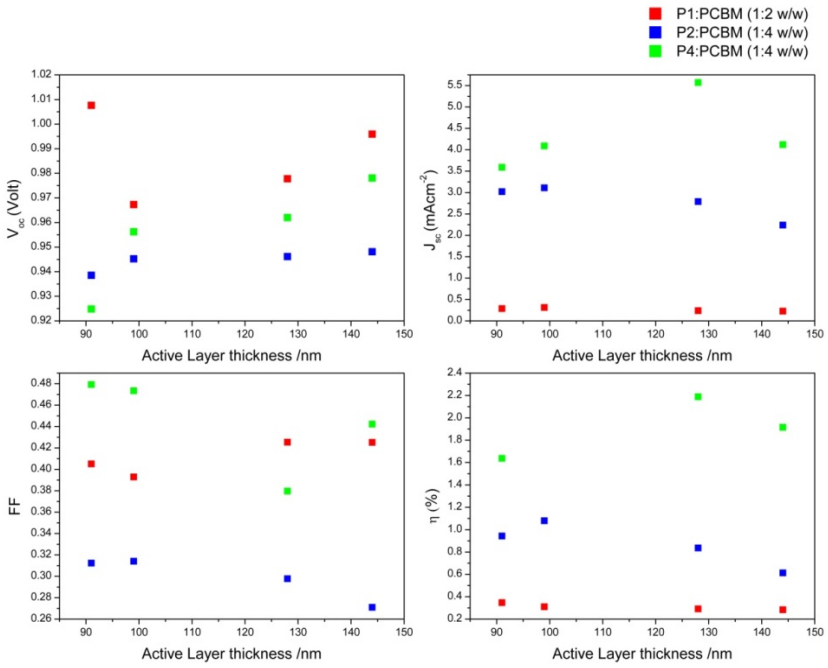

Figure 5.49 Photovoltaic parameters as a function of the active layer thickness for solar cells besed on **P1**:PCBM (1:2 w/w) in mixture of solvents (1:1 v/v) (red), **P2**:PCBM (1:4 w/w) in Chlorobenzene (blue), **P4**:PCBM (1:4 w/w) in Cholobenzene (green).

The best I-V curves in the dark and under illumination from solar simulator (AM1.5, 97mW/cm^2) of the bulk heterojunction solar cells are reported in **Figure 5.50**.

Autor's signature

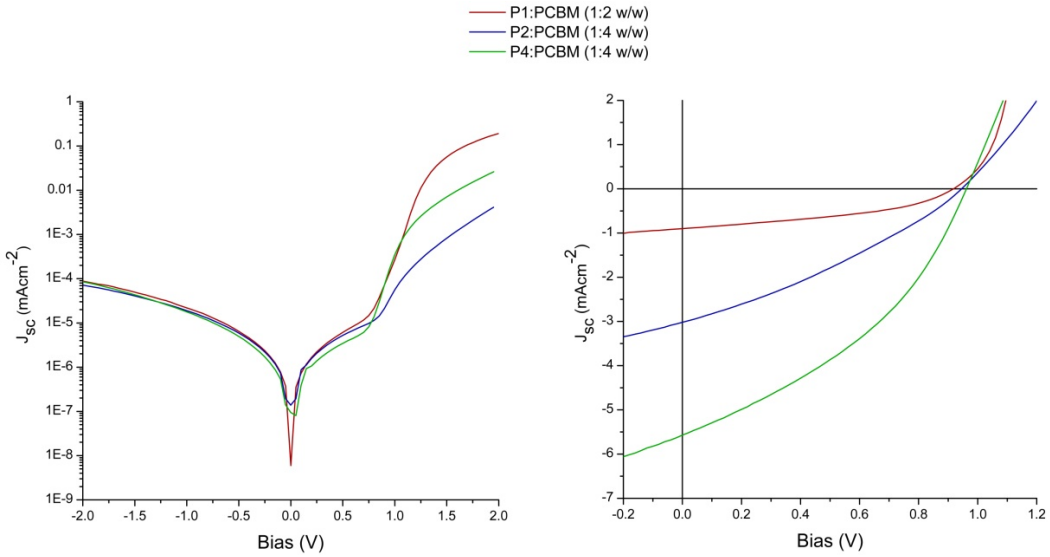

Figure 5.50 J-V curve of the best solar cells based on **P1** (red line), **P2** (blue line) and **P4** (green line) in the dark (*Left*) and under illumination (*Right*).

The photovoltaic parameters of the best cells are summarized in **Table 5.18**.

Table 5.18 Photovoltaic parameters for the best solar cells.

Donor	Acceptor	D/A ratio (w/w)	Solvent	Voc (V)	Jsc ($mAcm^{-2}$)	FF	η (%)
P1	PCBM	1:2	Chlorobenzene:Chloroform (1:1 v/v)	0.92	0.90	0.40	0.35
P2	PCBM	1:4	Chlorobenzene	0.94	3.43	0.31	1.08
P4	PCBM	1:4	Chlorobenzene	0.99	4.79	0.458	2.25

For all devices the active area was approximatively $22cm^2$.

The effects of thermal annealing were studied for all solar cells but it has shown a negative effect in all cases. The results clearly demonstrated that there is a correlation between the chemical structure and the HOMO levels determined from electrochemical studies as well as the V_{oc} values determined from photovoltaic devices. **P2** showed interesting photovoltaic properties with V_{oc} of 0.94 V and an efficiency over 1%.

Autor's signature

5.11 REFERENCES

[1] Schlüter, A. D.: The tenth anniversary of Suzuki polycondensation (SPC). J. Polym. Sci. A: Polym. Chem. . 39, 1533-1556 (2001)

[2] Kirschbaum, T., Briehn, C. A., Bauerle, P.: Efficient solid-phase synthesis of regioregular head-to-tail-coupled oligo(3-alkylthiophene)s up to a dodecamer. J.Chem. Soc. Perkin Trans. 1. 1211-1216 (2000)

[3] Forster, M., Annan, K. O., Scherf, U.: Conjugated Ladder Polymers Containing Thienylene Units. Macromolecules. 32, 3159-3162 (1999)

[4] Jayakannan, M., van Dongen, J. L. J., Janssen, R. A. J.: Mechanistic Aspects of the Suzuki Polycondensation of Thiophenebisboronic Derivatives and Diiodobenzenes Analyzed by MALDI−TOF Mass Spectrometry. Macromolecules. 34, 5386-5393 (2001)

[5] Zerbi, G.: Vibrational Spectroscopy of Conducting Polymers: Theory and Perspective. John Wiley & Sons, Ltd, (2006)

[6] Jespersen, K. G., Beenken, W. J. D., Zaushitsyn, Y., Yartsev, A., Andersson, M., Pullerits, T., Sundstrom, V.: The electronic states of polyfluorene copolymers with alternating donor-acceptor units. J. Chem. Phys. 121, 12613-12617 (2004)

[7] Slooff, L. H., Veenstra, S. C., Kroon, J. M., Moet, D. J. D., Sweelssen, J., Koetse, M. M.: Determining the internal quantum efficiency of highly efficient polymer solar cells through optical modeling. Appl. Phys. Lett. 90, 143506 (2007)

[8] Perdew, J. P.: Density-functional approximation for the correlation energy of the inhomogeneous electron gas. Physical Review B. 33, 8822 (1986)

[9] Moses, D., Dogariu, A., Heeger, A. J.: Ultrafast detection of charged photocarriers in conjugated polymers. Phys. Rev. B. 61, 9373-9379 (2000)

[10] Hou, Q., Xu, Y., Yang, W., Yuan, M., Peng, J., Cao, Y.: Novel red-emitting fluorene-based copolymers. J. Mater. Chem. 12, 2887-2892 (2002)

[11] Sariciftci, N. S., Smilowitz, L., Heeger, A. J., Wudl, F.: Photoinduced Electron Transfer from a Conducting Polymer to Buckminsterfullerene. Science. 258, 1474-1476 (1992)

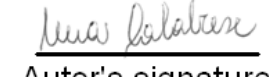

Autor's signature

[12] Hwang, S.-W., Chen, Y.: Synthesis and Electrochemical and Optical Properties of Novel Poly(aryl ether)s with Isolated Carbazole and p-Quaterphenyl Chromophores. Macromolecules. 34, 2981-2986 (2001)

[13] Johansson, T., Mammo, W., Svensson, M., Andersson, M. R., Inganas, O.: Electrochemical bandgaps of substituted polythiophenes. J. Mater. Chem. 13, 1316-1323 (2003)

[14] Segre, U., Pasimeni, L., Ruzzi, M.: Simulation of EPR and time resolved EPR lineshapes in partially ordered glasses. Spectrochimica Acta Part A: Molecular and Biomolecular Spectroscopy. 56, 265-271 (2000)

[15] Veldman, D., Meskers, S. C. J., Janssen, R. A. J.: The Energy of Charge-Transfer States in Electron Donor–Acceptor Blends: Insight into the Energy Losses in Organic Solar Cells. Adv. Funct. Mat. 19, 1939-1948 (2009)

[16] Brabec, C. J., Sariciftci, N. S., Schultz, N. A., Scharber, M. C.: Low-temperature recombination kinetics of photoexcited persistent charge carriers in conjugated polymer/fullerene composite films. Phys. Rev. B. 64, 245210 (2001)

[17] Marumoto, K., Takeuchi, N., Ozaki, T., Kuroda, S.: ESR studies of photogenerated polarons in regioregular poly(3-alkylthiophene)-fullerene composite. Synth. Met. 129, 239-247 (2002)

[18] Marumoto, K., Kato, M., Kondo, H., Kuroda, S., Greenham, N. C., Friend, R. H., Shimoi, Y., Abe, S.: Electron spin resonance and electron nuclear double resonance of photogenerated polarons in polyfluorene and its fullerene composite. Phys. Rev. B. 79, 245204 (2009)

[19] Hehre, W. J., L. Radom, P. v. R. Schleyer, Pople, J. A.: Ab Initio Molecular Orbital Theory John Wiley & Sons, Inc., USA (1986)

[20] Kronholm, D., Hummelen, J. C.: Fullerene-Based n-Type Semiconductors in Organic Electronics. Material Matters. 2, 16-20 (2007)

[21] Brabec, C. J., Hummelen, J. C., Sariciftci, N. S.: Plastic Solar Cells. Adv. Funct. Mater. 11, 15-26 (2001)

[22] Brabec, C. J., Cravino, A., Meissner, D., Sariciftci, N. S., Fromherz, T., Rispens, M. T., Sanchez, L., Hummelen, J. C.: Origin of the Open Circuit Voltage of Plastic Solar Cells. Adv. Funct. Mater. 11, 374-380 (2001)

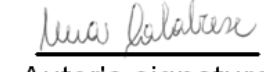

Autor's signature

6 CONCLUSIONS

That of novel materials for new generation solar energy technologies is an expanding research area. In this frame, polymer solar cells represent a hot topic and one of the most promising developments. The achievement of efficient polymer solar cells requires a multidisciplinary research encompassing the synthesis of new π-conjugated systems, the photophysical characterization of the photoactive materials, the design and fabrication of devices exhibiting nanostructured architectures, their electrical characterization and the study of the device physics. A large number of different donor and acceptor materials (both low molecular weight compounds and polymers) have been explored over the years to find the best performing photoactive system. It is possible, to some extent, to rationally design the structure of the donor polymer to tune its chemical, physical and electronic properties which, in turn, affect the devices performance. On the other hand, phenyl-C61-butyric acid methyl ester (PCBM) and phenyl-C71-butyric acid methyl ester are by far the most effective electron acceptors used in solar cells. A class of promising materials with these characteristics is represented by the alternating fluorene copolymers (APFO), which leads to solar cells having promising power conversion efficiencies. In particular, it is known from the literature that poly{9,9-bisalkylfluorene-2,7-diyl-*alt*-[4,7-bis(thien-2-yl)-2,1,3-benzothiadiazole]-5',5"-diyl} (alkyl = hexyl, 2-ethylhexyl, octyl, decyl, dodecyl), containing fluorene-thiophene-benzothiadiazole-thiophene units in a strictly alternating sequence, exhibit energy gaps around 1.9 eV and open circuit voltages (Voc) around 1 V.
In this work, the synthesis and the optoelectronic characterization of a novel family of 9,9-bisalkylfluorene (F)/thiophene (T)/benzothiadiazole (B) pseudo-random copolymers is described. The structure of the reported copolymers is pseudorandom: in turn each F, T, B monomer unit is alternated to the other randomly distributed two units. The polymers were prepared by Suzuki polycondensation method. The alternating copolymer F-T-B-T was also prepared as a reference material. The structure of the polymers was verified by Nuclear Magnetic Resonance (NMR) spectroscopy. The experimental monomer

Autor's signature

composition is in fairly good agreement with the nominal ratio expected on the basis of the monomers feed.

An advantage of random copolymers over the alternating copolymers commonly reported in the literature consists in the simplicity of synthesis: while the preparation of alternating copolymers requires a multistep synthesis to assemble the monomeric units in the desired sequence, random copolymers can be easily obtained in a one-pot polymerization from readily available precursors.

To study the effect of the molecular weight on the photophysical properties and photovoltaic performance of fullerene-based bulk heterojunction solar cells, these copolymers were prepared into two different version: low molecular weight and high molecular weight. However, only for the polymers having the higher solubility it was possible to obtain molecular weights greater than 10000. Moreover, to understand the effect of metal residues (from polymerization catalyst) samples with different degree of purity were prepared.

Preliminarly to polymer synthesis, a theoretical calculation of polymer energy levels was carried out. Quantum mechanical Hartree Fock methods (for the initial preparation of the monomeric units) and methods based on density functional theory approach were used. The calculations allowed to formulate two considerations: the first, of general applicability, on electron rich-electron poor monomer alternation approach applied to photovoltaics, the second specific to random conjugated polymers.

The on electron rich-electron poor monomer alternation approach is commonly used to obtain low-band gap copolymers, and such rule of design is confirmed by the reported calculation. In addition to that, from the distribution of HOMO and LUMO orbital densities on the molecule is clearly seen as the last occupied orbital is localized primarily on the electron-rich units of the molecule (fluorene and thiophene) while the first empty orbital is essentially localized on the benzothiadiazole. This means that, unlike what can be observed in a conjugate homopolymer as the P3HT, the molecular orbitals are not extended to the whole molecule, but are confined in a defined region of space. This has important implications both for the exciton formation and for the charge transfer. The excited electron cannot find itself anywhere on the molecule but must necessarily be localized on a

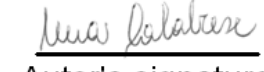

Autor's signature

benzothiadiazole unit and in turn if it would migrate within the polymer domains it must meet another LUMO or two benzothiadiazole units must be found at adequately close distance, because otherwise or the transfer cannot occur or, even worse, a intra-or intermolecular hole-electron recombination will happen. It therefore seems that in this type of polymers the hopping can be regarded as the main or only allowable transport mechanism, with all the limitations already discussed, and this could significantly reduce the charge mobility. Moreover, in order to obtain an electronic transfer between the polymer and the PCBM, the latter should be close to a benzothiadiazole unit.

Cyclic voltammetry (CV) was employed to determine redox potentials of polymers and to estimate their HOMO and LUMO energy.

Reduction and oxidation potentials decrease consistently with the trends expected on the basis of the balance of electron rich/electron poor groups in the polymer.

All the polymers have HOMO and LUMO levels higher than the commonly used [6,6]-phenyl-C_{61}-butyric acid methyl ester (PCBM) acceptor. **P1** is the polymer with the highest $E_{HOMOdonor}$-$E_{LUMOacceptor}$ difference. On this basis **P1** is expected to lead to photovoltaic devices with the better Voc. The $E_{HOMOdonor}$-$E_{LUMOacceptor}$ difference of **P2** is lower, but the smaller energy gap could compensate the expected lower Voc with a higher Jsc in designing an efficient solar cell. **P3**, is the polymer with the lower energy gap and this would make it also a good candidate for solar cell applications. Unfortunately, it has a very low solubility and a marked tendency to aggregate.

The energy gap estimated by UV-visible analysis are in agreement with those estimated by electrochemical analysis; although the absolute values are different (a discrepancy well documented in the literature for many conjugated polymers), the trend is the same. The metal residues do not affect the shape of the absorption spectra. All the polymers, except **P3**, are photoluminescent. The photoluminescence is quenched by PCBM, a clear indication that the charge transfer process in these systems is faster than the radiative dacay of the excited state.

Further evidences about the photoinduced charge transfer process arise from Electron Spin Resonance studies (both Light induced, LESR, and Time Resolved, TR-ESR, techniques). The TR-ESR measurements on the series of copolymers indicate, in all cases examined, the formation of triplet states with different efficiencies as a consequence of the

Autor's signature

photoexcitation. The TR-EPR measurements of the blend copolymer/PCBM showed at least two different types of behavior: (a) blends of **P2, P3** and the alternating polymer with PCBM showed the formation of independent states of the polymer and the PCBM triplet. However PCBM triplet energy is transferred quickly to the triplet state of the copolymer, which then is the excited at lower energy. Also in this case the charge separation can occur and immediate charge recombination can occur with production of the triplet state of the copolymer; (b) blend of **P1** with PCBM showed only the triplet state of PCBM, which gets the state to lower energy. Considering the simplified scheme introduced by Janssen, the cases examined fall into a category that involve a charge-transfer state located in energy below the triplet state (a situation favorable for the photovoltaic mechanism), where, however, the triplet state can be either the triplet state of PCBM (in the case of the blend **P1**/PCBM) or the triplet state of the copolymer (in the case of the blends **P2, P3**/PCBM).

Light induced ESR evidenced the formation of polarons in blends P2/PCBM and P3/PCBM illuminated with artificial light, while in P1:PCBM recombination phenomena are likely to take place.

The mobility of charge carries is still under way. The copolymer investigated (**P2**) shows a charge carrier mobility, in the purified version, four time greater than the charge carries mobility for the pristine copolymer. By the measurement already made is possible to understand the affects of impurity on the transport process.

In summary, the photophysical study confirm that fluorene, thiophene, benzothiadiazole pseudo random copolymers might act as donor materials for organic solar cells, in particular **P2** (the copolymer with thiophene units alternated to randomly distributed fluorene and benzothiadiazole) , matching both morphological and electronic requirements. The optical and electronic properties of **P2**, that can be easily obtained starting from commercially available monomers, do not differ significantly from those of the corresponding perfectly alternating polymer, thus paving the way to the preparation of materials useful for photovoltaic application in a much more simplified manner.

Photovoltaic devices were fabricated in a typical sandwich structure of glass-ITO/PEDOT:PSS/Copolymer:PCBM/Al, using copolymers as electron donors and the PCBM as electron acceptor. Photovoltaic characterization includes different approaches to optimize the efficiency of the devices as the selection of the best solvent, optimization of

Autor's signature

D:A weight ratio, optimization of the active layer thickness and analyzing annealing effects. The results clearly demonstrated that there is a correlation between the chemical structure and the HOMO levels determined from electrochemical studies as well as the V_{oc} values determined from photovoltaic devices. In particular **P2** showed interesting photovoltaic properties with V_{oc} of 0.94 V and an efficiency over 1%. Furthermore the **P1** copolymer was tested as active layer in a simple OLED. The device emits in the green and might be a promising candidate for electroluminescent materials due to its excellent luminescent properties, solubility, film-forming property and stability. It can conclude that this class of copolymer materials open a wide range of possible optoelectronic applications.

Autor's signature

7 EXPERIMENTAL

7.1 MATERIALS

2,1,3-Benzothiadiazole-4,7-bis(boronic acid pinacol ester) was purchased from Aldrich and purified by column chromatography (heptane/ethyl acetate 1:1). Toluene was distilled over lithium alluminium hydride. [9,9-Bis(2-ethylhexyl)-9*H*-fluorene-2,7-diyl]bisboronic acid, 4,7-Dibromobenzo[*c*]-1,2,5-thiadiazole, 9,9-Di-(2′-ethylhexyl)-2,7-dibromofluorene, 2,5-Dibromothiophene, Tricaprylylmethylammonium chloride (Aliquat® 336), Tetrakis(triphenylphosphine)palladium(0), methanol, isopropanol, chloroform, potassium carbonate, EthyleneDiamineTetraAcetic acid disodium salt (EDTA), were purchased from Sigma-Aldrich and used without further purification.

7.2 SYNTHESIS

7.2.1 LOW WEIGHT POLYMERS

P1 low Mw: Poly{[4'-(9,9-bis(2-ethylhexyl)fluoren-2-yl)-2',1',3'-benzothiadiazole-7,7'-diyl]-co-[2'-(9,9-bis(2-ethylhexyl)fluoren-2-yl)thien-7,5'-diyl]}

1.736 g (3.63 mmol) of 9,9-bis(2-ethylhexyl)fluorene-2,7-diboronic acid, 533 mg (1.81 mmol) of 4,7-dibromo-2,1,3-benzothiadiazol and 439 mg (1.81 mmol) of 2,5-dibromothiophene were dissolved in a mixture of 40 ml of toluene and 8 ml of degassed isopropanol under nitrogen atmosphere. Five drops of Aliquat 336 and 4 ml of a 4 M (16 mmol) potassium carbonate in degassed water were added and the mixture was heated to 70°C for 15 minutes; then, 52 mg (0.040 mmol) of $Pd(PPh_3)_4$ were added and the reaction

Autor's signature

was carried out for 40 hours under vigorous stirring. The reaction mixture was cooled, poured into 250 ml of methanol, and the solid that precipitated was collected by filtration. The solid was redissolved in 500 ml of chloroform, 500 ml of 30% aqueous ammonia were added and the mixture was vigorously stirred for 3 hours at reflux temperature. After cooling at room temperature the organic phase was separated. 400 mg of EDTA were added and the mixture was stirred overnight. Then the solution was extracted three times with 500 ml of water. The organic phase was separated, concentrated to about 10 ml and added dropwise to 200 ml of methanol. The coagulated polymer was collected by filtering through a Gooch filter and dried in a vacuum oven to yield 1.702 g (94 %) of a yellow-green powder.

P2 low MW: Poly{[2'-(thien-2-yl)-9',9'-bis(2-ethylhexyl)fluorene)-5,7'-diyl]-co-[4'-(thien-2-yl)-2',1',3'-benzo-thiadiazole-5-7'-diyl]}

627 mg (1.40 mmol) of 9,9-bis(2-ethylhexyl)fluorene-2,7-diboronic acid, 545 mg (1.40 mmol) of 2,1,3-benzothiadiazole-4,7-bis(4,4,5,5-tetramethyl)-1,3,2-dioxaborolane and 680 mg (2.81 mmol) of 2,5-dibromothiophene were dissolved in a mixture of 25 ml of toluene and 6 ml of degassed propanol under nitrogen atmosphere. Five drops of Aliquat 336 and 3 ml of 4 M (12 mmol) potassium carbonate in degassed water were added and the mixture was heated to 70°C for 15 minutes; then, 30 mg (0.035 mmol) of $Pd(PPh_3)_4$ were added and the reaction was carried out for 40 hours under vigorous stirring. The reaction mixture was cooled, poured into 250 ml of methanol, and the solid that precipitated was collected by filtration. The solid was redissolved in 500 ml of chloroform and the insoluble fraction was removed. 500 ml of 30% aqueous ammonia were added to the solution and the mixture was vigorously stirred for 3 hours at reflux temperature. After cooling at room temperature the organic phase was separated. 400 mg of EDTA were added and the mixture was stirred overnight. Then the solution was extracted three times with 500 ml of water. The organic phase was separated, concentrated to about 10 ml and added dropwise to 200 ml of methanol. The coagulated polymer was collected by filtering through a Gooch filter and dried in a vacuum oven to yield 472 mg (49 %) of a dark brown

Autor's signature

P3 low MW: Poly{[2'-(2,1,3-benzothiadiazole-4-yl)-9',9'-bis(2-ethylhexyl)fluorene-7,7'-diyl]-co-[2'-(2,1,3-benzothiadiazole-4-yl)thien-7, 5'-diyl]}

873 mg (1.59 mmol) of 2,7-dibromo-9,9-bis(2-ethylhexyl)fluorene, 1.239 g (3.19 mmol) of 2,1,3-benzothiadiazole-4,7-bis(4,4,5,5-tetramethyl)-1,3,2-dioxaborolane and 385 mg (1.59 mmol) of 2,5-dibromothiophene, were dissolved in a mixture of 180 ml of toluene and 6 ml of degassed ethanol under nitrogen atmosphere. Five drops of Aliquat 336 and 3 ml of a 4 M (12 mmol) potassium carbonate in degassed water were added and the mixture was heated to 70°C for 15 minutes; then, 369 mg (0.32 mmol) of $Pd(PPh_3)_4$ were added and the reaction was carried out for 40 hours under vigorous stirring. The reaction mixture was cooled, poured into 250 ml of methanol, and the solid that precipitated was collected by filtration. The solid was redissolved in 500 ml of chloroform, 500 ml of 30% aqueous ammonia were added and the mixture was vigorously stirred for 3 hours at reflux temperature. After cooling at room temperature the organic phase was separated. 400 mg of EDTA were added and the mixture was stirred overnight. Then the solution was extracted three times with 500 ml of water. The organic phase was separated, concentrated to about 20 ml and added dropwise to 200 ml of methanol. The coagulated polymer was collected by filtering through a Gooch filter and dried in a vacuum oven to yield 817 mg (70 %) of a dark brown powder.

7.2.2 HIGH WEIGHT POLYMERS

P1 high Mw: 1.736 g (3.63 mmol) of [9,9-Bis(2-ethylhexyl)-9H-fluorene-2,7-diyl]bisboronic acid, 533 mg (1.81 mmol) of 4,7-Dibromobenzo[c]-1,2,5-thiadiazole and 439 mg (1.81 mmol) of 2,5-dibromothiophene were dissolved in a mixture of 40 ml of toluene and 8 ml of degassed isopropanol under nitrogen atmosphere. Five drops of Aliquat 336 and 4 ml of a 4 M (16 mmol) potassium carbonate in degassed water were added and the mixture was heated to 70°C for 15 minutes; then, 52 mg (0.040 mmol) of Pd(PPh3)4 were added and the reaction was carried out for 40 hours under vigorous stirring. The reaction mixture was cooled, poured into 250 ml of methanol, and the

Autor's signature

coagulated solid was collected by filtration. The solid was redissolved in 500 ml of chloroform, 500 ml of 30% aqueous ammonia were added and the mixture was vigorously stirred for 3 hours at reflux temperature. After cooling at room temperature the organic phase was separated. 400 mg of EDTA were added and the mixture was stirred overnight. Then the solution was extracted three times with 500 ml of water. The organic phase was separated, concentrated to about 10 ml and added dropwise to 200 ml of methanol. The coagulated polymer was collected by filtering through a Gooch filter and dried in a vacuum oven to yield 1.702 g (94 %) of a yellow-green powder.

P2 high MW: 627 mg (1.40 mmol) of [9,9-Bis(2-ethylhexyl)-9*H*-fluorene-2,7-diyl]bisboronic acid, 545 mg (1.40 mmol) of 2,1,3-Benzothiadiazole-4,7-bis(boronic acid pinacol ester) and 680 mg (2.81 mmol) of 2,5-Dibromothiophene were polymerized following the same procedure described for **P1 high MW.** The coagulated polymer was collected by filtering through a Gooch filter and dried in a vacuum oven to yield 472 mg (49 %) of a dark brown powder.

7.2.3 PURIFICATION

The process of purification was carried out following the procedure described by Jansenn *et al.* [1].

7.2.4 REFERENCE COPOLYMERS

P4 high MW and purification: {[2,7-(9,9-bis-(2-ethylhexyl)-fluorene)]-alt-[5,5-(4,7-di-20-thienyl-2,1,3-benzothiadiazole)]}
479 mg (PM= 478.29 Da, 1,00 mmol) of 9,9-bis(2-ethylhexyl)fluoren-2,7-diboronic acid, 459 mg (PM= 458.20 Da, 1.00 mmol) of 4,7-di-2'-(5'-bromo)-thyenyl-2,1,3-benzothiadiazole were dissolved in a mixture of 11 ml of distilled toluene, 2 ml of degassed propanol and five drops of Aliquat 336 in nitrogen atmosphere. 4 ml of a 4 M

solution of potassium carbonate in degassed water were added, then the mixture was vigorously stirred at 70 °C for 15 minutes. In nitrogen atmosphere 12 mg (0.01 mmol) of $Pd(PPh_3)_4$ were added. After 40 hours the reaction mixture was cooled, poured into 250 ml of methanol and the solid precipitated was collected by filtration. The solid was dissolved again in 500 ml of chloroform and were added 500 ml of ammonia solution in water (30% v/v). The two phases was vigorously stirring at reflux of chloroform. After 3 hours the two phases were separated and 400 mg of EDTA were added to the organic solution, stirring overnight. Then the solution was extracted in succession three times with 500 ml of water. The organic phase was concentrated distilling the solvent and added drop wise to 200 ml of methanol. The polymer was collected by filtering through a Gooch filter and dried in a vacuum oven to yield 681 mg (98%) of a red-violet powder.
The synthesis of alternating copolymers $(F\text{-}T)_n$ and $(F\text{-}B)_n$ can be found elsewhere.

7.3 MEASUREMENTS

Molecular weight determinations were made using a Waters 150C chromatograph (Waters Corp. Milford, MA, USA) equipped with a refractive index detector on 1,2,4-trichlorobenzene solutions at 80°C. Molecular weight calibration was performed using monodisperse polystyrene standards.
NMR spectra were obtained with an Avance 400 spectrometer (Bruker Corp., Madison, WI, USA). Samples were dissolved in CDCl3 (reference: 7.26 ppm for 1H and 77.7 ppm for 13C). ^{1}H-NMR spectra were acquired with a 90° pulse width and 4 s. as delay time. 13C[1H]-NMR spectra were acquired with 30° pulse width and 2 s. as delay time.
UV-Vis absorption spectra were recorded at room temperature with a Lambda 950 spectrophotometer (Perkin-Elmer Inc. Waltham, MA, USA). Samples in solution were prepared by dissolving pristine polymer in $CHCl_3$ solutions in cell with 10 mm optical path length and optical density of typically 0.5 at max. absorption in the visible region of spectrum. Thin films (~100 nm) of pristine polymers and polymer/PCBM blends were prepared by spin-coating from chlorobenzene solution on quartz Suprasil substrates. The optical energy gaps were evaluated by the edge corresponding to the intersection between

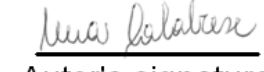

Autor's signature

the negative tangent line in the inflection point of lowest energy absorption band and the tangent line to linear portion of the absorption tail.

Steady-state PL spectra were recorded at room temperature with an Fluorolog 3 spectrofluorometer (Horiba Jobin-Yvon Inc., Edison, NJ, USA), with right angle geometry for liquid samples and front face (22°) for thin films. The same samples used for absorption was used for PL quenching measurement; emission spectra were corrected for the optical density of the sample at the excitation wavelength.

Electrochemical measurements were performed with an Autolab PGSTAT30 potentiostat/galvanostat (EcoChemie, The Netherlands) run by a PC with GPES software, in a one-compartment three-electrode cell in argon-purged acetonitrile with 0.1 M Bu4NBF4 as supporting electrolyte. A $CHCl_3$ solution 1mg/ml of the compound was coated on the Glassy Carbon working electrode (Amel Electrochemistry, Milano, Italy) having a surface of 0.071 cm2. A Platinum counter electrode and an aqueous saturated calomel (SCE) reference electrode were used. The film formed on the electrode was analyzed at a scan rate of 200 mV/s. The data have been referred to the Fc^+/Fc redox couple (ferricenium/ferrocene), according to IUPAC [2].

IR spectra were recorded at 2 cm^{-1} resolution on a Nicolet Nexus FT-IR spectrometer; the polymers were analysed in transmission as KBr pellets.

Raman spectra were recorded at 4 cm^{-1} resolution on a Bruker FRA 106 FT-Raman module attached to a Bruker IFS88 FT-IR spectrometer, equipped with Nd:YAG excitation laser (1064 nm) and a high sensitive Ge detector. The polymers were analysed as powder in an aluminium solid sample holder in back-scattering configuration with delocalized laser beam of about 150 mW power.

EPR samples in toluene or o-DCB solution (C=1 mg/ml) were degassed by repeated freeze-pump-thaw cycles and sealed under vacuum in 3 mm-OD quartz tubes. Films of copolymers/PCBM (1:1 w/w) in o-DCB were prepared by pouring approximately 0.3ml of toluene solution into a 3 mm EPR quartz tube and letting the solvent evaporate slowly. After, the sample were leaved for 30 min within under vacuum (10^{-5} Torr). Finally the tubes were sealed under vacuum to eliminate oxygen traces. EPR measurements were carried out with a Bruker ER200D spectrometer equipped with a broadband preamplifier

Autor's signature

(6.5MHz) using the direct detection mode, i.e. without magnetic field modulation. The direct detection implies that the line shapes are in true absorption mode, i.e. not in first-derivative mode as in conventional field modulated spectra. The optical excitation was generated with a pulsed laser beam from a frequency-doubled Nd:YAG laser (Quantel Brilliant, pulse length 5 ns, repetition rate 20 Hz, pulse energy 5mJ) with second and third harmonic (532 nm e 355 nm). The time resolution of the experimental setup was about 150 ns. The sample temperature was controlled in the 100-300 K range by a variable temperature nitrogen flow system (Bruker ER4112VT). The transient signal was recorded with a LeCroy LT344 digital oscilloscope. The transient signal was recorded, digitized and averaged over 100-200 laser pulses by the oscilloscope and collected for each magnetic field value. After a systematic intensity correction and background signal subtraction a 2-D dataset is obtained, which represents the variation of the magnetization with respect to magnetic field and time. For the spectral analysis a slice of the 2-D dataset taken at constant time was considered, corresponding to the maximum of the transient signal. The spectra were analysed with a simulation program built with EasySpin routines in Matlab environment.

Mobility measurements were carried out The sandwich type structure consisting of on ITO-coated transparent electrode, PEDOT layer, active layer (1_2 Am thick)
prepared by spin coating of 1:1 weight ratio mixture of PCBM
and RR-P3HT and Al evaporated on top of structure. The sample
was illuminated through ITO by 532 or 1164 nm laser pulse.

Organic solar cells devices were fabricated by first spin-coating poly(ethylenedioxythiophene: polystyrenesulfonic acid) (PEDOT-PSS) on top of cleaned, pre-patterned indium-tin-oxide (ITO) coated glass substrates as polymer anode (50 nm in thick). The anode polymer film was then annealed at 120°C for 10 min. The copolymers blended with PCBM in solution were deposited on the top of PEDOT:PSS by spin-coating. The cathode consisting of Al (70 nm) was then sequentially deposited on top of the active layer by thermal evaporation in vacuum lower than 10^{-6} Torr giving a sandwich solar cell structure of ITO/PEDOT:PSS/Copolymer:PCBM/Al. Current density-voltage

Autor's signature

characteristics were measured using a Solar Simulator Abet 2000 (Class A, AM1.5G). The current-voltage curves were taken with a Keithley 2400 source-measure unit. All devices was made in air while all characterization was carried out in an ambient environment. For light-intensity dependent measurements, a set of quartz neutral filters was used to vary the incident light power.

7.4 REFERENCES

[1] Bijleveld, J. C., Shahid, M., Gilot, J., Wienk, M. M., Janssen, R. A. J.: Copolymers of Cyclopentadithiophene and Electron-Deficient Aromatic Units Designed for Photovoltaic Applications. Adv. Funct. Mat. 19, 3262-3270 (2009)

[2] Gritzner, G., Kuta, J.: Recommendations on reporting electrode potentials in nonaqueous solvents: IUPC commission on electrochemistry. Electrochimica Acta. 29, 869-873 (1984)

Autor's signature

APPEND A

Local density approx:	Vosko Wilk Nusair,	
Basis:	III-TZP (small core) Restricted	
Exchange:	Becke88,	
Correlation:	Perdew86,	
Correction	after SCF,	
Convergence parameters:	SCF:	5.0E-05 Ha
	Geom. Energy:	2.250E-03 Ha/step
	Geom. Gradient:	1.0E-02 Å/step
	Geom. Lenght:	1.0E-02 Å /step
	Geom. Angle: 0.5 deg/step	
SCF integration accuracy:	4.0	
DIIS vectors:	5	
Max DIIS coeff:	5.0	
Limits:	Hessian update	
Minimization algorithm:	BFGS	
Convergence parameters:	Max SCF cycles:	250 steps
	Max lenght step:	0.3 Å
	Max angle step:	5.0 deg
	Max opt cycles:	100 steps

Autor's signature